APPLICATION OF NOVEL METHODS FOR THE MEASUREMENT OF ACIDIC ULTRAFINE PARTICLES IN THE ATMOSPHERE

LU HAOXIAN

PhD

The Hong Kong Polytechnic University

2022

The Hong Kong Polytechnic University
Department of Civil and Environmental Engineering

Application of Novel Methods for the Measurement of Acidic Ultrafine Particles in the Atmosphere

Lu Haoxian

A thesis submitted in partial fulfillment of the requirements for the degree of Doctor of Philosophy

June 2021

CERTIFICATE OF ORIGINALITY

I hereby declare that this thesis is my own work and that, to the best of my knowledge and belief, it reproduces no material previously published or written, nor material that has been accepted for the award of any other degree or diploma, except where due acknowledgement has been made in the text.

_____(Signed)

LU Haoxian (Name of student)

ABSTRACT

The adverse effects of acidic ultrafine particles (AUFPs) have been widely recognized in scientific communities. AUFPs pollution is closely correlated with total mortality, morbidity and hospital admissions for respiratory diseases. In addition to health issues, AUFPs have impacts on climate, visibility and secondary organic aerosol (SOA) production. However, AUFPs have been rarely measured in the past due to the limitations of reliable measurement technique. Moreover, the existing methods for measuring AUFPs through atomic force microscope (AFM) scanning have several drawbacks such as offline, complicated and time-consuming. There is a need to acquire more AUFPs data, and refine/revise the previous method and develop a new method to achieve semi-automatic measurement of AUFPs without using AFM. Therefore, in the thesis, extensive measurements of AUFPs were firstly conducted in different land-use areas and cities in China using the previous method to better understand the pollution of AUFPs. After the samplings, the disadvantage of the previous method was highlighted and emphasized (*i.e.*, the usage of AFM). To achieve the identification and quantification of AUFPs without using an AFM, a unique method was proposed to remove the non-acidic particles and retain the acidic particles on the surface. With the help of the aforementioned method, a novel system was then developed for semi-automatic measurement of AUFPs in the atmosphere by establishing the relationship between mass of deposited particles and the frequency change detected by the quartz crystal microbalance (QCM).

To explore the AUFPs pollution, six measurements were conducted in the roadside, urban and rural areas in Hong Kong, and the urban area in Shanghai between 2017 and 2020 using the previous diffusion sampler (DS)+AFM method. The concentrations of AUFPs and UFPs, and the proportions of AUFPs in UFPs were obtained with the aid of AFM. The concentration of UFPs was the highest at the roadside site, followed by that at the urban site and the rural site, while the proportion of AUFPs

in UFPs showed a contrary trend, *i.e.*, rural > urban > roadside. The difference, on one hand, might indicate potential transformation of AUFPs from non-acidic UFPs through condensation of acidic vapor on the surface of non-acidic particles and/or heterogeneous reaction of acidic vapor with non-acidic particles during the transport and aging of air masses, and on the other hand, suggested the minor contribution of anthropogenic sources to the emission of AUFPs. The levels of UFPs ((1.21±0.49) $\times 10^4/cm^3$) (mean ± standard deviation (SD)) and AUFPs ((0.27±0.19) $\times 10^4/cm^3$) in urban Shanghai were lower than those ((1.48±0.64) $\times 10^4$ and (0.40±0.27) $\times 10^4/cm^3$, respectively) in Hong Kong ($p < 0.05$). Moreover, the size distributions of AUFPs and UFPs together with the proportions of AUFPs in UFPs in different size bins were investigated. The sizes of UFPs and AUFPs both followed the normal distribution. The proportion of AUFPs in UFPs was peaked in the size range of 35-50 nm in roadside area, while in urban area it was characterized by a hysteretic peak (50-75 nm), probably suggesting the aggregation of AUFPs with non-acidic UFPs during the transport from source areas to receptor areas. In rural area, the peak was observed in the size range of 5-10 nm, which might indicate the stimulation of new particle formation (NPF) with the AUFPs as seeds that were not easy to be aggregated by other low-concentration preexisting particles in a relatively clean environment. Furthermore, in the urban areas of Hong Kong and Shanghai, no significant difference was found for the geometric mean diameters (GMDs) of UFPs and AUFPs ($p > 0.05$), suggesting similar emission sources and/or chemical formation mechanisms of UFPs and AUFPs in these two cities. At last, the sulfuric acid proxy (Q_{sa}) was positively correlated with the proportions of AUFPs in UFPs (R^2=0.71) but not well correlated with the AUFPs levels (R^2=0.17). The results suggested the important roles of both Q_{sa} and preexisting particles in AUFPs formation. At high Q_{sa} level, AUFPs were favorably formed through heterogeneous reaction of sulfuric acid vapor with non-acidic UFPs and/or condensation of sulfuric acid vapor on non-acidic UFPs, which led to high proportion

of AUFPs in UFPs. However, the AUFPs level is not necessarily high if the concentration of preexisting particles is low even though sulfuric acid vapor is sufficient (*i.e.,* high Q_{sa}). Due to the significant reduction of sulfuric dioxide (SO_2) in China during the last decade, the pollution of AUFPs in urban areas was alleviated with the evidence of lower AUFPs concentrations and proportions of AUFPs in UFPs. Specifically, significant reductions in SO_2 levels were observed in Hong Kong and Shanghai. The reduction in Hong Kong was attributed to the increasingly stringent standards of low sulfur fuel oil (LSFO) used in vehicles and the elimination of old diesel vehicles, while the combustion of low sulfur coal in industries and power plants was the important cause for the decrease in SO_2 emissions in Shanghai, in addition to the use of LSFO. Nevertheless, this DS+AFM method was high-cost and time-consuming.

In order to develop a method without using AFM, one possible way is to use an online microbalance (*i.e.*, quartz crystal microbalance (QCM)), which is able to obtain the correlations between the mass of deposited particles and the frequency changes of the QCM. Moreover, if the above idea works, a method that can differentially remove non-acidic particles and retain acidic particles on a surface is a necessity. Subsequently, the acidic particles can be simply quantified based on the frequency change of a QCM. Therefore, in the study, three methods were attempted for differential removal of non-targeted nanoparticles on the surface, including air jet, nanobubble and ultrasonic methods. Acidic particles were taken as the targeted particles while non-acidic particles were regarded as non-targeted particles. Results showed that, regardless of methods, acidic particles were retained on the surface due to the strong particle-surface interaction. The air jet treatment and nanobubble treatment were not able to completely remove non-acidic particles from the surface with the removal efficiency of 5.1% ± 3.4% and 89.3% ± 4.1%, respectively, while the non-acidic particles were entirely removed in the ultrasonic treatment. Ethanol rather than deionized (DI) water was the proper solution in the

ultrasonic treatment to avoid contamination. In conclusion, ultrasonic by ethanol was fully efficient for differential removal of non-acidic particles on the surface. The principle of differential removal of particle is the differences of particle-surface interaction force between non-acidic particles (*i.e.*, physically attached particles) and acidic particles (*i.e.*, chemically-formed particles). Non-acidic particles are removed from the surface through cavitation to form bubbles in the gap between a non-acidic particle and the surface in the ultrasonic treatment. In contrast, the space between an acidic particle and the surface is filled by the reaction, and thus bubbles cannot enter the crevice to remove the acidic particle. The developed method is useful for aerosol research, especially for AUFPs.

By combining the differential removal method, a convenient, rapid and accurate measurement system was developed for semi-automatic measurement of AUFPs in the atmosphere through integrating a DS with three QCMs, namely a QCM+DS system. The QCM detectors were coated with a nano-film of metal (metal-QCM detectors) and then placed inside the DS at three sampling spots for collection and detection of ultrafine particles (UFPs). The frequency changes obtained from the metal-QCM detectors were converted into the weights of deposited particles and used to determine the proportions of AUFPs in UFPs through the differential removal process of non-AUFP particles. Prior to sampling, the sensitive response of the QCM system and collection efficiencies of the QCM+DS system were calibrated using standard acidic and non-acidic particles. Reactions between the AUFPs and nano-film of metal were guaranteed by confirming much lower than one-layer deposition of particles on the detectors based on theoretical calculation and experimental results. Eventually, the QCM+DS system was validated in a field measurement by comparing the results with those obtained from the previously developed method and a commercial measurement system, *i.e.*, Scanning Mobility Particle Sizer (SMPS). All the three methods showed good agreements in measuring AUFPs and UFPs concentrations, indicating the reliability of the QCM+DS system for the quantification of

ambient UFPs and AUFPs.

THE NOVELTY OF THIS STUDY

Acidic ultrafine particles (AUFPs) are ubiquitous in the atmosphere with significant impacts on human health, visibility, and climate. Nevertheless, reliable techniques for measuring AUFPs in the atmosphere were lacking. Only a few studies successfully obtained the concentrations of AUFPs in the atmosphere previously. With the limited techniques and studies, the information of AUFPs in the atmosphere was poorly understood. Moreover, while the previous methods can identify and quantify AUFPs, the usage of atomic force microscope (AFM) makes the methods complicated and time-consuming. There is a need to refine the previous methods for identification and quantification of AUFPs without using an AFM. In addition, the offline measurement techniques of the previous methods consumed enormous resources, which indicated an urgent necessity to develop a resource-saving semi-automatic method. To fill the above research gaps, studies were conducted to unravel these scientific puzzles of AUFPs in this thesis. The novelty of this study is summarized as follows:

(i) The concentrations and size distributions of AUFPs were for the first time measured in different cities in China and different land-use areas in Hong Kong to explore the spatial variations of AUFPs pollution. Higher proportion of AUFPs in UFPs was found in rural area than in urban and roadside areas, probably suggesting the potential transformation of AUFPs from non-acidic UFPs by condensation of acidic vapor on the surface of non-acidic particles and/or heterogeneous reaction of acidic vapor with non-acidic particles during the transport and aging of air mass and proving the minor contribution of anthropogenic sources to the emission of AUFPs. Moreover, the proportion in urban area was characterized by a peak in a larger size range (*i.e.*, 50-75 nm) than that in roadside area (*i.e.*, 35-50 nm), implying the growth and aggregation of AUFPs with non-acidic UFPs during the transport from source areas to receptor areas. However, in rural area, the proportion peaked in the smallest size

range (*i.e.*, 5-10 nm) and then gradually decreased with size. The peaked nucleation mode AUFPs indicated the stimulation of NPF with the AUFPs as seeds, which were not easily aggregated by other low-concentration preexisting particles in the relatively clean environment. Compared to the urban area of Hong Kong, urban Shanghai suffered from less pollution of AUFPs and UFPs, evidenced by their lower concentrations. However, no significant difference was found for the geometric mean diameters (GMDs) of UFPs and AUFPs between the two cities ($p > 0.05$), indicating similar emission sources and/or chemical formation mechanisms of UFPs and AUFPs in these two cities. Lastly, close relationship between the sulfuric acid vapor (Q_{sa}) and the proportions of AUFPs in UFPs was found (R^2=0.71), while the correlation of Q_{sa} with AUFPs level was poor (R^2=0.17). The findings suggested that an important pathway of AUFPs formation was the heterogeneous reaction of sulfuric acid vapor with non-acidic UFPs and/or the condensation of sulfuric acid vapor on non-acidic UFPs. Thus, both Q_{sa} and the level of preexisting particles were the important factors to determine the concentration of AUFPs and the proportion of AUFPs in UFPs. The high Q_{sa} facilitated the transformation of non-acidic UFPs to AUFPs and thus led to the high proportion of AUFPs in UFPs but did not necessarily result in high concentration of AUFPs if the level of preexisting particles was low. Compared to the values measured in urban Hong Kong ten years ago, the concentrations of AUFPs and their fractions in UFPs were reduced in urban areas, proving the alleviation of AUFPs pollution in the past decade due to the nationwide successful reduction of ambient SO_2 level. The reduction of SO_2 was mainly attributed to the usage of low sulfur fuel oil (LSFO) with increasingly stringent standards in vehicles, the elimination of old diesel vehicles and the combustion of low sulfur coal in industries and power plants.

(ii) For the first time, a novel method was developed to semi-automatically determine the concentrations of ambient AUFPs and UFPs, namely quartz crystal microbalances (QCM) + diffusion sampler (DS) method. The method was accomplished by combining the previous DS and three QCM systems. The QCM is an extremely sensitive online mass sensor with a detection capacity in the sub-nanogram range. Modifications were made to the inlet of the DS and the sampling spots inside the DS. Furthermore, the QCM detector was altered by coating a nano-metal film on its surface to generate a metal-QCM detector for collecting and identifying AUFPs. AUFPs were identified and quantified based on the frequency change of the metal-QCM detectors during ultrasonic processing and sampling. Prior to field measurements, calibration experiments were conducted to determine the sensitivity factor of the modified QCM detector and the relationship of collection efficiency of QCM+DS system with particle size and sampling flow rate. The developed QCM+DS system was validated by comparing with the results of other two methods (*i.e.*, Scanning Mobility Particle Sizer (SMPS) and DS+AFM) in a field sampling campaign. The results of UFPs and AUFPs measured by the QCM+DS system showed fairly good agreements with the results of the other two methods. To sum up, the QCM+DS system is satisfactory and reliable for the measurements of ambient UFPs and AUFPs.

(iii) Previous methods removed all the particles on the surface regardless of particle properties. To facilitate the collection and analysis of AUFPs, a unique method was developed for differential removal of non-acidic particles on the surface in this study. Three methods were trialed for differential removal of nanoparticles on the surface of the nano-metal film, including air jet, nanobubble and ultrasonic methods. It was proved that ultrasonic treatment with ethanol can completely remove the non-acidic particles and retain the acidic particles on

the surface of nano-metal film. In the process of differential removal of particles, the physically adhered particles (*i.e.*, non-acidic particles) are removed from the surface due to cavitation collapse pressure. The space between non-acidic particles and the surface acts as a crevice, which entraps gas and improves cavitation erosion. In contrast, for the acidic particles that react with the surface of the nano-metal film, the space between the particles and the surface is filled and no crevice exists. Under such circumstance, no cavitation occurs, and bubbles cannot enter the gap to remove the particles.

RESEARCH OUTPUTS

1. **Lu, H.**, Lyu, X., and Guo, H.* 2021. A novel semi-automatic method for measuring acidic ultrafine particles in the atmosphere. *Atmospheric Environment*, *245*, 118044. (IF: 4.039).
2. **Lu, H.**, Yao, D., Yip, J., Kan, C. W., and Guo, H.* 2020. Addressing COVID-19 Spread: Development of Reliable Testing System for Mask Reuse. *Aerosol and Air Quality Research*, *20*(11), 2309-2317. (IF: 2.735).
3. **Lu, H.**, Lyu, X., Cheng, H., Ling, Z., and Guo, H.* 2019. Overview on the spatial-temporal characteristics of the ozone formation regime in China. *Environmental Science: Processes and Impacts*, *21*(6), 916-929. Invited review paper. (IF: 3.238).
4. **Lu, H**., Huang, F., Guo, H.* 2021. Differential removal of nanoparticles on the surface of a thin film substrate. ACS Omega (Accepted) (IF: 2.87).
5. **Lu, H**., Lyu, X., and Guo, H.* 2019. Atmospheric Acidic Ultrafine Particle Measuring Device. Gold Medal and Special Merit Award in the 71st International Trade Fair for Ideas, Inventions & New Products (iENA), 31 October to 3 November, Germany.
6. **Lu, H**., and Guo, H.* 一种用于检测大气中酸性超细微颗粒的半在线方法及装置. (Patent)
7. Yao, D. W., Lyu, X. P., **Lu, H. X.**, Zeng, L. W., Liu, T. Y., Chan, C. K. and Guo, H.* 2020. Characteristics, sources and evolution processes of atmospheric organic aerosols at a r oadside site in Hong Kong. *Atmospheric Environment*, *252*, 118298. (IF: 4.039).
8. Lyu, X., Guo, H.,* Yao, D., **Lu, H.**, Huo, Y., Xu, W., Kreisberg, N., Goldstein, A., Jayne, J., Worsnop, D., Tan, Y., Lee, S., and Wang, T. 2020. In Situ Measurements of Molecular Markers Facilitate Understanding of Dynamic Sources of Atmospheric Organic Aerosols. *Environmental Science and Technology*, *54*(18), 11058-11069. (IF: 7.864).
9. Liu, T., Zhou, L., Liu, Q., Lee, B. P., Yao, D., **Lu, H.**, Lyu, X., Guo, H., and Chan, C. K.*

2019. Secondary organic aerosol formation from urban roadside air in Hong Kong. *Environmental Science and Technology*, *53*(6), 3001-3009. (IF: 7.864)

10. Lyu, X. P., Guo, H.,* Cheng, H. R., Wang, X. M., Ding, X., **Lu, H. X.**, Yao, D. W. and Xu, C. 2017. Observation of SOA tracers at a mountainous site in Hong Kong: Chemical characteristics, origins and implication on particle growth. *Science of the Total Environment*, *605*, 180-189. (IF: 6.551)
11. Lyu, X., Huo, Y., Yang, J., Yao, D., Li, K., **Lu, H.**, Zeren, Y., and Guo, H.* 2021, Real-time molecular characterization of air pollutants in a Hong Kong residence: Implication of indoor source emissions and heterogeneous chemistry. Indoor Air. 00:1–13. (IF: 4.739)
12. Guo, H.,* Ling, Z. H., Cheng, H. R., Simpson, I. J., Lyu, X. P., Wang, X. M., Shao, M., **Lu, H. X.**, Ayoko, G., Zhang, Y. L., Saunders, S. M., Lam, S. H. M., Wang, J. L., and Blake, D. R. 2017. Tropospheric volatile organic compounds in China. *Science of the Total Environment*, *574*, 1021-1043. (IF: 6.551)

ACKNOWLEDGEMENTS

The years of my PhD study in the Hong Kong Polytechnic University will be the most unforgettable memory in my life. I want to express my sincere gratitude to a lot of people for their assistance and support.

Firstly, I would like to give my most sincere thanks to my supervisor, Professor Hai Guo, for his constant help and meaningful guidance for my PhD study. He is always selfless to share his knowledge with me and provide necessary resources on my research. He spent a lot of time on helping me overcome difficulties and leading me the direction of my PhD study. His rigorous research attitude impresses me a lot and will always influence me in my future study and work.

My sincere thanks also go to Prof. Chak K. Chan from City University of Hong Kong, who lent an equipment to me for calibration experiments; to Prof. Gewei Wang in East China Normal University, whose group helped me collect samples in Shanghai; to the lab technicians, Mr. Tam and jazz Chan, in the Air Pollution Laboratory, who helped me a lot for sampling campaigns as well as sample analysis; and to the Hong Kong Environmental Protection Department for providing the Hok Tsui sampling site to collect my samples.

Furthermore, this study was supported by the Strategic Focus Area scheme of The Research Institute for Sustainable Urban Development at The Hong Kong Polytechnic University (1-BBW9), the Environment and Conservation Fund (ECF) of the Hong Kong Special Administrative Region (ECF59/2015), the Hong Kong PhD Fellowship (Project Number: RULW) and the University Strategic Importance scheme at The Hong Kong Polytechnic University (1-ZE1M).

I am also grateful to members in our group, Dr. Xiaopu Lyu, Dr. Yu Wang, Dr. Lewei Zeng, Dr. Xufei Liu, Mr. Dawen Yao and Miss Yangzong Zeren. They supported me in my research and my daily life. Lastly, I would like to thank my families and my girlfriend for their love, care and

encouragement. They are always my solid support.

ABBREVIATIONS

Table Methods and substances in this thesis with their abbreviations.

Full name	Abbreviations
Ultrafine Particles	UFPs
Acidic Ultrafine Particles	AUFPs
Scanning Mobility Particle Sizer	SMPS
Differential Mobility Analyzer	DMA
Diffusion Sampler	DS
Atomic Force Microscope	AFM
Quartz Crystal Microbalance	QCM

CONTENTS

Chapter 1 Overview

1.1 Research background

Accumulated evidence strongly suggested that the number of acid-containing ultrafine particles was closely correlated with total mortality, morbidity and hospital admissions for respiratory diseases (Lippmann, 1989; Thurston et al., 1989, 1992, 1994; Lippmann and Thurston, 1996; Peters et al., 1997; Wichmann et al., 2000; Cohen et al., 2000). In addition, acidic ultrafine particles (AUFPs) affect climate, visibility and secondary organic aerosol (SOA) production (Kim et al., 1994; Kulmala et al., 2004a; Zhang et al., 2007; Li et al., 2010; Han et al., 2016). Moreover, AUFPs contribute to new particle formation (NPF) as AUFPs may act as seeds to catalyze/trigger the particle formation and growth (Guo et al., 2012; Wang et al., 2014a). Hence, it is critical to distinguish AUFPs from the total ultrafine particles (UFPs), and to quantify the AUFPs in the atmosphere. Only with this information, can the formation mechanism of AUFPs be understood and effective control measures be formulated and implemented. To measure AUFPs, some pilot studies were carried out to quantify the number of acidic particles. Lodge and Havlik (1960) used the changes of light transmission and resistance of thin metal films to indicate the atmospheric pollution. Horstman et al. (1967) used iron-coated detectors to size acidic particles (> 0.1 μm) by electron microscope. In the early 2000s, Cohen et al. (2004a) adopted iron nanofilm detectors for the measurements of acidic particles in New York. The nanofilm detectors were examined by Scanning Probe Microscope (SPM) for the enumeration of acidic particles. However, no acidic particles were detected in their study, probably due to the insufficient sampling duration which led to undetected levels of AUFPs. Later, Cohen et al. (2004b) conducted further measurements of AUFPs for a longer duration (1 week) and firstly reported the concentrations of AUFPs (100-1800 /cm^3) in New York state. However, they did not conduct method validation with other instruments.

In 2012, a method with the use of iron nanofilm detectors for enumeration and size measurement of acidic aerosols was developed (Wang et al., 2012). Briefly, standard sulfuric acid (H_2SO_4) or ammonium hydrogen sulfate (NH_4HSO_4) droplets and sulfuric acid-coated particles were generated and deposited on the specially designed detectors to cause reaction spots. The dimensions of the reaction spots were examined with Atomic Force Microscopy (AFM) to establish the correlations between the diameter of the particle and the size of the reaction spot. Collection of particles in the atmosphere was achieved by using an electrostatic precipitator (ESP), thus forming the ESP+AFM method. The method was validated by field measurement data collected at a mountain site in Hong Kong. Results indicated that the particle number concentrations and geometric mean diameter (GMD) obtained from the ESP+AFM method were comparable to those derived from the Scanning Mobility Particle Sizer (SMPS) measurements ($p > 0.05$). The concentration of AUFPs was about 2×10^3 /cm^3, which accounted for about 30% of total UFPs. Wang et al. (2012) proved that the ESP+AFM method with iron nanofilm detectors was a reliable tool for the measurement and analysis of acidic particles in the atmosphere.

However, this method has limitations for the assessment of long-term exposure to AUFPs due to the fact that (1) the detector is saturated after only several hours of sampling using the ESP, and it is highly time-consuming if this method is used to assess long-term variations of AUFPs because numerous short-term samples are needed for AFM analysis; and (2) the cost is high for the operation and maintenance of AFM if the sample size is tremendous for a long-term measurement. Therefore, in 2014, a diffusion sampler (DS) with the iron nanofilm detectors was successfully developed for the long-term measurement (2-4 days) of the number concentration and size distribution of AUFPs in the atmosphere (Wang et al., 2014a), namely the DS+AFM method. The iron nanofilm detectors were deployed on rectangular recesses inside the sampler at three different

locations along the length of the channel to collect the ultrafine particles. The exposed detectors were then scanned using an AFM to numerate and distinguish the AUFPs from the non-acidic UFPs. Prior to sampling, the semi-empirical equations for the diffusive deposition efficiency of particles at the different detector locations in the sampler were obtained on the basis of theoretical diffusive mechanism and modified by the experimental data using polystyrene latex (PSL) standard particles. After calibration, the DS + AFM method and a commercially available online measurement system (*i.e.,* SMPS) were simultaneously used in a 4-week field sampling campaign at an urban site in Hong Kong for method validation. The DS+AFM method showed good agreement with the SMPS results of total particle number concentration and size distribution indicating that the DS+AFM provides an additional approach for the long-term measurements of ambient AUFPs. With this method, the concentrations of AUFPs and UFPs at this urban site were approximately 9×10^3 /cm^3 and 2×10^4 /cm^3, respectively. Overall, only a few studies successfully measured and reported the concentrations of AUFPs in the atmosphere, suggesting the poor understanding of AUFPs pollution in the atmosphere. Therefore, in this thesis, for the first time, AUFPs were extensively measured in different land-use areas and cities through six sampling campaigns using the DS+AFM method. The spatial variations of AUFP concentrations and size distributions were acquired. The results would help establish a database of AUFPs and provide a valuable reference for the future air-quality study.

While the aforementioned methods can identify and quantify the concentration of AUFPs, they are offline and require enormous resources to support the required AFM analysis. The AFM instrument is neither inexpensive, timesaving, small, nor easy to operate (Kessler et al., 2020; Li et al., 2016). These deficiencies have been highlighted and emphasized after extensive measurements of AUFPs. The AFM is unable to scan the nanoparticles on the entire surface in an acceptable period. Multiple

scans of a sample are required to reduce the uncertainty, which consume a lot of resources and cause high costs, in particular when the sample size is huge. Hence, there is a need to refine/revise the above methods, which will not use the expensive AFM to enumerate acidic particles on the detectors after collection and can realize the semi-automatic measurement. To develop a semi-automatic method without using AFM, an online microbalance (*i.e.*, quartz crystal microbalance (QCM)) is a possible way, which links the mass of deposited UFPs and/or AUFPs with the frequency change. The QCM is an extremely sensitive online mass sensor with a detection capacity in the sub-nanogram range (McCallum, 1989, Ward and Buttry, 1990; Chen et al., 2016). Generally, the mass of deposited substance is linearly related with the frequency change of the QCM. Due to its high sensitivity, it is widely used as detector/sensor to measure the gaseous and particulate pollutants (Marple et al. 2001; Liang et al., 2010; Subramanian et al., 2016). In the study, the previous DS was refined by integrating with the QCM to form a new system which did not use the AFM. Moreover, to determine the proportion of AUFPs in UFPs without using AFM, a method is required to differentially remove the non-AUFPs and reserve the AUFPs on the surface. In this way, the AUFPs levels could be determined by excluding the frequency change caused by the non-AUFPs in the QCM system. To our best knowledge, previous methods removed all the particles on a surface regardless of particle properties (Kim et al., 2013; Park et al., 2012; Kawamoto and Guo, 2018). This is the first study that developed a differential removal system for nanoparticles on the surface based on the property of particles. The method is useful for the purposeful collection and subsequent component analysis of AUFPs in aerosol study. Eventually, with the aid of the differential particle removal method and the system of previous DS with QCM, a convenient, rapid and reliable method was developed for the semi-automatic measurement of AUFPs in the atmosphere.

1.2 Scope of this study

The objectives of this study are shown below:

- To understand the spatial variation of AUFPs pollution by conducting field measurements in different land-use areas and different cities in China.
- To realize identification and purposeful collection of AUFPs without using an AFM by developing a method which can differentially remove non-acidic particles and retain acidic particles on the surface.
- To develop a novel system for semi-automatically measuring AUFPs in the atmosphere by combining the previous DS with three QCM systems, and to validate the developed system in the field measurement with two other methods (*i.e.*, SMPS and DS+AFM).

The broad objectives of this study are to improve the understanding of AUFPs pollution through extensive field measurements, refine the previous methods and develop a new method to achieve semi-automatic measurement of AUFPs without using an AFM. The findings are expected to provide a valuable database of AUFPs for further study, and the developed methods are useful for purposeful particle collection and measurement of atmospheric AUFPs in the future.

1.3 Outline of the thesis

In order to better present the work in my PhD study, this thesis was divided into seven chapters, including Overview, Literature Review, Methodology, Results and Discussion (Chapters 4-6), and one chapter summarizing all sub-conclusions for this study, namely, Conclusions and Suggestion for Future Study. The brief introduction of each chapter is given below.

Chapter 1 (*Overview*) included three sections. The *Research background* part introduced the previous studies and illustrated the research gaps in the research area of acidic ultrafine particles (AUFPs). The *Scope of this study* part presented the research objectives of this study. Then the research content was listed and briefly introduced in the *Outline of the thesis*.

Chapter 2 (*Literature Review*) introduced the previous studies on ultrafine particles (UFPs) and AUFPs, reviewed the previous methods for offline measurement of AUFPs and presented possible techniques which could be utilized to develop a method for online measurement of AUFPs.

Chapter 3 (*Methodology*) summarized the materials and methods used in the thesis, including *Preparation of nano-metal film detectors, Generation of standard particles, Verification of nano-metal film detectors, diffusion sampler (DS)+atomic force microscope (AFM) system, QCM+DS system, Methods for differential particle removal, Sampling campaign* and estimation of *concentration of sulfuric acid (SA) vapor*.

Chapter 4 (*Ambient acidic ultrafine particles in different land-use areas and in different Chinese cities*) for the first time measured the concentrations and size distributions of AUFPs and UFPs in different land-use areas and cities in China. The relationship of sulfuric acid vapor with AUFPs was investigated. Moreover, the AUFPs pollution was compared with that in the previous studies.

Chapter 5 (*Differential removal of nanoparticles on the surface of a thin film substrate*) examined three methods to differentially remove non-acidic particles and retain acidic particles on the surface of a nano-metal film. Removal efficiencies of different methods were determined with the aid of AFM. In addition, the mechanism and implication of differential removal of particles on the surface were discussed.

Chapter 6 (*A novel semi-automatic method for measuring acidic ultrafine particles in the atmosphere*) developed a novel method of QCM+DS system for semi-automatic measurement of AUFPs in the atmosphere. The response of the QCM and the collection efficiency of the QCM+DS system were calibrated through laboratory experiments. After calibration, the developed method was validated by the results of two other methods (*i.e.*, scanning mobility particle sizer (SMPS) and DS+AFM) in a field measurement.

Chapter 7 (*Conclusions and suggestion for future study*) concluded major findings of the thesis and emphasized innovative contributions of this work to the scientific communities. In addition, suggestions for future studies in this research area were provided.

Here, I clarify that all the data in my thesis were mainly collected by myself, except for the samples collected in Shanghai. Moreover, the data analyses in Chapters 4-6 were carried out by me.

Chapter 2 Literature Review

2.1 Atmospheric ultrafine particles (UFPs) and acidic UFPs (AUFPs)

2.1.1 UFPs

UFPs are particles with an aerodynamic diameter of 0.1 μm (100 nm) or less (Kulmala et al; 2004a; Kumar et al., 2014; Morawska et al., 2020). They are ubiquitous in the atmosphere because around 90% of particles are UFPs in term of number concentration in both outdoor (*e.g.*, Wichmann et al., 2000; Guo et al., 2008; Solomon et al., 2008; Hagler et al., 2009; Buonanno et al., 2009; Karottki et al., 2015) and indoor environments (*e.g.*, Morawska et al., 2009; Guo et al., 2010; Zhang and Zhu, 2010; González et al., 2011; Karottki et al., 2015; Rim et al., 2016). In general, atmospheric UFPs can be classified into three modes, *i.e.*, nucleation mode (5-25 nm), Aitken mode (25-100 nm) and accumulation mode (100-300 nm). Nucleation mode particles are formed through direct source emissions and/or atmospheric chemical reactions (Lingard et al., 2006), while Aitken mode particles are mainly produced from the growth or coagulation of nucleation mode particles and the emission from primary combustion sources (Kulmala et al., 2004b). Accumulation mode particles (100-300 nm), sometimes called soot mode, are carbonaceous (soot and/or ash) agglomerates (Lingard et al., 2006), which are mainly emitted from the combustion of fuel and lubricant oil by vehicles (Wehner et al., 2009) and from the coagulation of nucleation and Aitken mode particles (Hinds, 1999). Ultrafine particles discussed in the thesis are the combination of the above three modes of particles. Due to high diffusion coefficients and tiny sizes, ultrafine particles can penetrate deep into the fluids and alveoli of the lungs (Morawska et al., 2004; Oberdörster et al., 2005; Sturm, 2016; Weichenthal et al., 2017) and bloodstream (Oberdörster et al., 2004; Baldauf et al., 2016). The accumulation of UFPs in human body

significantly contributes to adverse health effects, including aggravated respiratory symptoms, decreased lung function, chronic bronchitis, irregular heartbeat, and premature death in people with heart or lung disease (Bräuner et al., 2007; Hoek et al., 2010; Oh and Park, 2014; Heinzerling et al., 2016; Clifford et al., 2018).

2.1.2 AUFPs

2.1.2.1 Health effect of AUFPs

Although the substantially toxicological effects of UFPs are evidenced, the components of UFPs are not equally toxic (Hazi et al., 2003; Yang et al., 2013; Adams et al., 2015). For example, Oberdörster et al. (2000) reported that inhalation of nonreactive, low-solubility ultrafine particles did not cause inflammation in young healthy rats. Among all the components, sulfuric acid (H_2SO_4) and ammonium bisulfate (NH_4HSO_4) are important chemicals that cause significantly adverse health effects in airborne UFPs, forming AUFPs. Since the early 20th century, studies have pointed out the adverse effects of acidic particles on human health (Lioy and Waldman, 1989; Dockery et al., 1993; Wyzga and Folinsbee, 1995). Adverse health effects caused by the inhalation of AUFPs include the prevalence of bronchitis and lung function decrements (Lung et al., 1992; Chen et al., 1995; Lippmann, 2000; Thurston et al., 2000). In a real case in West Germany, an acidic pollution episode was observed in January 1985 by Wichmann et al. (1989). The episode led to significant excesses in respiratory mortality and morbidity. Dassen et al. (1986) also pointed out the persistent decrements in lung function among schoolchildren of the same case. Hattis et al. (1987) indicated the importance of number concentration in the health effect of acidic particles. An "irritation signaling" model was developed in his study to evaluate the harm of atmospheric acid sulfate particulates. The model revealed that acid sulfate particulates carried

irritant acid signals to the distal tracheobronchial epithelium, and those signals contributed to chronic bronchitis over time. Moreover, animal exposure tests were conducted to understand the health effect of acidic particles. Amdur and Chen (1989) found that concentrations of H_2SO_4 particles as low as 20 $\mu g/m^3$ produced cumulative pulmonary effects in guinea pigs through repeated daily 3 hours exposures for 5 consecutive days. Decrements in total lung capacity (TLC), vital capacity (VC), functional residual capacity (FRC), and pulmonary diffusing capacity (DL_{CO}) persisted for 48 to 72 hours after the exposure. Lung et al. (1992) indicated that acidic sulfate was the most toxicologically important sulfur oxide in the ambient air. To determine if particle size influences toxic effects of sulfuric acid, they investigated the effects of sulfuric acid aerosols of two different sizes on biochemical and cellular parameters of bronchoalveolar lavage fluid from exposed guinea pigs. Guinea pigs were exposed to fine (mass median diameter = 0.3 μm), and ultrafine (mass median diameter = 0.04 μm) sulfuric acid aerosols at 300 $\mu g/m^3$ for 3 hours/day. Lungs were of lavage after the euthanasia of animals. Elevated β-glucuronidase, lactate dehydrogenase activities, and total protein concentration as well as decreased cell viability were observed in the lavage after exposure to sulfuric acid aerosols of both sizes. Chen et al. (1995) proved that the number concentration of acidic particles played an important role in cellular response. Guinea pigs were exposed to varying amounts of H_2SO_4 (50 to 300 $\mu g/m^3$ layered onto 10^8 ultrafine carbon core particles/cm^3) and to a constant concentration of acid (350 $\mu g/m^3$ layered onto 10^6, 10^7, or 10^8 particles/cm^3). Indicators of irritant potency in macrophages harvested from the lungs of guinea pigs were clearly increased with the increase of acid in particles. Thus, it is important to distinguish AUFPs from UFPs for epidemiologic studies.

2.1.2.2 Other effects of AUFPs

In addition to adverse health effects, AUFPs also affect the secondary organic aerosol (SOA) formation. Acid-catalyzed heterogeneous reactions, for instance, have been proposed as an important mechanism that might significantly enhance SOA production in the atmosphere (Zhang et al., 2007; Han et al., 2016). With the aid of acidic seed particles, the yield of SOA was increased up to several folds in chamber studies (Jang et al., 2002; Edney et al., 2005). Moreover, AUFPs play an important role in the new particle formation (NPF). Previous studies confirmed a positive relationship of sulfuric acid with particle grow rate and particle formation rate in a NPF event, implying that AUFPs might catalyze/trigger the particle formation and growth (Kulmala et al., 2000; Guo et al., 2012; Wang et al., 2014a). Sufficient concentrations of condensational vapors, such as sulfuric acid and possibly other organic compounds with a low saturation vapor pressure, strongly promote the nucleation and the growth of freshly formed particles to Aitken mode (Boy et al., 2005; Riipinen et al., 2007; Sipilä et al., 2010). This process not only happened in the remote environments (Kulmala et al., 2004a; Morawska et al., 2008; Holmes, 2007; Wang et al., 2012) but also in the urban environments (Fernández-Camacho et al., 2010; Wang et al., 2014a). Lastly, acidic particles were suggested to be hygroscopic according to the positive correlations of particle acidity with measured water content, and deliquescence relative humidity of particles with NH_4^+/SO_4^{2-} ratio (Hu et al., 2010; Xue et al., 2011). Since the impairment to visibility would be worse at a high humidity due to the enlarged light scattering cross-sectional areas of particles (Tsai, 2005), a high proportion of AUFPs would enhance the particle ability to scatter lights due to a large hygroscopicity, and thus impair the visibility (Malm and Day, 2001).

2.1.2.3 Formation of AUFPs

In general, AUFPs are both emitted directly from primary sources and formed through chemical reactions of primary pollutants in the atmosphere. Direct production/emission of AUFPs mostly occurs in the combustion process, especially when fuel with high sulfur content is used (Ushakov et al., 2013). However, secondary formation is usually the main source of AUFPs (Wang et al., 2012, 2014a). The formation mechanism of AUFPs was not comprehensively studied and/or discussed in previous studies due to lack of AUFPs data. Nevertheless, some previous studies provided some hints on how the AUFPs were formed through reactions. For instance, sulfuric acid and nitric acid are produced from the reactions of sulfur dioxide and nitrogen dioxide with hydroxyl radicals, respectively. Once formed, these liquid chemicals either condense on preexisting particles or coagulate with each other to form new particles. Previous study indicated that ultrafine particles generally contain sulfuric acid and/or nitric acid at the initial formation stage because nitric acid, ammonia and sulfuric acid vapors with the low vapor pressures could condense onto freshly nucleated particles as small as a few nanometers in diameter (Schlesinger and Cassee, 2003; Wang et al., 2020a). When sulfuric acid production is high and the existing particle number (PN) concentration is low, a large number of new nuclei mode sulfate particles can be formed, significantly contributing to the total particle number concentration (Narsto, 2003). In order to better understand the atmospheric AUFPs, *e.g.*, their formation mechanism and impacts on human health, SOA formation, NPF and visibility, it is essential to develop reliable techniques to measure them.

2.2 Previous techniques for measuring AUFPs

Due to the significant effects but insufficient understanding of AUFPs, some pilot studies tried to develop methods for quantifying the concentration of acidic particles. In the earliest study, Gerhard

and Johnstone (1955) successfully observed the reaction spots of acidic particles in the gelatinous films. However, due to the limit of microscope technique, it was impossible to individually survey particles with diameter less than 1.0 μm at that time. Lodge and Havlik (1960) used the changes of light transmission and resistance of thin metal films as the indicators of atmosphere pollution. The exposed films showed extensive surface mottling and pitting under the observation of an electron microscope. Hayashi et al. (1961) used metal-coated glass slides to detect acid aerosols which were nebulized to form holes as reaction spots on the metal film and compared the sizes of observed reaction spots to the diameters of aerosol droplets. Unfortunately, the smallest diameter of generated acidic droplets was several microns. Similarly, Horstman et al. (1967) used thin iron-coated detectors to collect and size acidic particles with diameter much larger than 0.1 μm. Reaction pits of acidic particles on the iron film were observed by an electron microscope. Moreover, Bigg et al. (1974) developed a method for spot reaction by applying a thin film of reagent on the surface. Sulphuric acid, sulphates, nitrates, halides, persulphates and urban aerosols were adopted as the samples to be collected on the thin film and were visualized by an electron microscope. Later, Mamane and De Pena (1978) modified and improved this method for measuring sub-micrometer size sulfate particles by coating a barium chloride film on the substrate based on the reaction of sulfate ion with barium chloride. Furthermore, Huang and Turpin (1996) noticed the ring formation of H_2SO_4 particles on carbon film substrates using the scanning electron microscopy (SEM). In the early 2000s, Cohen et al. (2004a) developed iron nanofilm detectors for the measurements of acidic particles in New York. The nanofilm detectors were examined with Scanning Probe Microscope (SPM). In principle, this method could identify and quantify the ambient AUFPs. However, no acidic particles were detected in their study due to the insufficient

sampling time. After that, Cohen et al. (2004b) conducted a longer period of sampling (1 week) and reported the concentrations of acidic particles. Most recently, Wang et al. (2012 and 2014b) developed two methods to quantify the number concentrations of AUFPs in the atmosphere with method validation. Wang et al. (2012) coated an iron nanofilm on the silicon detectors using the thermal vacuum evaporation and magnetron sputtering deposition methods. Standard sulfuric acid droplets and sulfuric acid-coated particles were generated and deposited on both detectors to cause reaction spots. Atomic force microscopy (AFM) was used to examine the reaction spot, and enumerate and size the acidic particles. Collection of particles in the atmosphere was achieved by using an electrostatic precipitator (ESP), thus forming the ESP+AFM method. The method was validated through a field measurement at a mountain site in Hong Kong with a commercial measurement system, *i.e.,* Scanning Mobility Particle Sizer (SMPS). The results obtained from the ESP+AFM method were comparable to those derived from the SMPS, suggesting the reliability of the method. However, the method is not suitable for the assessment of long-term measurement of AUFPs as the detector is easily saturated. Therefore, later, Wang et al. (2014b) developed a diffusion sampler (DS) for the long-term measurement (2-4 days) of AUFPs in the atmosphere with the same detectors of Wang et al. (2012). The detectors were deployed on rectangular channel inside the DS at three different locations to collect the UFPs. The particle deposition in a DS relied on the diffusive properties of UFPs, whereby the particles adhered when they hit a surface (Knutson, 1999). The exposed detectors were also scanned by an AFM to distinguish the AUFPs from the non-acidic UFPs and numerate them. Thus, the method was called DS+AFM. Prior to sampling, the collection efficiency of particles in the DS was calibrated. After calibration, the method and a SMPS were simultaneously used in a field measurement at an urban

site in Hong Kong for method validation. The good agreement of results between the DS+AFM method and the SMPS indicated the availability of the DS+AFM method.

Literature review indicates that only a few studies successfully acquired the concentrations of AUFPs in the atmosphere due to the immaturity of measurement technique. Moreover, although the above methods are available to identify and quantify AUFPs, they are offline and require enormous resources to support the microscopic technique. All the microscopic techniques are neither cheap, timesaving, small, nor easy to operate (Kessler et al., 2020; Li et al., 2016). Multiple scans of a sample are required to reduce the uncertainty. As a manual and offline technique, the resources consumption and cost of the microscopic technique will be extremely high if the sample size is huge. Hence, there is a need to refine/revise the above methods, which will not use the microscopic techniques to quantify acidic particles on the exposed detectors and can realize the semi-automatic measurement.

2.3 Possible techniques for online measurement of AUFPs

Although several instruments have been developed for online measurement of concentrations and size distributions of UFPs, no instruments are capable of online measurement of AUFPs at present. Instruments for online measurement of UFPs can be mainly divided into two categories, i.e., measurement of number concentration and measurement of mass concentration, using different mechanisms. For measuring number concentration, the most common technique is the optical particle counter, such as aerodynamic particle sizer (APS), laser aerosol spectrometer (LAS) and scanning mobility particle sizer (SMPS) (Wiedensohler et al., 1986; Wang and Flagan, 1990; Stolzenburg and McMurry, 1991; Kumar et al., 2010). Online particle measurements using the optical technique are based on the fact that when a particle passes through a beam of light, some of the light is scattered.

Particle number can be determined simply by counting the pulses of scattered light reaching the detector. Therefore, the technique can mainly obtain the information of particle number but not the property. As for measuring mass concentration, microbalance is the most commonly used technique for continuous particle weight monitoring (*e.g.*, tapered element oscillating microbalance (TEOM) and cascade impactor) (Wang et al., 2020b). Mass concentration is acquired based on the mass of deposited particles on the detector over time. Among all the microbalances, quartz crystal microbalance (QCM) is considered as an appropriate tool for the measurement of UFPs due to its portability and high sensitivity (Ngo et al., 2019). Moreover, previous studies proved the possibility of applying the QCM into the measurement of different air pollutants according to their properties (Reipa et al., 2010; Venkatasubramanian et al., 2012; Lv et al., 2017; Zhang et al., 2017).

2.3.1 QCM

The QCM is an extremely sensitive mass sensor with detection capacities ranging from micrograms to fractions of a nanogram as demonstrated in a number of gas and vapor systems (King, 1964; Ward and Buttry, 1990; McCallum, 1989). A very short response time of QCM make it suitable for real-time sensing applications (Tzou, 1999). The microbalance is designed around a piezoelectric wafer sliced from a single crystal of quartz. The electrical, mechanical, and chemical properties of quartz make it the most useful of the many possible piezoelectric materials. As a piezoelectric material, the quartz wafer deforms slightly in the presence of an electric field. The changes in resonant frequency can be used as a direct measurement of mass changes on the surface of the QCM according to the Sauerbrey's equation. Hence, if the QCM is used for the collection of particulate matters (PM), the mass change can be readily detected (Subramanian et al., 2016). For example, the most widely used QCM

instrument for ambient particle measurement is the cascade impactor (Savolainen and Pietroiusti, 2017). It collects size-fractionated particles by inertial impaction with the particle size ranged from a few nanometers to tens of micrometer. Cascade impactor with real-time measurement of particles is achieved by the QCMs. QCMs are flush mounted to the impaction plates. After particles impact on the QCMs, the resonance frequencies of the QCMs decrease proportionally to the mass added. The mass of particles can be calculated based on the frequency shift using the Sauerbrey's equation, i.e., $\Delta f = -k \cdot \Delta m$, where Δf is the measured frequency shift, k is the sensitivity factor of QCM system, and Δm is the mass change. Another system using the QCM to measure particles is the virtual impactor (Liang et al., 2010; Zhao et al., 2016). Compared to the cascade impactor, the virtual impactor is miniature. Its advantage is that the cascade impactors are often too complicated and bulky for in-situ applications. The virtual impactor separates different sizes of particles by their inertial forces and then uses the QCM to quantify the mass of particles. For QCM measurements, particle bounce due to the deficient coupling of collected particles on the QCM surface (*i.e.*, failure of deposited particles to oscillate with the crystal) is a source of error (Sauerbrey, 1959; Marple et al., 2001). An accurate impactor measurement requires particle bounce to be completely eliminated and the collected particles to be rigidly attached (*i.e.*, coupled) to the surface of the crystal.

2.3.2 Modification of QCM detector for measuring AUFPs by coating films

By functionalizing the QCM detector surface with a proper layer, many sensors have been developed. The principle is to use/apply the interactions between the surface of a quartz covered with thin film layers and the analytes. The aim is to get quantitative information on the analyte (Ward and Buttry, 1990). The mass change on the thin film layer leads to a change in the resonant frequency of the quartz.

For example, by coating the urea formaldehyde resin/nano silica composite films on the QCM detector, Lv et al. (2017) developed a highly sensitive and linear humidity sensor. Under the optimum conditions, the humidity sensor exhibited a good linearity (R^2=0.9998), short response time (12s), good stability and reproducibility. Moreover, graphene oxide/chitosan (GO/CS) nanocomposite was employed as the sensing film of the QCM sensor to detect amine vapors (Zhang et al., 2017). In addition to gaseous substances, film coating on the QCM detector was also applied in the measurement of particular matters (Ngo et al., 2019). Multiple materials were adopted as films to increase the adhesion of particles with the surface and thus reduce the dislodging of particles on the QCM detector, such as grease (Zampetti et al., 2017), photoresist (Zhao et al., 2016) and hydrogel (Liang et a., 2010). Jang et al. (2019) integrated a thin film of carbon nanotubes (CNTs) on a QCM for an accurate mass sensing of in-liquid particles. The CNT layer provided a controllable nm-resolution roughness on the surface, and such roughness affected the nucleation behavior of ionic particles and attachment parameters of colloids, ultimately improving the particle adhesion on the QCM detector. To sum up, QCM is capable of measuring different substances using an appropriate film coating. Hence, there is a possibility to modify the original QCM detector for online measurement of AUFPs by coating the previously developed metallic nanofilm.

Here is the assumption. The QCM detector is coated with the metal nanofilm (Cohen et al., 2004a; Wang et al., 2012). The coated detector is then used for the collection of ambient UFPs. The total mass of all particles collected onto the detector is obtained by the QCM (as W_{total}). The weighed detector is stored in a clean environment (*i.e.*, a desiccator filled with nitrogen gas) for a certain period of time to ensure that collected AUFPs have fully reacted with the metal nanofilm on the QCM surface. Then a

suitable method is used to remove those non-acidic particles from the surface of the detector which do not react with the metal nanofilm. After that, the weight of particles remaining on the QCM surface is measured again, which is the mass of collected AUFPs (as W_{acid}). The mass of non-acidic ultrafine particles is thus ($W_{total} - W_{acid}$). In principle, this approach is able to quantify acidic particles based on the frequency change of QCM if a differential particle removal method exists.

2.3.3 Differential particle removal

To measure AUFPs using the QCM system, a feasible approach is to remove the non-acidic particles and retain the acidic particles on the surface of QCM detector on the basis of the principle that the attractive forces between acidic particles and metal nanofilm are different from those between non-acidic particles and metal nanofilm. To our best knowledge, no method was available to selectively remove the particles on the surface according to the properties of particles previously.

Removal of nanoparticles from the surface of a substrate is an imperative but challenging issue in micrometer-scale manufacturing and research (Salih et al., 2019; Kohli, 2019). The main components of the adhesion force are the Van Der Waals' force, the electrical double layer force, the electrostatic image force and the capillary force. In particular, Van Der Waals' force is the dominant force. Removal of nanoparticles is especially challenging since, as the particle size decreases, the average adhesion stress between the particle and substrate increases by a fractional power law. In general, the traditional particle removal methods can be divided into two types, *i.e.*, dry-cleaning and wet-cleaning methods. On one hand, dry-cleaning method is proposed since wet-cleaning methods may have several drawbacks, such as recontamination of surfaces by dissolved chemicals during rinsing and dry process, water marks, haze, crystal originated particles (COP), etc (Otani et al., 1995). The most common dry-

cleaning method is the blown-off method by air or nitrogen (N_2). Xu et al. (2009) used a jet spray nozzle to generate N_2 gas jet to remove 60% - 80% of SiO_2 particles from the surface. However, it has been reported that the traditional blown-off cleaning is more effective to remove particles above 10 μm in size (Donovan, 1990). Therefore, other novel types of blown-off method were developed for effectively removing nanoparticles from the substrate's surface. A cryogenic particle beam is a promising means of removing nanosized contaminant particles. For instance, Kim et al. (2012) generated bullet particles using CO_2 to remove the 10 nm contaminant particles from the Si wafers. Similarly, argon was used to generate cryogenic particle beam by a contoured laval nozzle to remove the 20 nm particles on the surface (Lee et al., 2009). Nevertheless, both methods required an extreme environment to conduct the treatment (greatly low temperature: -170 ℃ and ultrahigh vacuum: 10 Torr).

On the other hand, due to the high effectiveness, wet-cleaning methods with ultrapure water and other cleaning liquids are commonly used to remove nanoparticles from various surfaces. Brems et al. (2013) reviewed the removal techniques of acoustics and pointed out the high effectiveness of the technique in removing nanoparticles. In general, acoustics cleaning encompasses two cleaning methods: ultra-sonics (less than 100 kHz) and mega-sonics (0.8 to 1.2 MHz) (Busnaina et al., 1995; Wang et al., 2019). In ultra-sonics cleaning, a part is immersed in a suitable liquid medium and sonicated or agitated at a high frequency (18-120 kHz or 20-80 kHz). The ultra-sonic cleaning method is thorough because the bubbles can penetrate whenever the liquid does. For instance, Bakhtari et al. (2006) removed 63 nm polystyrene latex (PSL) particles from bare silicon wafers and wafers with 4 nm Si-cap film by acoustic streaming and the removal efficiency on both surfaces was ~99% in less than 10 min of processing

time. Mega-sonics cleaning is another method which basically consists of the same steps as ultra-sonic cleaning: immersion, agitation or sonication, rising and drying. The cleaning action in mega-sonic cleaning comes from high pressure waves pushing and tugging at contamination lodged on a part's surface. However, damage of surface/materials may appear as the frequency increases, especially in the range of mega-sonic (Brems et al., 2013).

Although no methods were reported to differentially remove nanoparticles on the surface, it is worth noting that the effectiveness of traditional particle removal methods can be controlled. For example, the effect of blowing/air jet method is related to the pressure of air supply and time interval (Xu et al., 2009). As for the wet-cleaning method, the effect is related to the frequency used and processing time. Therefore, a suitable method with an appropriate effect should be able to realize differential removal of non-acidic particles on the surface on the basis of different attractive forces between acidic particles and non-acidic particle with the metal nanofilm.

All in all, although a lot of efforts have been made on the study of AUFPs, research gaps still exist. Bearing in mind the significant roles of AUFPs with limited measurement data and the complicated methods for measuring AUFPs previously, studies on AUFPs measurements and method development are worth conducting. In this study, to improve the understanding of AUFPs pollution, extensive measurements were carried out in different land-use areas and cities in China using the previous DS+AFM method (Chapter 4). After the sampling campaigns, deficiencies of the previous method were highlighted and/or emphasized (*i.e.*, usage of AFM). To desert the use of AFM, a method was firstly developed for the differential removal of non-acidic particles and retainment of acidic particles on the surface of metal nanofilm (Chapter 5). With the help of the differential particle removal method,

a novel system was developed for semi-automatic measurement of AUFPs in the atmosphere by integrating the previous DS with QCM, forming the DS+QCM system (Chapter 6).

Chapter 3 Methodology

3.1 Preparation of metal nanofilm detectors

Metal-silicon detectors

A silicon wafer was chosen as the substrate, and a magnetron sputtering system (MSS) was adopted to coat a nanofilm of metal on the surface of the silicon wafer to form the metal-silicon detector. Before sputtering, the silicon wafer was firstly cut into silicon chips with the size of 5cm × 5cm using laser. Each chip was ultrasonically cleaned with sulfuric acid solvent (1 mol/L) and ethanol, successively, to remove impurities on its surface. In the MSS process, the base pressure of the chamber was lower than 4×10^{-5} Torr before magnetron sputtering deposition, and the total pressure for sputtering was maintained at 1.3×10^{-2} Torr. In an ultrahigh vacuum environment, the metal target was activated at a high voltage of ~ 400 volts to generate plasma, and then metallic atoms were sputtered onto the surface of the chip. To obtain a metal film thickness of ~25 nm, a sputtering time of 2.5 min was used. After sputtering, the metal-silicon detectors were stored in a nitrogen atmosphere to avoid oxidation of the nanofilm metal.

Metal-QCM detectors

Apart from metal-silicon detector, a nanofilm of metal was sputtered on the QCM detector to generate the new-generation detector, namely metal-QCM detector. MSS was still used to coat the nanofilm of metal on the QCM detector. Similarly, each pure QCM detector was ultrasonically cleaned in sulfuric acid solvent (2 mol/L), ethanol and purified water, successively, to remove all the small particles and impurities on its surface. After cleaning, the detectors were taken for sputtering. The parameters used in MSS were the same as those to generate metal-silicon detectors (*i.e.*, base pressure: 4×10^{-5} Torr;

total pressure: 1.3×10^{-2} Torr; voltage: ~400 volts and duration: 2.5 min). It was clearly seen that the nanofilm of metal was successfully coated on the surface, compared to the pure detectors (Fig. 3-1). In the end, the metal-QCM detectors were also stored in a nitrogen atmosphere to avoid oxidation of the nanofilm metal.

The oxidation of metal film is a major concern for the application of the metal detectors in field measurements. On the one hand, previous studies have investigated the oxidation of thin iron film (Kumari and Vaidyan, 1988; Martin et al., 1994; Marczyńska et al., 2015). It was proved that the initial iron film was oxidized instantaneously (within 100 second) after the generation of detector, whereby 2.5 nm of metal was transformed into oxides. Nevertheless, the iron film remained stable in the ambient environment for more than 10 days after the initial oxidation. Moreover, the metal-QCM detector in the study was ever put in ambient environment to conduct blank experiment. Results showed that the frequency of the detector did not change after two-day exposure. On the other hand, Wang et al., (2012) already examined the stability of nano-metal film detector by putting the detectors in extreme weather conditions (i.e., 85% RH/35◦C and 90% RH/20◦C) for 3 months. Results showed that the surface structure of the detectors did not change after 3-month exposure in both conditions. These two weather conditions are often observed in subtropical Hong Kong. Therefore, the oxidation of metal film will not be a problem for the application of metal detector in the study.

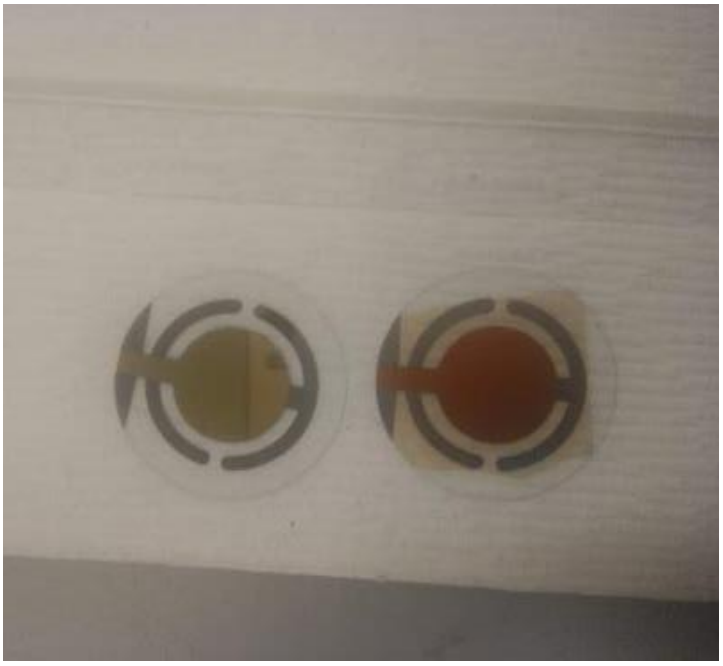

Fig.3-1 Original QCM detector (left) and coated QCM detector (right).

3.2 Generation of standard particles

3.2.1 Non-acidic particles

Non-acidic particles were produced by nebulizing the solution of sodium chloride (NaCl) or polystyrene latex (PSL) by dispersing NaCl or PSL microspheres (*i.e.*, 32, 52 and 102 nm) in Milli-Q water, respectively, to minimize the concentrations of impurities that may be present in tap water. To collect monodispersed particles, the generated particles were charge-neutralized and size-selected by the differential mobility analyzer (DMA) and deposited onto the metal-coated detectors using an electrostatic precipitator (ESP). To generate the NaCl aerosol standards, an aerosol generator (Model 7.811, GRIMM, Germany) was used to produce submicron-sized NaCl particles. The particle production rate was adjusted by the flows of the atomizer and the dryer (dilution air), and the mass concentrations of the NaCl solution. To generate the PSL particle standards, a few drops of PSL

standard were added into Milli-Q water to dilute the suspension. In my experiments, both NaCl and PSL particles, generated from the aerosol generator, were diluted in a 1.5-liter bottle and dried by a silica gel dryer (40 cm long × 5 cm diameter), and then were introduced into the measurement system (*e.g.*, scanning mobility particle sizer (SMPS)) or the collection system (*e.g.*, ESP). The generation and collection system of standard non-acidic particles is shown in Fig. 3-2.

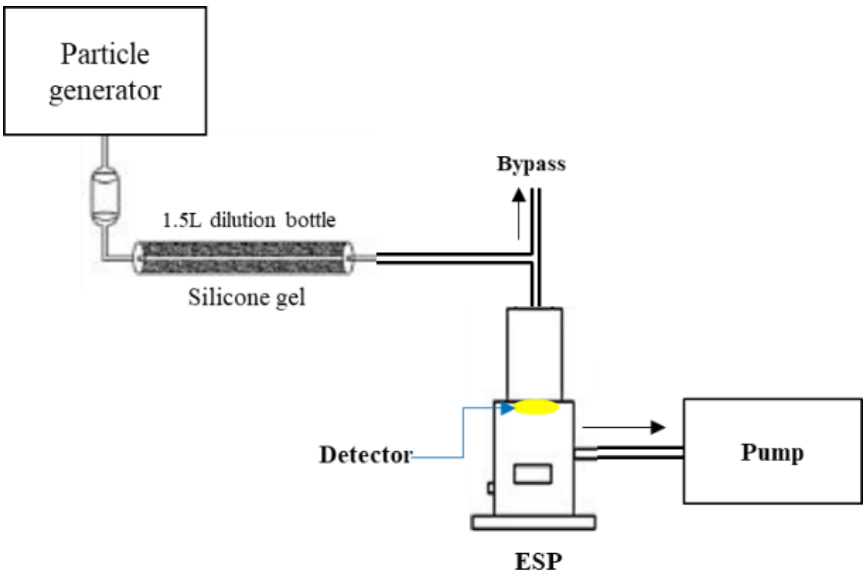

Fig. 3-2 Generation and collection system of standard non-acidic particles.

3.2.2 Acidic particles

To generate acidic particles, a standard acidic particle generation (SAPG) system was established which included a nano-carbon particles generation system, a H_2SO_4 aerosol generation system and a sample collection system. In the nano-carbon particles generation system, a high temperature of 700°C was remained in a quartz tube furnace. A large quantity of glucose aerosols generated by an ultrasonic atomizer was introduced into a quartz tube in the furnace. At high temperature, without sufficient oxygen supply for complete combustion, the glucose aerosol underwent thermal decomposition, producing ultrafine carbon particles. The carbon particles were then diluted and cooled down

immediately with two conical flasks and passed over the headspace of highly pure H_2SO_4 solution heated on a wire coil heater. A filter was placed before the carbon particles passed through the acidic vapor to remove the large particles. The mixture of nanocarbon and sulfuric acid vapor then passed through a thermos-stated water-cooled condenser. Sulfuric acid was coated onto the carbon particles during the condensation process, forming acidic ultrafine particles (AUFPs). Ultimately, the AUFPs were collected on the detectors placing in the ESP (Fig. 3-3).

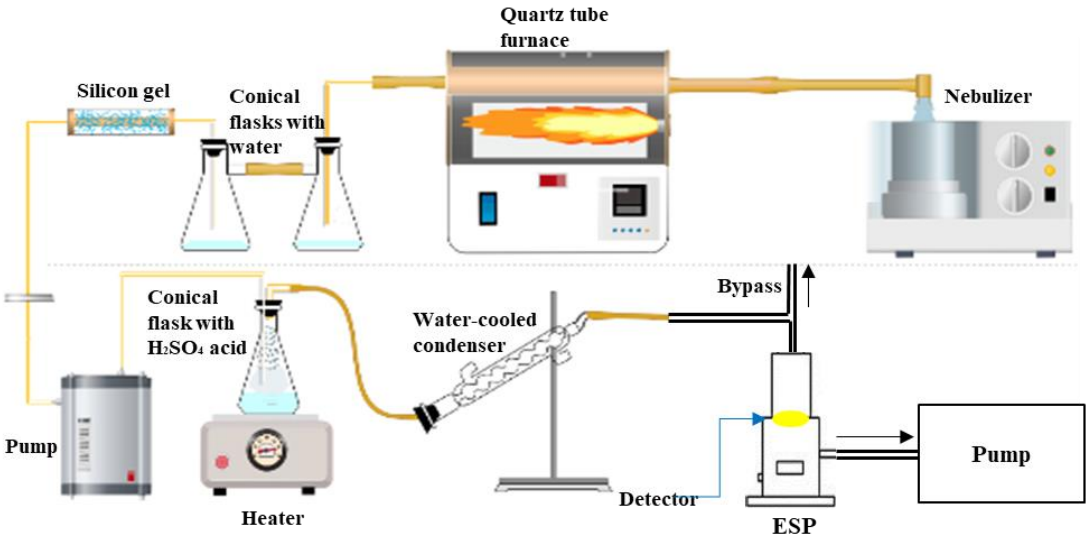

Fig.3-3 The schematic of generation and collection system of standard acidic particles.

3.3 Verification of the nanofilm of metal coated

Standard acidic and non-acidic particles were generated and collected on the nanofilm of metal for verification. Atomic force microscope (AFM) was used to observe the morphology of particles collected on the metal film. The AFM images of standard acidic particles (both 2D and 3D) are shown in Fig. 3-4. Clear reaction spots were found in the images. The reaction spots were circular and had one large bump in the center. The same reaction spot was also observed and reported in the previous study (Wang et al., 2012), indicating the availability of the nanofilm of metal detector in the study.

That is, under AFM scanning, the acidic particles deposited on the nanofilm of metal would have clearly recognizable and unique reaction spots that formed a central elevation with a surrounding yellow halo. Noteworthily, although the standard acidic particles are mainly generated from sulfuric acid, the detector in the study did not have selectivity to SO_2-induced particles. Acidic SOA collected on the detector will also react with the metal film and contribute into the concentration of AUFPs and proportions of AUFPs in UFPs.

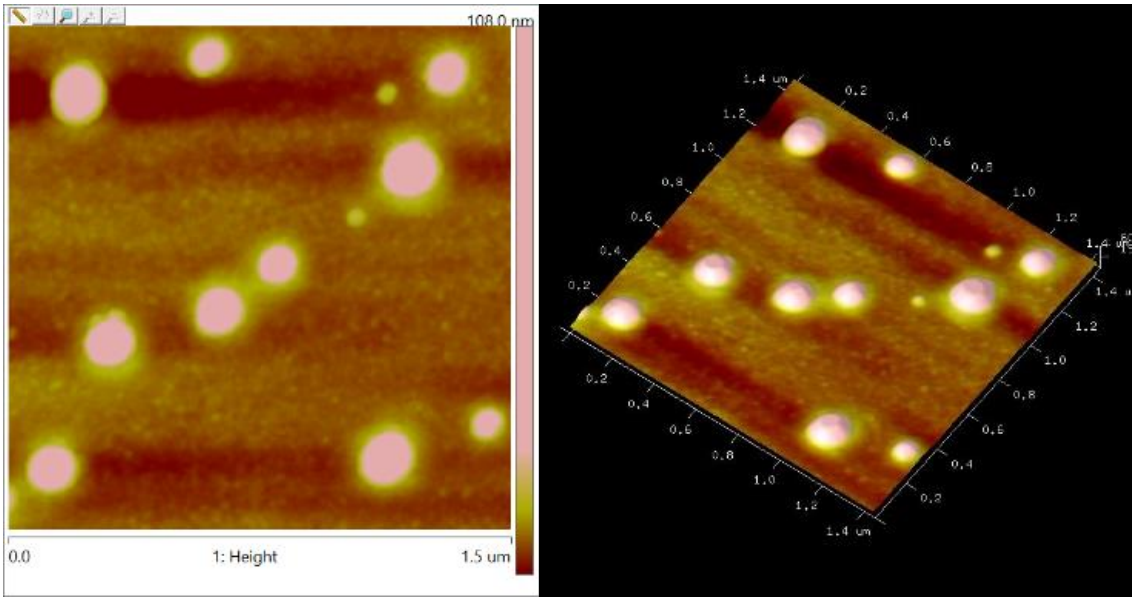

Fig. 3-4 AFM images (2D and 3D) for standard acidic particles

In comparison, standard non-acidic particles (NaCl particles) were also generated and collected on the metal film. The detectors containing standard non-acidic particles were also scanned by AFM. The AFM images are shown in Fig. 3-5. It can be seen that no reaction spots were observed around the non-acidic particles, proving the good performance of nanofilm of metal in distinguishing acidic particles and non-acidic particles.

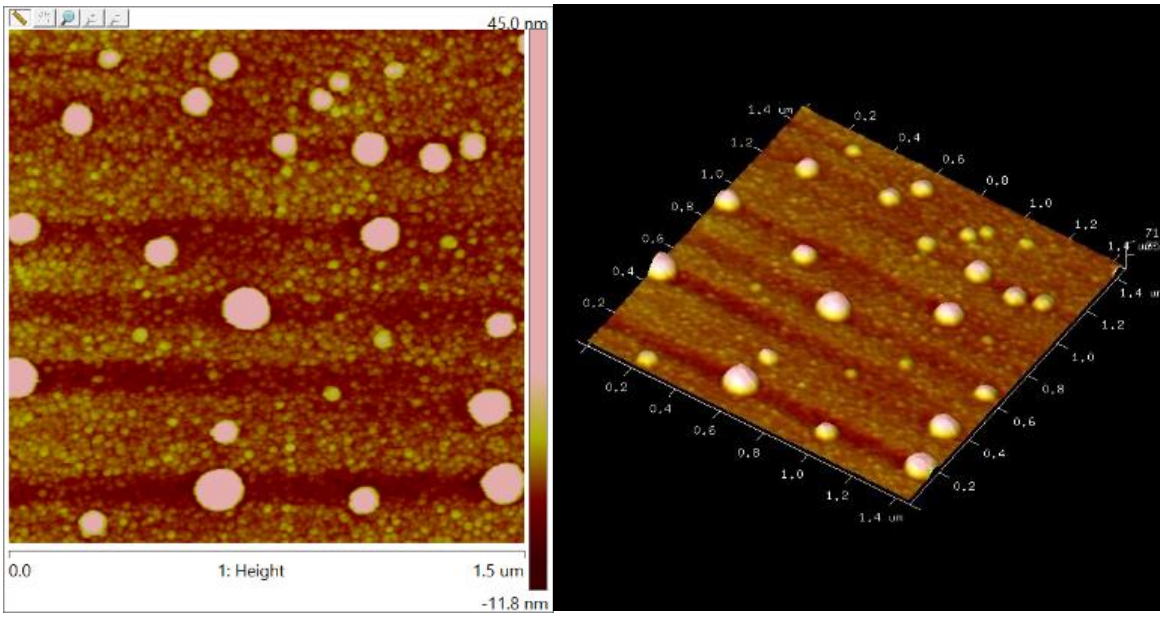

Fig. 3-5 AFM images (2D and 3D) for standard non-acidic particles

3.4 DS+AFM system

3.4.1 Structure of diffusion sampler (DS)

The DS was originally developed in the previous study to measure AUFPs in the atmosphere (Wang et al., 2014b). The DS was made of stainless steel with a flat and rectangular channel with 1.0 mm height, 50 mm width, and 500 mm length. The size of the DS inlet was 1×50 mm (height × width). The DS had nine circular sampling spots to place the metal-silicon detectors (diameter × height: 7×0.4 mm) comprising three groups (Wang et al., 2014b; Fig. 3-6). The locations of the three sampling spots were at 7.0, 201.5, and 472.5 mm (midpoint of the circular recess) from the inlet along the length of the channel, respectively. The L1~L2, L3~L4, and L5~L6 were the distances of left and right sides of metal-silicon detectors from the inlet at the three locations, respectively. Air was drawn through the DS by a low-flow pump (0.05 L/min). Air leakage was avoided by sealing the channel with a layer of rubber. The detectors collected by the DS were topographically analyzed by the AFM (NanoScope, Multi-mode 8, Veeco Instrument Inc., USA) to identify and enumerate the acidic and non-acidic

particles and obtain the sizes of particles. In a field measurement, the sampling durations were 2-4 days, depending on the concentrations of atmospheric particles.

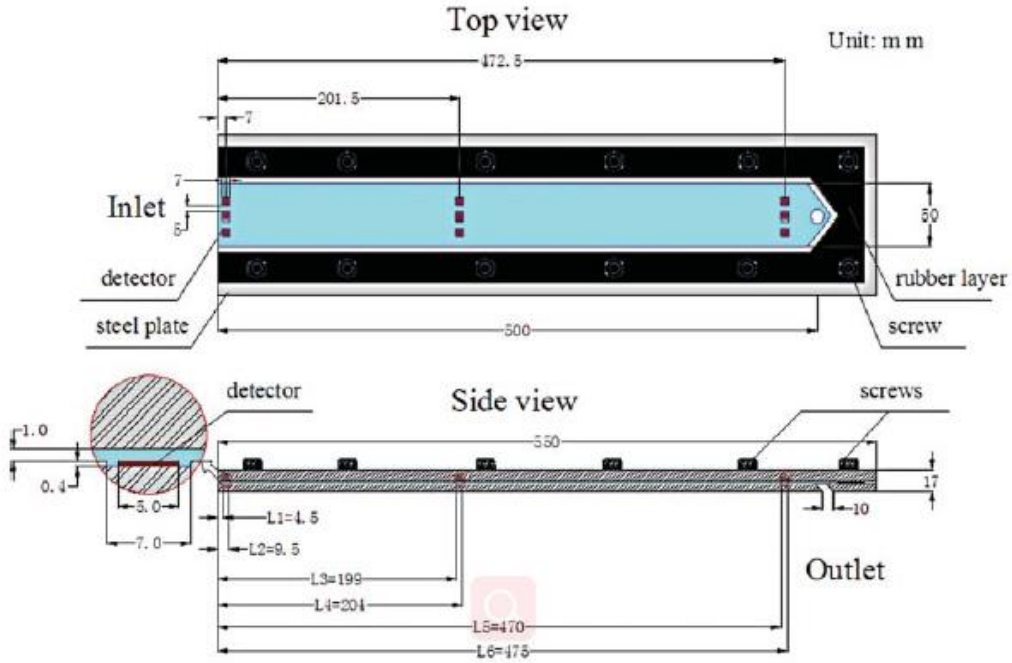

Fig. 3-6 Schematic diagram of the DS (Wang et al., 2014b).

3.4.2 Collection efficiency of DS

The collection efficiencies of the DS at each spot were calibrated in the previous study (Eqs. 3-1, 3-2, 3-3, 3-4 and 3-5; Wang et al., 2014b).

$$\Delta\eta_a = 3.20 \times \mu_{L2}\text{^}0.576 - \mu_{L1}\text{^}0.576 \quad \text{Eq. 3-1}$$

$$\Delta\eta_b = 1.844 \times [\exp(-8.04\mu_{L3}) - \exp(-8.04 \times \mu_{L4})] \quad \text{Eq. 3-2}$$

$$\Delta\eta_c = 1.957 \times [\exp(-7.43\mu_{L5}) - \exp(-7.43 \times \mu_{L6})] \quad \text{Eq. 3-3}$$

$$\mu_{Li} = (D \times L_i \times W)/(Q \times h) \quad \text{Eq. 3-4}$$

$$D = (k \times T \times Cc \times 10\text{^}10)/(3\pi \times \gamma \times dp) \quad \text{Eq. 3-5}$$

where $\Delta\eta_a$, $\Delta\eta_b$, and $\Delta\eta_c$ are the collection efficiencies at the sampling spots A, B and C, respectively, μ is deposition parameter, L is channel length (cm), W is channel width (cm), Q is flow rate (cm^3/sec),

and h is channel height (cm); D is the diffusion coefficient of the particle (cm^2/sec), k is Boltzmann's constant (1.38×10^{23}), T is the absolute temperature, C_c is the slip correction factor, γ is the air viscosity (1.79×10^{-5} Pa·sec), and d_p is the particle diameter (μm). The collection efficiency of particles with different sizes at each spot at the flow rate of 0.05 L/min are calculated and plotted (Fig. 3-7).

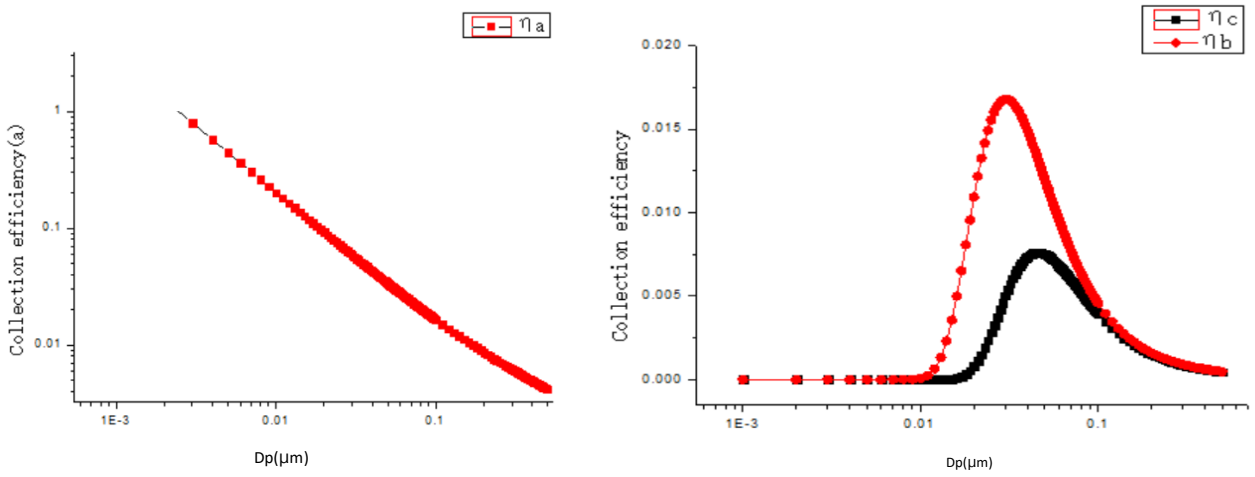

Fig. 3-7 The stepwise particle collection efficiency of the three sampling spots.

Thus, the particle concentrations in the atmosphere, derived from the number of deposited particles on the detectors scanned by the AFM, are given as follows (Eq. 3-6).

$$\text{Concentration}=(2.5\times10^7)/A\times\Sigma\{N_{dpi}/(\eta_i\times Q\times t)\} \quad \text{Eq. 3-6}$$

where 2.5×10^7 is the area of the metal-silicon detector (5mm × 5mm = 2.5×10^7 μm^2); A is the scanning area on the detector by AFM (μm^2); N_{dpi} is the counted number of particles in the i^{th} size bin; η_i is the deposition efficiency of the particles in the same size bin; and t is the sampling time (sec.). By summing up the calculated number concentration in each size bin, the average number concentrations of particles were obtained.

3.5 QCM+DS system

3.5.1 Fabrication of quartz crystal microbalance (QCM)+DS system

The developed QCM+DS system was fabricated by integrating the previous DS with three QCMs. Introduction of the previous DS was described above and in previous study (Wang et al., 2014b). To integrate the QCMs with the DS, modifications were made, including the inlet and the sampling spots. In the QCM+DS system, a differential mobility analyzer (DMA) was deployed in front of the inlet of the DS for the size selection of ultrafine particles (UFPs). The inlet of previous DS was a flat and rectangular channel which was unable to connect to the DMA. Thus, the inlet was modified to be a hollow cube with an inlet tube (Fig. 3-8). The inlet unit was fastened with the DS screws. Air tightness was guaranteed by the rubber between the inlet unit and the DS. In this way, the QCM+DS system was able to connect with the DMA for collection of size-resolved particles.

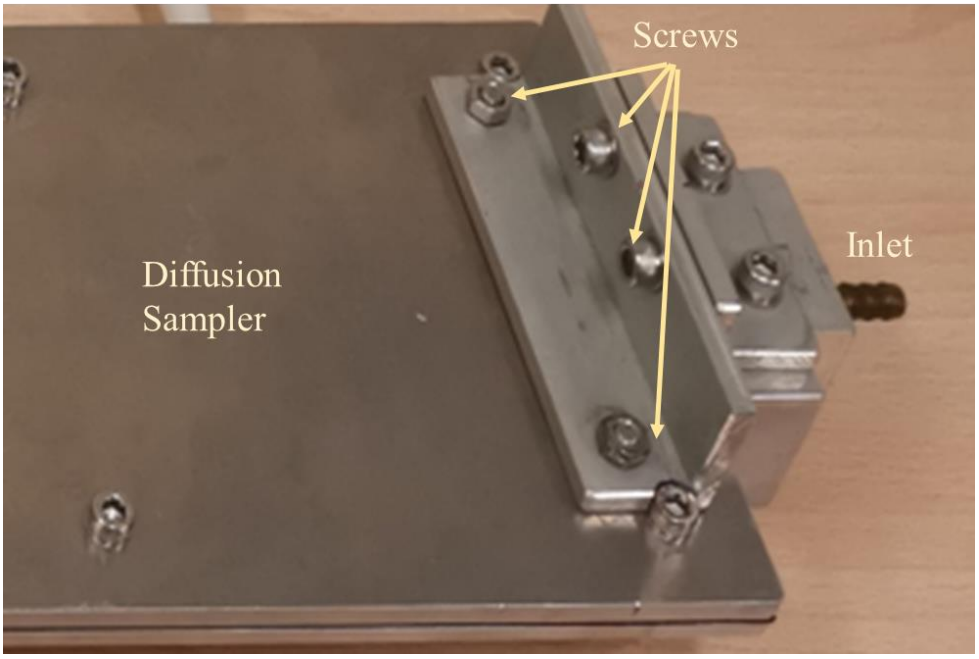

Fig. 3-8 Inlet of the QCM+DS system.

To integrate the previous DS with the QCM system, QCM holders were inserted into the DS sampler from the bottom panel of the DS and hence modification of sampling spots was conducted. The structure of new sampling spot is shown in Fig. 3-9. To firmly place the metal-QCM detector into the

sampling spot, the drilled spot was fabricated to be slightly larger than the metal-QCM detector. Specifically, diameter of the sampling spot was 2.65 cm with the depth of 0.4 mm, which was almost the same size as the metal-QCM detector. Two contact springs of the QCM holder were traversed to the surface of the sampling spot from the bottom panel of the DS and evenly distributed in the sampling spot as so to becomingly contact with the electrode of the metal-QCM detector. Indeed, the contact springs of the QCM holder were two gold electrons with resilience. Therefore, a flexible space for placing the metal-QCM detector was provided in height. To fix the detector on the sampling spot properly and tightly, two black rubbers protruding 1 mm in height were fixed on the upper panel of the DS and set at the exact position of the sampling spot (Fig. 3-9). The detector was pressed by the stretchy rubber and fixed tightly when the DS was installed by combining the upper and bottom panels.

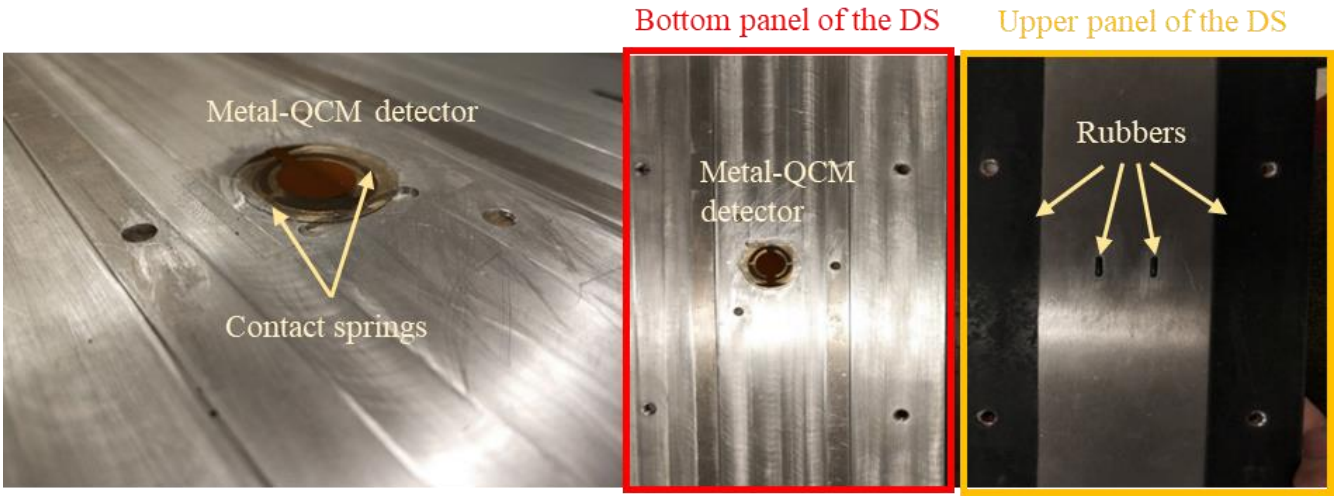

Fig. 3-9 Sampling spot of the QCM+DS system placing a metal-QCM detector.

The schematic diagram of the QCM+DS system is shown in Fig. 3-10. Specifically, 1 is the inlet unit (Fig. 3-8 for detail). 2 is the rubber used to seal the sampler. 3 is the metal-QCM detector which is put inside the system. 4 is the channel for collecting air sampler. 5 is the outlet of the sampler. 6 is the inlet tube for connecting with other parts outside. 7 is the upper panel of the diffusion sampler. 8 is the

installation groove which can suitably place the detector. 9 are the two QCM pins which enable the connection between the detector and digital controller. 10 is the QCM digital controller. A is the sampling spot inside the QCM+DS system. Sectional view of A is also displayed in Fig. 3-10. In particular, the locations of the three sampling spots (*i.e.*, spot A, spot B and spot C) were at 85.0, 201.5, and 472.5 mm (midpoint of the rectangular recess) from the inlet along the length of the channel, respectively. The L1, L2, L3, L4, L5 and L6 were the distances of left and right sides of metal-QCM detectors from the inlet at the three locations, respectively. During the sampling, the air containing particles was first drawn into the QCM+DS system through the inlet. The particles were diffusely deposited on the metal-QCM detectors placed at sampling spots A, B and C. Simultaneously, the QCM system obtained the frequency changes caused by the deposition of particles. Finally, the exhaust air with excess particles was discharged through the outlet.

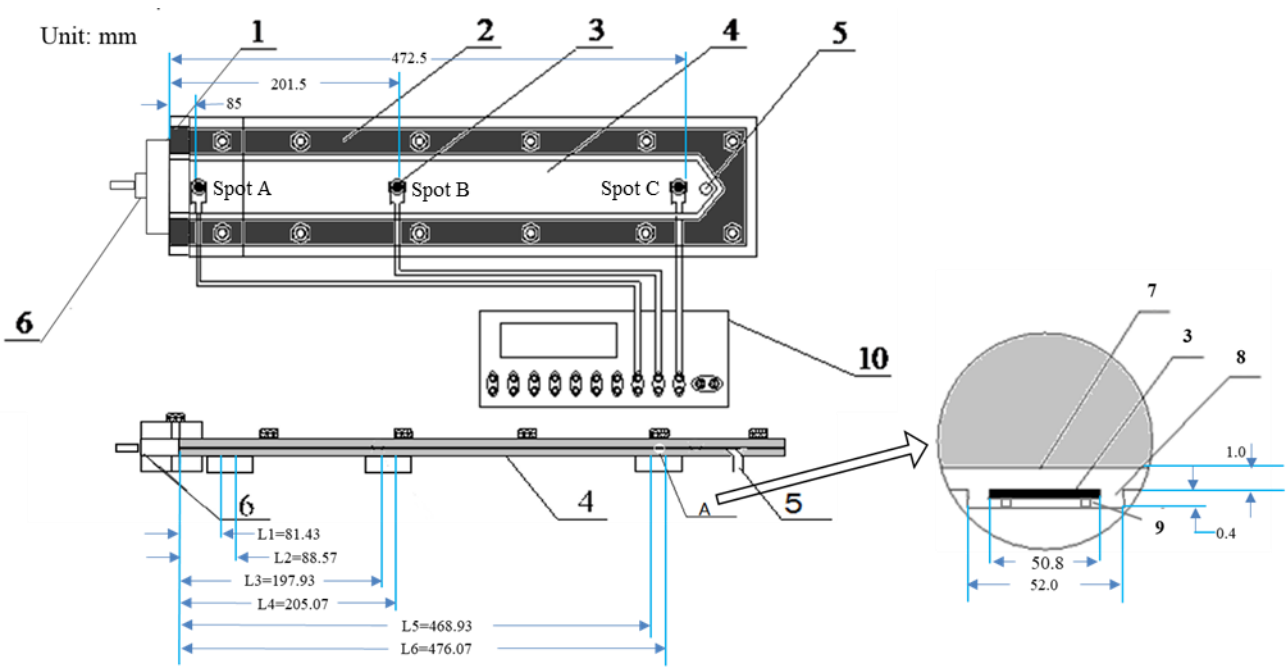

Fig. 3-10 Schematic diagram of the QCM+DS system.

3.5.2 Calibration

3.5.2.1 Sensitivity factor of QCM detector

A quartz crystal microbalance (QCM) measures a mass variation per unit area by detecting the change in frequency of a detector. The resonance is disturbed by the addition or removal of a slight mass. High-precision (0.01 Hz) and high-resolution frequency (1 second) measurements are readily made. As a gravimetric instrument, the QCM measures mass ranging from micrograms to fractions of a nanogram. Its detection limits correspond to sub-monolayers of atoms. In the study, the QCM200 (Stanford Research Systems) were adopted. The changes in resonant frequency are used as a direct measurement of mass changes on the surface of the QCM detector according to the Sauerbrey's equation (Eq. 3-7) below,

$$\Delta f = -K \cdot \Delta m \qquad \text{Eq. 3-7}$$

where Δf is the measured frequency change in Hz, K is the sensitivity factor for the detector in $Hz \cdot cm^2/\mu g$, and Δm is the change in mass per unit area in $\mu g/cm^2$. Hence, if the QCM is used for the collection of particulate matters (PM), the mass change can be readily detected. In this study, three QCM200 systems were adopted and integrated with the previous DS to develop the QCM+DS system. The purpose of using three QCM systems was to understand the collection efficiency at different distances from the inlet. The QCM200 system includes a controller, crystal oscillator electronics, a crystal holder and detectors.

The Sauerbrey's equation relies on a linear sensitivity factor, K, which is a fundamental property of the QCM. Sauerbrey's equation is only strictly applicable to uniform, rigid, and thin-film deposits (Buttry, 1991). As the QCM detector was modified and different sizes of particles would be measured in this study, calibration of the sensitivity factor of the QCM after modification was needed. In the

calibration process, the particle mass concentration obtained from the QCM system was compared with the particle number concentration derived from the SMPS. With the density and size of a particle, the number concentration derived from SMPS was converted to mass concentration (Sarangi et al., 2016; Franken et al., 2019). The details of conversion are shown in Eq. 3-8 and Eq. 3-9.

$$\Delta m = C_{num} \cdot Q \cdot T \cdot (\frac{4}{3}\pi r^3 \cdot \rho) \quad \text{Eq. 3-8}$$

$$K = \frac{\Delta f \cdot A}{C_{num} \cdot Q \cdot T \cdot (\frac{4}{3}\pi r^3 \cdot \rho)} \quad \text{Eq. 3-9}$$

where C_{num} is the number concentration of particles derived from CPC (count/cm^3), Q is the flow rate (cm^3/min), T is the sampling time (min), ρ and r are the density (g/cm^3) and radium (cm) of particles, respectively, and A is the area of the metal-QCM detector (cm^2). The total mass change was calculated based on the number concentration of particles derived from SMPS. By combining Eq. 3-7 and Eq. 3-8, K value was calibrated and shown in Eq.3-9. Both standard acidic and non-acidic particles were used to calibrate the sensitivity factor to exclude the influence of reactions between the acidic particles and the nanofilm of metal. In my system, ESP was used to collect the particles and the collection efficiency of ESP was assumed to be 100% when the particle size smaller than 200 nm according to the previous research (Wang et al., 2012).

A calibration system was set up using standard non-acidic particles (Fig. 3-11). The system comprised a particle generation unit, a particle collection unit and a condensation particle counter (CPC; Model 5.400, Grimm, Germany). In the particle generation unit, a particle generator (Model 7.811, Grimm, Germany) was used to generate standard non-acidic particles of PSL (Thermo Scientific, USA) and NaCl. After generation, particles passed through a dilution bottle and a silicone gel dryer to buffer and remove water vapor, respectively. A differential mobility analyzer (DMA) was used to select

monodisperse particles for follow-up collection. After size selection, particles were collected on a metal-QCM detector mounted in the ESP at a flow rate of 0.3 L/min. Frequency change of the metal-QCM detector was obtained through an offline collection of particles in a certain sampling period, which was then put back to the QCM system. A CPC measured particle number concentration simultaneously during the calibration process at the same flow rate as ESP (*i.e.*, 0.3 L/min). As for the calibration system using standard acidic particles, the particle collection unit and the CPC were the same, while the particle generation unit was altered to the SAPG system (Fig. 3-3).

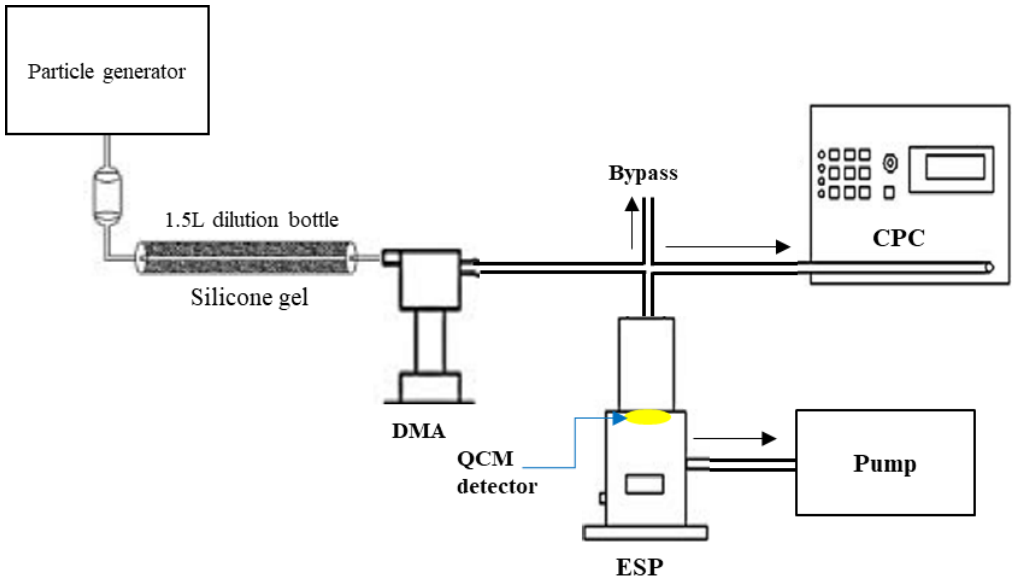

Fig. 3-11 The schematic of calibration system of non-acidic particles.

3.5.2.2 Mixing and airtightness of the chamber

The collection efficiency of the QCM+DS system was calibrated in a chamber. The chamber size was 70 (H)×60 (W)×90 (L) cm. Prior to calibration, an experiment was conducted to examine the mixing of the chamber. Firstly, particle generator generated a certain number concentration of NaCl particles. After passing through the dilution bottle and silicone gel dryer, it was guided directly into the chamber and mixed uniformly with the aid of a fan inside the chamber. SMPS was used to detect the number

concentration of particles in the chamber. The concentration was considered as stable if the data was stable for about 30 min. The bypass hole was used to balance the pressure in the chamber.

The results are shown in Fig. 3-12. Firstly, particle-free air was injected into the chamber. It can be seen that particle number concentration in the chamber gradually decreased from around 2500 /cm^3 (pre-existing particles in the chamber) to less than 100 /cm^3. Afterwards, sodium chloride particles were generated and guided into the chamber. The number concentration of particles sharply increased to around 150,000 /cm^3 in 30 min. and then remained relatively stable for more than one hour. Thus, it was concluded that the mixing of the chamber was satisfactory and the chamber was able to achieve a relatively stable number concentration of particles for calibration purpose.

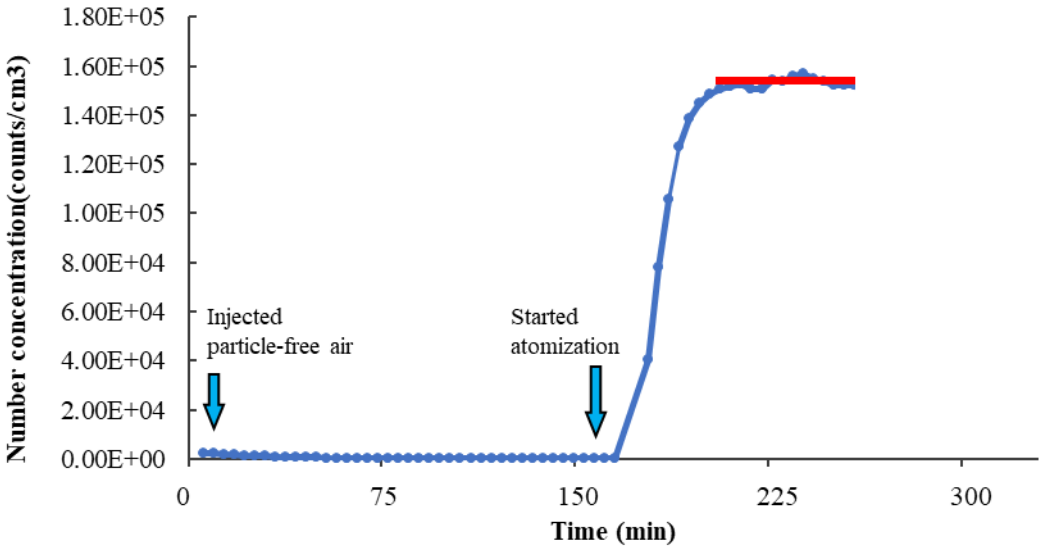

Fig. 3-12 Total number concentration of particles in the chamber (red line: stabilized average concentration (1.53 E+05 counts/cm^3)).

Apart from the mixing capability, the airtightness of the chamber was tested. CO_2 with the mixing ratio of 1000 ppm was injected into the chamber and the concentration of CO_2 in the chamber was monitored simultaneously and continuously by a Q-Trak Plus (TSI, Model 8554). Fig.3-13 shows the temporal variation of CO_2 concentrations in the chamber during the experiment. At the beginning, the

concentration of CO_2 in the chamber was around 500 ppm which was closed to the indoor CO_2 level. Once the Q-Trak reading became stable, the CO_2 with mixing ratio of 1000 ppm was injected into the chamber. The CO_2 concentration inside gradually increased and reached the peak value of about 1030 ppm in 80 minutes. The chamber was then sealed and the injection of CO_2 was stopped at the same time to examine the airtightness of the chamber. The concentration of CO_2 inside remained constant for more than 1.5 hours, suggesting the good airtightness of the chamber. Overall, the airtightness and mixing of the chamber were tested and the performance of the chamber in these two aspects was satisfactory.

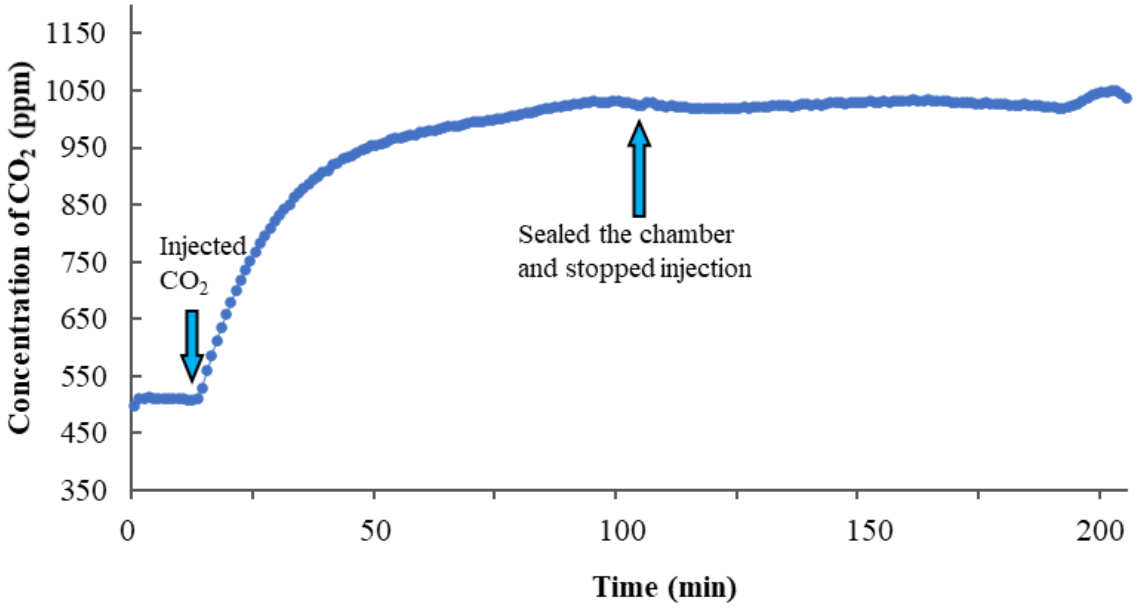

Fig. 3-13 The temporal variation of the concentration of CO_2 in the chamber.

3.5.2.3 Collection efficiency of the new DS+QCM system

As a modified diffusion sampler, the collection efficiency is dependent upon the theory of diffusion presented by Hinds (1999), which is related to the deposition parameter (μ). The deposition parameter (μ) is determined by Eq. 3-4 and Eq. 3-5.

Collection efficiencies of particles in the QCM+DS system were calibrated using three sizes of PSL

particles (53 nm, 102 nm and 200 nm) at four different sampling flow rates (0.05, 0.1, 0.2 and 0.5 L/min). In total, 12 experimental scenarios were conducted at each sampling spot. The schematic of calibration experiment setup is illustrated in Fig. 3-14. A few drops of PSL standards in each size were added into 8 mL Milli-Q water to generate PSL-particle aqueous solutions. The PSL particles, generated by the particle generator and diluted with filtered air using a 1.5 L bottle, were dried by a silica gel dryer (70 cm length×15 cm diameter), and then introduced into an environmental chamber. Every 2h, 5 mL PSL-particle aqueous solution was added into the particle generator to keep the generated particles at a stable level of about 10^3–10^4/cm^3, *i.e.*, ~1.0× 10^4/cm^3 for 50 nm, 4.0×10^3/cm^3 for 102 nm, and 2.0×10^3/cm^3 for 200 nm PSL particles, respectively. The QCM+DS system was placed in the centre of chamber (Fig. 3-14). During the experiments, the frequency change of the system was recorded. To obtain sufficient frequency change for statistical analysis, totally 8~12 hours were required for sampling PSL particles. Simultaneously, a SMPS (Model 5.400, Grimm, Germany) measured the concentrations of monodisperse PSL aerosols inside the chamber every 4 min. throughout the entire experimental period. Eventually, the frequency change (Δf) was converted into the mass of deposited particles, which was compared with the total mass of particles passing through the QCM+DS system, measured by the SMPS. Thus, the collection efficiencies of the system on the three sizes of particles at four different sampling flow rates were obtained. The relationship of collection efficiencies of the QCM-DS system with sizes of particles and sampling flow rates was then quantified using the above experimental data (Origin Pro 2017, USA).

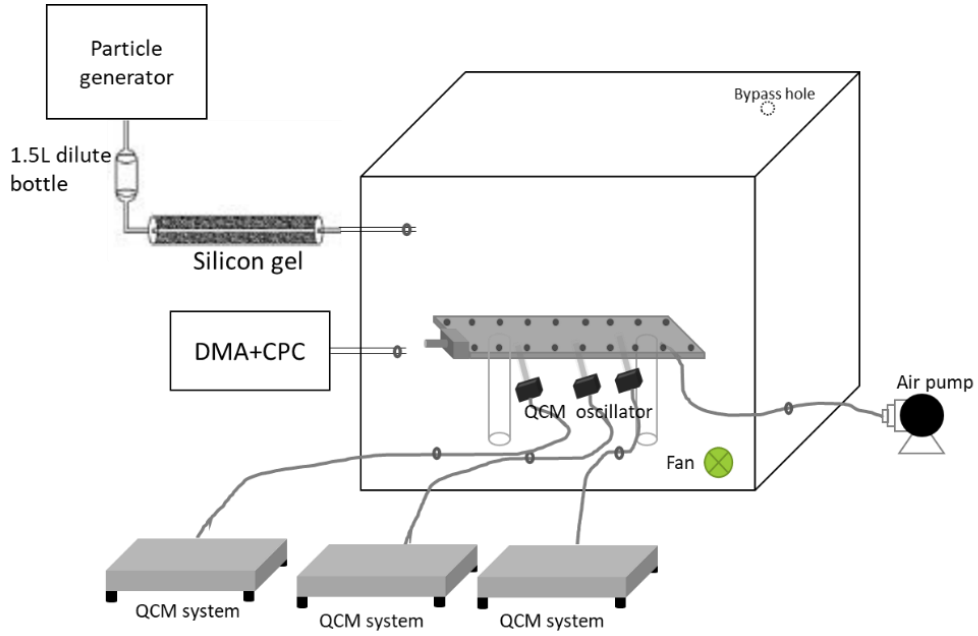

Fig. 3-14 The schematic setup of the calibration experiment.

3.6 Differential particle removal

3.6.1 Air jet method

The schematic of the air jet treatment system in the study is shown in Fig. 3-15. Compressed air was used to provide high-pressure airflow. The air pressure was controlled by a valve and then led into a HEPA filter to remove all the particles in the compressed air. At the outlet of the HEPA filter, a nozzle was connected to generate an air jet. The particle-free air ejected from the nozzle flushed the surface of a substrate at a high pressure of 0.5 MPa. The angle between the nozzle and the surface of the detector was set to ~ 30° (Lee et al., 2009). Air jet treatment was conducted for 60 min.

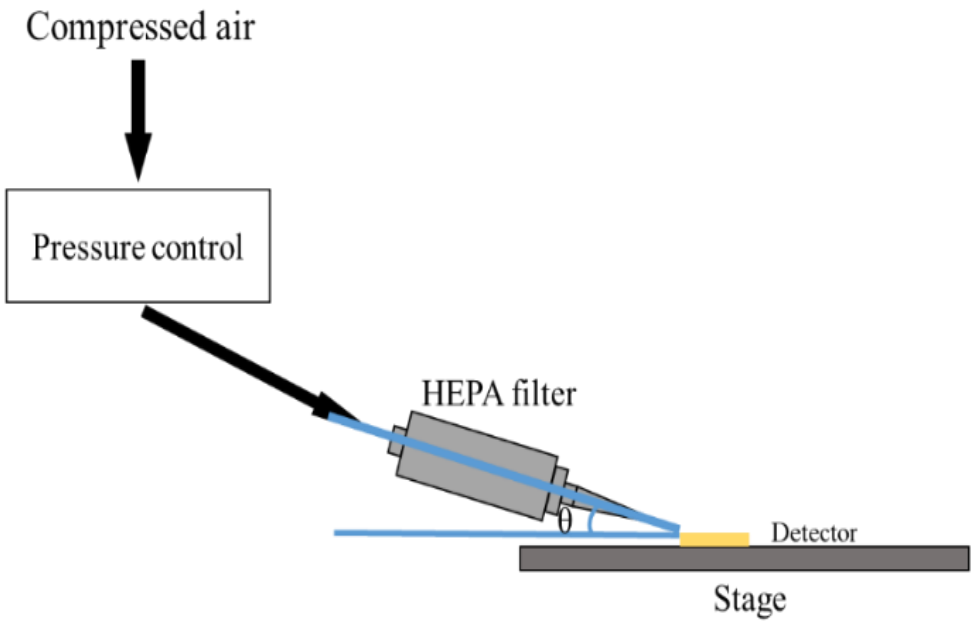

Fig. 3-15 Schematic of the air jet treatment.

3.6.2 Nanobubble method

Nanobubble is a method that can effectively remove nanoparticles from the surface. In the nano-bubble process, the surface of a substrate is first covered with ethanol, and then rinsed with deionized water (DI water). A large number of nanobubbles are generated through the ethanol-water exchange process to remove nanoparticles and the coverage rate of nanobubbles on the surface are remarkably high (Yang and Duisterwinkel, 2011). To adopt this method, a small device (*i.e.*, a diminutive chamber) was developed to provide a suitable space for the ethanol-water exchange process. The schematic of nano-bubble process is shown in Fig. 3-16. The detector was first placed in the middle of the diminutive chamber. Ethanol was then poured into the chamber until the surface of the detector was completely covered. A hole was drilled at the top of the diminutive chamber for injection of DI water. The pinhead of a needle was as close as possible to the surface of the detector to flush the surface. The extra ethanol-water solution was discharged from the bypass hole on the left side of the chamber. The

removal efficiency of the method is related to the treatment time. Previous study claimed that ~ 80% of nanoparticles were removed from a plain silicon wafer after one-time nanobubble treatment and the removal efficiency was further enhanced to ~ 90% after 3 times treatment (Yang and Duisterwinkel, 2011). In the study, to take advantage of this method, detectors containing particles were processed 5 times and 10 times with the nanobubble method, respectively.

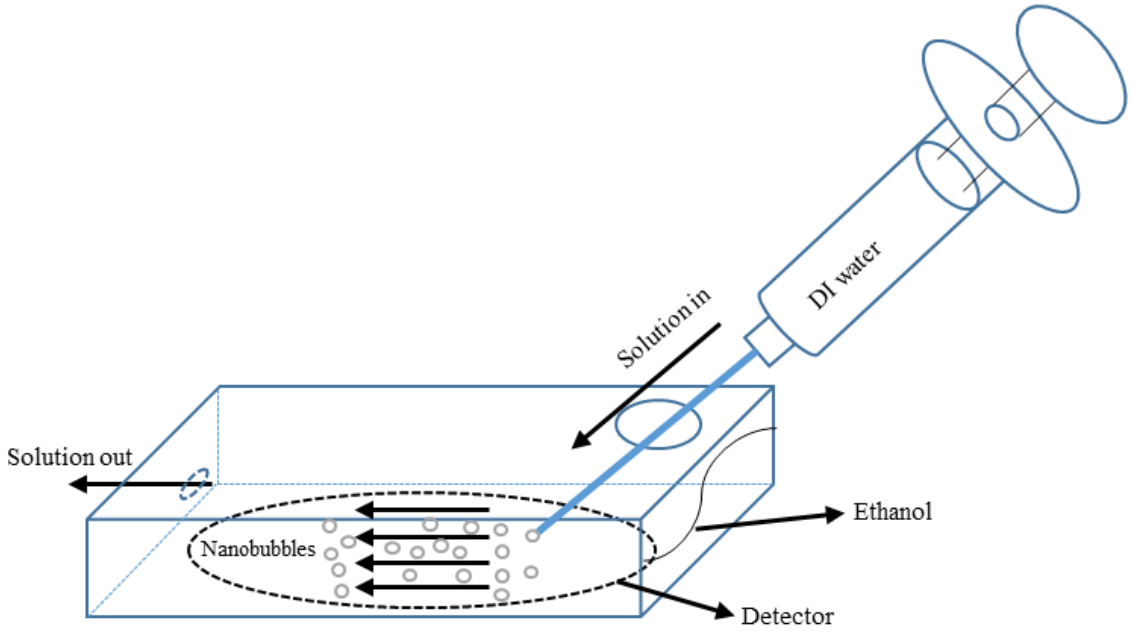

Fig. 3-16 Schematic of the nanobubble process.

3.6.3 Ultrasonic method

In this study, ultrasonic treatment was conducted with ethanol and DI water as a solution. Particle-containing detectors were put into a beaker, and immersed in ethanol and DI water, respectively. The beaker with the immersed detectors was then agitated in an ultrasonic bath (Crest Ultrasonic, model 275HTAE) at an ultrasonic frequency (~ 40 kHz) for 30 min. The frequency was commonly used for ultrasonic equipment in previous studies (Charasseangpaisarn and Wiwatwarrapan, 2015; Paniwnyk et al., 2017).

3.6.4 Particle removal efficiency

The tapping mode of an AFM (NanoScope, Version 5.31R1, Veeco Instrument Inc., USA) was used to evaluate the particle removal efficiency of the different methods. AFM images were scanned with the parameter settings as follows: scan rate: 0.6 - 1 Hz; amplitude setpoint: 0.65 - 0.80 V; integral gain: 0.2; and proportional gain: 0.5. The scanning areas were from 5 × 5μm to 10 × 10μm. The particle removal efficiency was determined using the following equation (Eq. 3-10):

$$\eta = 1 - \frac{n_a \cdot S_i}{n_i \cdot S_a} \quad \text{Eq. 3-10}$$

where η is the particle removal efficiency, n_i is the number of particles on the surface before the particle removal treatment, n_a is the number of particles on the surface after the particle removal treatment, S_i is the AFM scanning area before the particle removal treatment, S_a is the AFM scanning area after the particle removal treatment.

3.7 Sampling campaign

In this study, AUFPs were measured using novel methods (*i.e.*, DS+AFM and DS+QCM) at different sites in Hong Kong and Shanghai from 2017 to 2020 through six sampling campaigns. SMPS was also used in one sampling campaign for method validation with the DS+AFM and DS+QCM methods. SMPS is an analytical instrument that online measures the size and number concentration of particles (Model 5400, Grimm, Germany). It employs a continuous, fast-scanning technique to provide high-resolution measurements with 44 size bins from 5.5 nm to 350 nm with a fixed air flow rate of 0.3 L/min. Field measurements were conducted in three land-use areas in Hong Kong, including an urban site, a roadside site and a rural site. At the urban site, two campaigns were carried out from 6 January to 17 February 2017 and from 11 April to 25 April 2019 (Fig. 3-17). At the roadside site, two measurements were also conducted from 23 November to 14 December 2017 and from 10 July to 17

July 2019 (Fig. 3-17). The one at the rural site (Hok Tsui) was performed from 2 November to 23 November 2020 (Fig. 3-18). Outside Hong Kong, the sampling in Shanghai was implemented at an urban site from 11 September to 29 September 2019 (Fig. 3-19). In the thesis, the measurements above were marked as samplings I, II, III, IV, V and VI, for 2017 Hong Kong roadside sampling, 2017 Hong Kong urban sampling, 2019 Hong Kong roadside sampling, 2019 Hong Kong urban sampling, 2020 Hong Kong rural sampling and 2019 Shanghai urban sampling, respectively. In samplings I, II, III, V and VI, only DS+AFM method was adopted to measure the concentrations of atmospheric UFPs and AUFPs, while in sampling IV, DS+AFM, QCM+DS and SMPS were all used for comparison and method validation.

The urban site (22.303°N, 114.180°E) is on the rooftop of a building in the campus of Hong Kong Polytechnic University at Hung Hom, Kowloon (Z Core). This site is significantly affected by the anthropogenic emissions as it is located near main roads and surrounded by residential areas. The roadside site (22.306°N, 114.179°E) is near the cross-harbour tunnel (CHT), which is one of the busiest roads in Hong Kong. Traffic emission is the primary source at the roadside site.

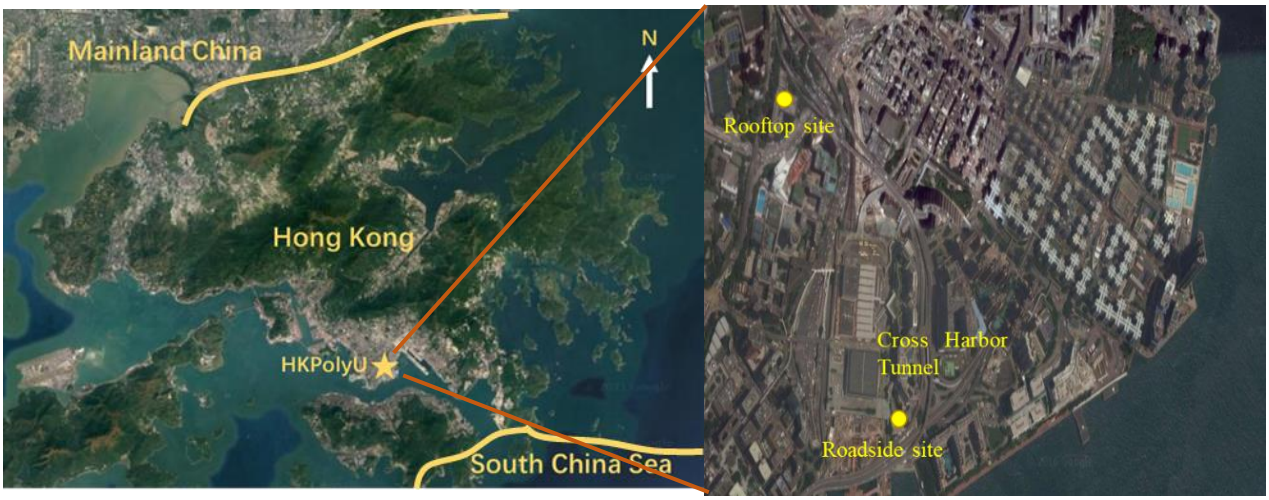

Fig. 3-17 Geographical location and scene pictures of the urban and roadside sites in Hong Kong

The Hok Tsui (HT) site (22.209°N, 114.253°E) is a relatively remote coastal site, located at the southeastern tip of Hong Kong. A country park locates 2 km to the north of the sampling site, and there are many broad-leaved trees within 500 m of the site. The site has long been regarded as a regionally urban background site in South China, given that air pollutants in the adjoining Pearl River Delta reached the site within a few hours (Zhang et al., 2012).

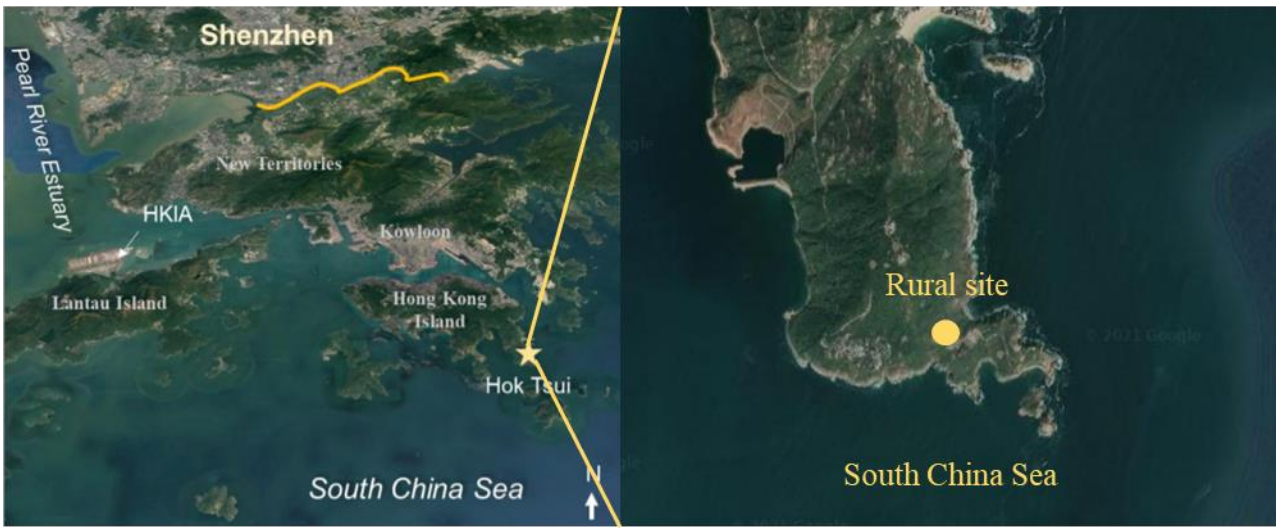

Fig. 3-18 Geographical location and scene pictures of the rural site in Hong Kong

The urban site in Shanghai is in the East China Normal University (Minhang Campus) (31.228°N, 121.407°E). Sampler was put on the top of a container located in a playground of the university. The site is located in the south of downtown Shanghai, where residential activities and vehicle emissions are the main sources of air pollutants.

Fig. 3-19 Geographical location and scene picture of the urban site in Shanghai

3.8 Validation of QCM+DS system in sampling IV

3.8.1 Sampling technique and setup

Several instruments were employed in the field measurement, including the QCM+DS system, the previous DS+AFM system and a SMPS (Model 5.400, Grimm, Germany). Results obtained from the previous DS+AFM method and SMPS were compared with those of the QCM+DS system. Schematic of the setup of sampling system is shown in Fig. 3-20. Ultrafine particles (UFPs) passing through the PM_1 cyclone were divided into two streams. The first stream went into the previous DS directly and particles were collected on the metal-silicon detectors. The other stream was further divided into two

sub-streams. One sub-stream went through a differential mobility analyzer (DMA) firstly for size selection to obtain monodisperse particles. Afterwards, the monodisperse particles were collected by the QCM+DS system. The other sub-stream after the DMA was delivered to a CPC to monitor the number concentrations of UFPs. During sampling, both QCM+DS system and CPC measured the time-integrated size-resolved concentrations of ambient particles with a range of 5.5–150 nm at a 120-min scan interval. The QCM+DS system with three metal-QCM detectors inside continuously measured the mass of deposited particles (via frequency changes) at a flow of 0.1 L/min for 2 days for each sample, while the SMPS monitored size-classified particle number concentrations at a fixed flow rate of 0.3 L/min. At the end of each sampling, a HEPA filter was connected to the inlet of the QCM+DS to conduct blank experiment for at least 3 hours. On one hand, the blank experiment measured the frequency change when particle-free air was collected, which was considered in the data analyses. On the other hand, the system was cleaned by the particle-free air before the next sampling. For the previous DS, nine metal-silicon detectors were placed inside it for exposure. Ambient air was drawn through the sampler by a low-flow pump with a fixed flow rate of 0.05 L/min. Sampling duration of each sample was 2-4 days, dependent on the level of particle number in the air. Noteworthily, although the sampling was non-isokinetic, the measurement of ultrafine particles in the study was not affected (Arouca et al., 2010; https://www.ldxsolutions.com /particulate-matter-isokinetic-sampling/).

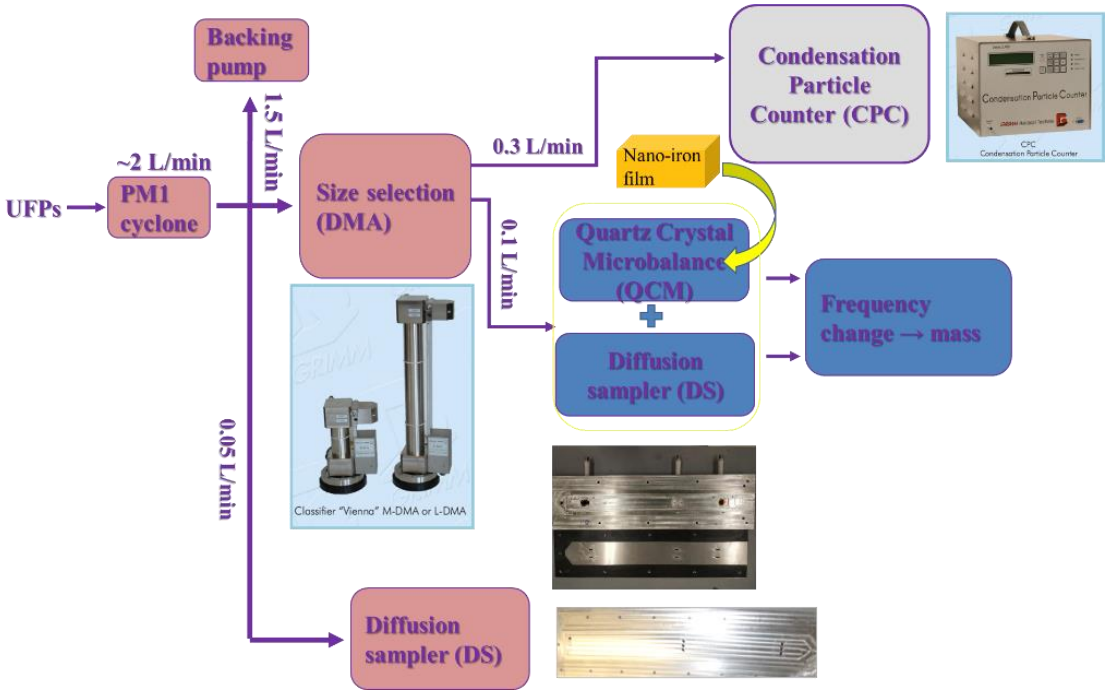

Fig. 3-20 Schematic diagram of the setup of sampling system in the field measurement

3.8.2 Data processing

After the field measurement, results obtained from the QCM+DS system were compared with those measured by the DS+AFM method and SMPS. The DS+AFM method was described in the section 3.4 and the previous study (Wang et al., 2014b). The SMPS is a commercial instrument, which can measure number concentrations of UFPs online (maximum time resolution of 4 min). As for the new QCM+DS system, real-time frequency of metal-QCM detector was obtained during sampling. To determine concentrations of UFPs in the atmopshere, frequency changes were converted into the masses of the deposited particles. By taking into account the collection efficiency, sampling flow rate and sampling duration, the concentrations of AUFPs and UFPs were determined. Specifically, in the QCM+DS system, particles ranged from 5.5 nm to 150 nm were categorized into 8 size bins (124~150 nm, 75~112 nm, 47~69 nm, 30~43 nm, 19~27 nm, 17~12 nm, 11~8 nm, and 7~5 nm) in one scanning interval (*i.e.* 2 hours) for calculation and comparison with the results of SMPS and DS+AFM method.

Frequency change of one size bin corresponded to the sampling duration (15 min) in one scanning interval. However, due to the tiny frequncy change in the smaller size bins (*i.e.* 17~12 nm, 11~8 nm and 7~5 nm), the three size bins were merged into one category for calculation (*i.e.* 17~5 nm). In collecting one sample, sampling duration of the QCM+DS system was 2 days. Thus, sum of frequency changes for each size bin in one sample was used to calculate the particle concentraions in the 2 days. Eq. 3-10 explains the details of quantifying the concentrations of UFPs (C_m) using the QCM+DS system.

$$C_m=(\sum m_i/\eta_i)/(Q\times T) \quad \text{Eq. 3-10}$$

where C_m is the mass concentration of UFPs in the atmosphere; m_i is the mass of particles in i^{th} size bin, calculated using the Sauerbrey's equation (Eq. 3-7); η_i is the corresponding collection efficiency of particles in i^{th} size bin; Q is the sampling flow rate; T is the sampling time. Moreover, to convert mass concentration into number concentration, the density of ambient particles was assumed to be 2.5 g/cm^3 (Ferro et al., 2004; Cha and Olofsson, 2018). The conversion equation is as follows (Eq. 3-11).

$$n_i= m_i/(4/3\times\pi\times r_i^3\times\rho) \quad \text{Eq. 3-11}$$

where n_i is the total number of particles in i^{th} size bin; m_i is the mass of particles in i^{th} size bin; ρ is the particle density and r_i is the average radius of particles in the i^{th} size bin. Therefore, the total number concentration of UFPs (C_n) is further determined (Eq. 3-12).

$$C_n=(\sum n_i/\eta_i)/(Q\times T) \quad \text{Eq. 3-12}$$

Furthermore, to determine the concentrations of AUFPs, sampled metal-QCM detectors were immersed in the ethanol solution for ultrasonic treatment for 30 min after a certain storage time (longer than one day) in the inert gas. The storage time was to ensure a sufficient reaction between acidic

particles and metal nano-film (Wang et al., 2012). Frequency changes before and after ultrasonic treatment were obtained. Frequency change after ultrasonic treatment was corresponded to the mass of non-acidic particles collected, while the frequency change in the field measurement referred to the mass of total UFPs. Thus, the mass of AUFPs was determined by the difference between the frequency changes in the field measurement and those after the ultrasonic treatment.

3.9 Estimation of concentration of sulfuric acid (SA) vapor

To investigate the relationship of sulfuric acid vapor (Q_{sa}) with the concentration of AUFPs, a predictive proxy based on solar radiation, SO_2 concentration, condensation sink (CS) and relative humidity (RH) was used to estimate sulfuric acid concentration (Mikkonen et al., 2011). In the study, the SO_2 data for Q_{sa} estimation in Hong Kong were obtained from Hong Kong Environmental Protection Department (HKEPD) (https://cd.epic.epd.gov.hk/EPICDI/air/station /?lang=zh), while in Shanghai they were collected from China National Environmental Monitoring Center (http://106.37.208.233:20035/). Meteorological data in Hong Kong and Shanghai were acquired from Hong Kong Observatory (https://www.hko.gov.hk/tc/) and the fifth generation European Centre for Medium-Range Weather Forecasts reanalysis data (https://www.ecmwf.int/), respectively. The average atmospheric conditions used to calculate the Q_{sa} in different samplings are listed in Table 3-1.

Table 3-1 Average radiation, SO_2 level and relative humidity in different samplings

Sampling	Radiation (W/m^2)	SO_2 (ppb)	RH (%)
2017 winter roadside Hong Kong	133.00	1.80	57.48
2019 summer roadside Hong Kong	185.17	1.20	56.93
2017 winter urban Hong Kong	139.22	1.40	57.73

2019 summer urban Hong Kong	194.95	1.08	59.45
2020 rural Hong Kong	163.72	3.40	71.20
2019 urban Shanghai	192.20	1.90	65.00
2010 rural Hong Kong	162.61	5.25	82.00
2010 urban Hong Kong	140.19	6.37	60.15

The CS, presented as the loss rate of molecules onto existing particles, was calculated based on the particle size distribution. The equations for calculating Q_{sa} and CS are shown in Eq. 3-11 and Eq. 3-12.

$$Q_{sa} = 8.21\times10^{-3}\cdot k\cdot[SO_2]^{0.62}\cdot[SR]\cdot(CS\cdot RH)^{-0.13} \quad \text{Eq. 3-11}$$

where k is a constant value 1.035, SO_2 is the measured concentration in ppb, SR is the solar radiation in W/m^2, RH is the relative humidity in % and CS is the condensation sink in s^{-1}.

$$CS = 2\pi d\int D_p\cdot\beta_M(D_p)N(D_p)dD_p = 2\pi d\sum\beta_{Mi}D_{pi}N_i \quad \text{Eq. 3-12}$$

where d is the diffusion coefficient of the condensing vapor, β_{Mi} is the transitional regime correction factor in size bin *i*, D_{pi} is the average particle diameter in size bin *i*, and N_i is the particle number concentration in the corresponding size bin.

Chapter 4 Ambient acidic ultrafine particles in different land-use areas in different Chinese cities

4.1 Introduction

Aerosol is defined as airborne particles, which contain more than 90% ultrafine particles (UFPs) in terms of number concentration (Karottki et al., 2015; Rim et al., 2016). It is believed that UFPs are able to carry the greatest amount of inflammation per unit PM mass because of high particle number (PN), high lung deposition efficiency and surface area compared to fine and coarse particles (Wang et al., 2012). However, components of UFPs are not equally detrimental (Utell et al., 1982; Schlesinger, 1989; McGranahan and Murray, 2012). Among all the chemical components in ambient UFPs, sulfuric acid (H_2SO_4) and ammonium bisulfate (NH_4HSO_4) are the significant and harmful chemicals, forming acidic ultrafine particles (AUFPs). AUFPs have been proved to be closely associated with total mortality, morbidity and hospital admissions for respiratory diseases (*e.g.*, Thurston et al., 1989, 1992, 1994; Lippmann and Thurston, 1996; Peters et al., 1997; Wichmann et al., 2000; Cohen et al., 2000). In addition to health effect, AUFPs are closely related to new particle formation (NPF) as AUFPs can facilitate the particle formation and growth (Guo et al., 2012; Wang et al., 2014a). However, the relationships of AUFPs with NPF and particle growth were only evidenced by the concentrations of sulfuric acid vapor and/or *pH* of particles in the NPF events in previous studies, rather than the concentration of AUFPs (Riipinen et al., 2007; Sipilä et al., 2010). Thus, it is crucial to collect sufficient data of AUFPs in the atmosphere to better understand the association of AUFPs with health impact and the direct connection of NPF with AUFPs.

A handful of studies successfully measured AUFPs in the atmosphere. In 1990s, Cohen et al. (2000, 2004a) firstly applied an iron nanofilm detector to measure the AUFPs in downtown New York, but no acidic particles were detected due to insufficient sampling duration. Later, Cohen et al. (2004b) reported AUFPs levels of 100-1800 /cm^3 in Tuxedo town of New York state after a longer sampling duration. More than 10 years later, Wang et al. (2012) successfully observed and quantified the AUFPs at a mountain site of Hong Kong by collecting airborne UFPs onto a nanofilm detector mounted in an electrostatic precipitator (ESP) and then scanning the detector using an Atomic Force Microscope (AFM). They found that the concentration of AUFPs was ~ 2 × 10^3 /cm^3, which accounted for ~30% of total UFPs. Further, to overcome the shortage of the previous method, Wang et al. (2014b) applied their own developed diffusion sampler (DS) together with the sample nanofilm detectors to measure UFPs and AUFPs at an urban site in Hong Kong. The concentrations of AUFPs and UFPs were ~ 9 × 10^3 /cm^3 and ~ 2 × 10^4 /cm^3, respectively. These limited studies clearly showed that the measurements of ambient AUFPs are far from enough, not to mention the inconsistent methods used in these previous studies. As such, the abundance, size distribution, and spatiotemporal characteristics of AUFPs in the atmosphere are poorly understood.

To fill the gap, in the study, AUFPs were extensively measured in different land-use areas in different Chinese cities using the method developed by Wang et al. (2014b) (*i.e.*, DS + AFM). Specifically, two field measurements were carried out at an urban site (one on 6 January-17 February 2017 and another on 15 - 25 April 2019) and at a roadside site (23 November-14 December 2017 and 10 -17 July 2019, respectively) in Hong Kong, while another sampling campaign was conducted in a rural area of Hong Kong from 2 November to 23 November 2020 to understand the spatiotemporal variations of AUFPs

pollution in Hong Kong. In addition, to investigate the difference of AUFPs pollution in different cities, a sampling campaign was undertaken in Shanghai on 11 - 29 September 2019. Shanghai was specifically chosen for inter-comparison of AUFPs pollution because of its distinct geographical feature, meteorological conditions, anthropogenic emissions, and urban infrastructures. This is the first comprehensive attempt to unravel the concentrations, size distributions and spatiotemporal variations of AUFPs. The findings are expected to enhance our understanding of AUFPs in the atmosphere, help establish a database of AUFPs and provide additional references for future air quality research.

4.2 Concentrations of UFPs and AUFPs

Fig. 4-1 presents the concentrations of AUFPs and UFPs in different land-use areas and cities together with the proportions of AUFPs in UFPs. The concentrations of UFPs (mean ± standard deviation (SD)) were (1.48±0.64) $\times 10^4$, (1.39±0.65) $\times 10^4$, (1.71±0.92) $\times 10^4$, (1.57±0.84) $\times 10^4$, (0.60±0.20) $\times 10^4$ and (1.21±0.49) $\times 10^4$ /cm^3 for sampling I (2017 Hong Kong roadside), II (2017 Hong Kong urban), III (2019 Hong Kong roadside), IV (2019 Hong Kong urban sampling), V (2020 Hong Kong rural sampling) and VI (2019 Shanghai urban sampling), respectively. In comparison, the concentrations of UFPs were the lowest in the rural area in Hong Kong ($p < 0.05$) due to sparse anthropogenic emissions. The levels of UFPs at the roadside site were slightly higher than those at the urban site because the roadside site was closer to emission sources, *i.e.*, motor vehicles which directly emit abundant UFPs (Zhai et al., 2016; Campagnolo et al., 2019). Nevertheless, the difference was not significant ($p > 0.05$). In addition, despite different years and seasons when the measurements were conducted at the roadside site or the urban site, no significant differences in the concentrations of UFPs were found (both $p > 0.05$), suggesting the pollution associated with UFPs was relatively stable in both urban and roadside

areas of Hong Kong in these years and in different seasons. Noteworthily, the concentration of UFPs in urban area of Shanghai was lower than that in urban area of Hong Kong ($p < 0.05$), implying less pollution of UFPs in urban Shanghai.

For AUFPs, the concentration was (0.31±0.18) $\times 10^4$, (0.37±0.30) $\times 10^4$, (0.37±0.26) $\times 10^4$, (0.42±0.28) $\times 10^4$, (0.22±0.10) $\times 10^4$ and (0.27±0.19) $\times 10^4$ /cm^3 for sampling I, II, III, IV, V and VI, respectively. Clearly, the concentration of AUFPs was the lowest in rural area ($p < 0.05$). No significant spatial and temporal differences were found in the concentration of AUFPs between the urban site and the roadside site in Hong Kong between 2017 and 2019 (all $p > 0.05$), consistent with the stable level of UFPs pollution in both urban and roadside areas. Similar to UFPs, the concentration of AUFPs in urban area of Shanghai was lower than that in urban Hong Kong ($p < 0.05$).

The AUFPs concentration accounted for the highest proportion of UFPs in rural area (*i.e.*, 36%) (Fig. 4-1), followed by that in urban areas (*i.e.*, sampling II: 27%, sampling IV: 26% and sampling VI: 23%) and in roadside areas (*i.e.*, sampling I: 20% and sampling III: 21%). The proportion of AUFPs in UFPs had inverse correlation with the distance to the emission sources, implying that the AUFPs emitted from anthropogenic sources was minor and the AUFPs might be potentially transformed from non-acidic UFPs by heterogeneous reaction of acidic vapors with preexisting non-acidic particles and/or condensation of acidic vapor on the surface of non-acidic particles during the transport and aging of air masses. Noteworthily, the field measurements in the study were basically short-term, which may exist some uncertainties for the above comparisons since the ambient particulates vary with the atmospheric conditions as well as the source emission profiles. Therefore, it is strongly suggested that prolonged sampling be conducted in future study.

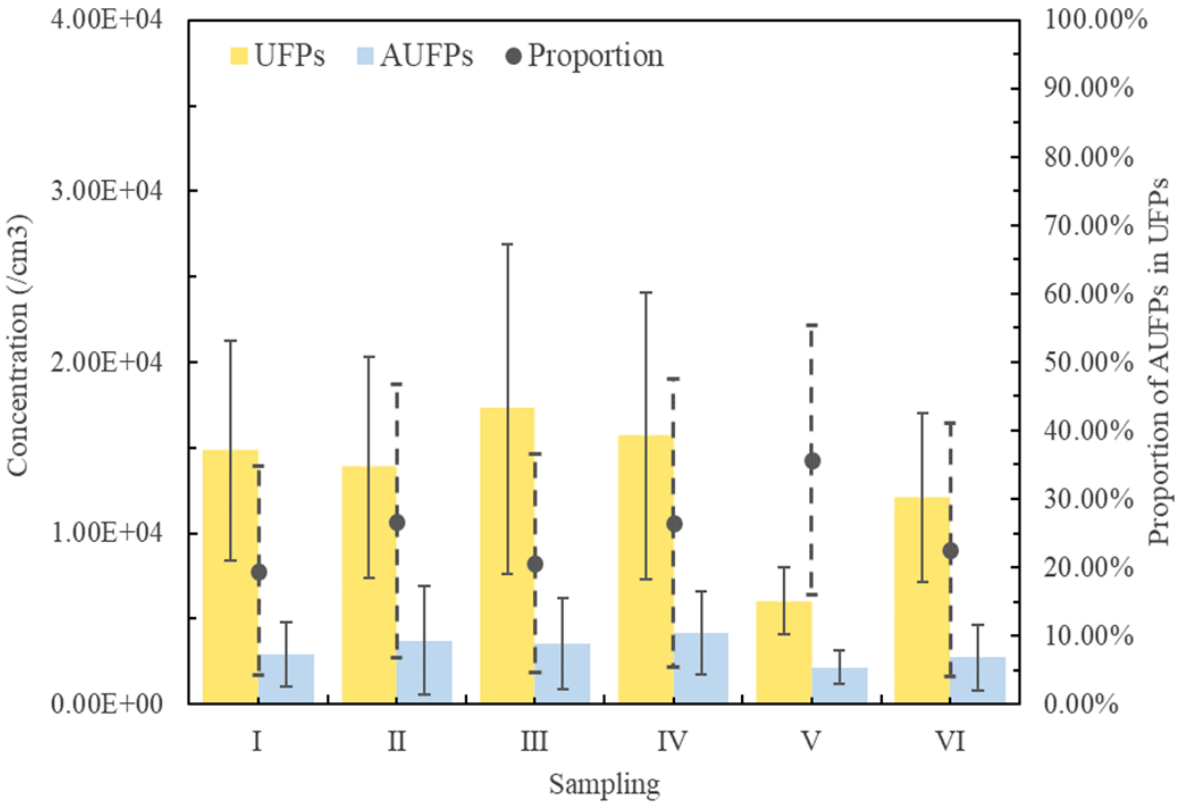

Fig. 4-1 Concentrations of UFPs and AUFPs, and proportion of AUFPs in UFPs in different land-use areas and cities

4.3 Size distributions of UFPs and AUFPs

Fig. 4-2 shows the size distributions of AUFPs and UFPs in different land-use areas and cities, as well as the proportions of AUFPs in UFPs in different size bins. Eight size bins were categorized for particles with sizes from 5 nm to 200 nm (*i.e.*, 5-10 nm, 10-20 nm, 20-35 nm, 35-50 nm, 50-70 nm, 70-100 nm, 100-150 nm and 150-200 nm). The geometric mean diameter (GMD) of the size distribution was calculated using the following equation (Eq. 4-1):

$$GMD = \Sigma N_i \cdot d_{pi} / N \quad \text{Eq. 4-1}$$

where N_i is the particle number concentration in i_{th} size bin, d_{pi} is the average particle diameter (nm) in i_{th} size bin, and N is the total particle number concentration of all size bins.

The size distributions of UFPs were normal in all the six sampling campaigns. Concentration of UFPs generally peaked in the size range of 20-35 nm or 35-50 nm, in line with the results of previous studies (Li et al., 2007; Cheng et al., 2012). The nucleation-mode and Aitken-mode particles (<100 nm) dominated the UFPs concentration, accounting for ~90% of the total particle number concentration. The GMD of UFPs was 28.0 nm, 35.8 nm, 33.6 nm, 34.5 nm, 38.1 nm and 35.4 nm in samplings I, II, III, IV, V and VI, respectively. The highest GMD value was found in rural area (*i.e.*, 38.1 nm), while the GMD values in urban areas (34.5 – 35.8 nm) were similar to those in roadside areas (28.0 – 33.6 nm). The GMD values were generally associated with the age of air masses in different land-use areas. The transport of pollutants from an urban area to a rural area provided enough time for particles to coagulate and grow and thus increased the GMD (Yao et al., 2010; Šmejkalová et al., 2020).

Similarly, the size distributions of AUFPs were normal with peaks at 20-35 nm or 35-50 nm. The GMDs of AUFPs were 28.7 nm, 34.3 nm, 36.1 nm, 36.0 nm, 32.8 nm and 34.3 nm for samplings I, II, III, IV, V and VI, respectively, analogous to the corresponding GMDs of UFPs ($p > 0.05$). Further, over 90% of AUFPs composed of particles in nucleation and Aitken modes. Few AUFPs were in the size range of 150-200 nm, consistent with the results of previous studies, which found that sulfuric acid and/or nitric acid are usually present in UFPs at the initial formation stage to promote particle formation and growth (Schlesinger and Cassee, 2003; Wang et al., 2020a). In addition, no significant difference in GMDs of AUFPs and UFPs was found in urban area between Hong Kong and Shanghai ($p > 0.05$), perhaps suggesting similar emission sources and/or chemical formation mechanisms of UFPs and AUFPs in these two cities.

The proportion of AUFPs in UFPs showed distinct patterns in different land-use areas. In roadside areas, the proportion peaked at 35-50 nm, while the maximum proportion in urban areas was in the size range of 50-75 nm. The hysteretic peak in urban areas might indicate the aggregation of AUFPs with non-acidic UFPs during the transport from source areas to receptor areas. However, the highest proportion in rural area was observed in the range of 5-10 nm. The high proportion of AUFPs in UFPs in small size range in rural area might suggest the stimulation of new particle formation (NPF) with the AUFPs as seeds, that were not easy to be aggregated by other low-concentration preexisting particles in a relatively clean environment. In addition, anthropogenic sources are scarce in rural area, especially vehicle emissions. Automobile exhaust is an important source of particles smaller than 20 nm (Mathis et al., 2004; Casati et al., 2007). Hence, a large amount of automobile exhaust emissions in urban and roadside areas resulted in a lower proportion of AUFPs in UFPs in the small size range than in rural areas.

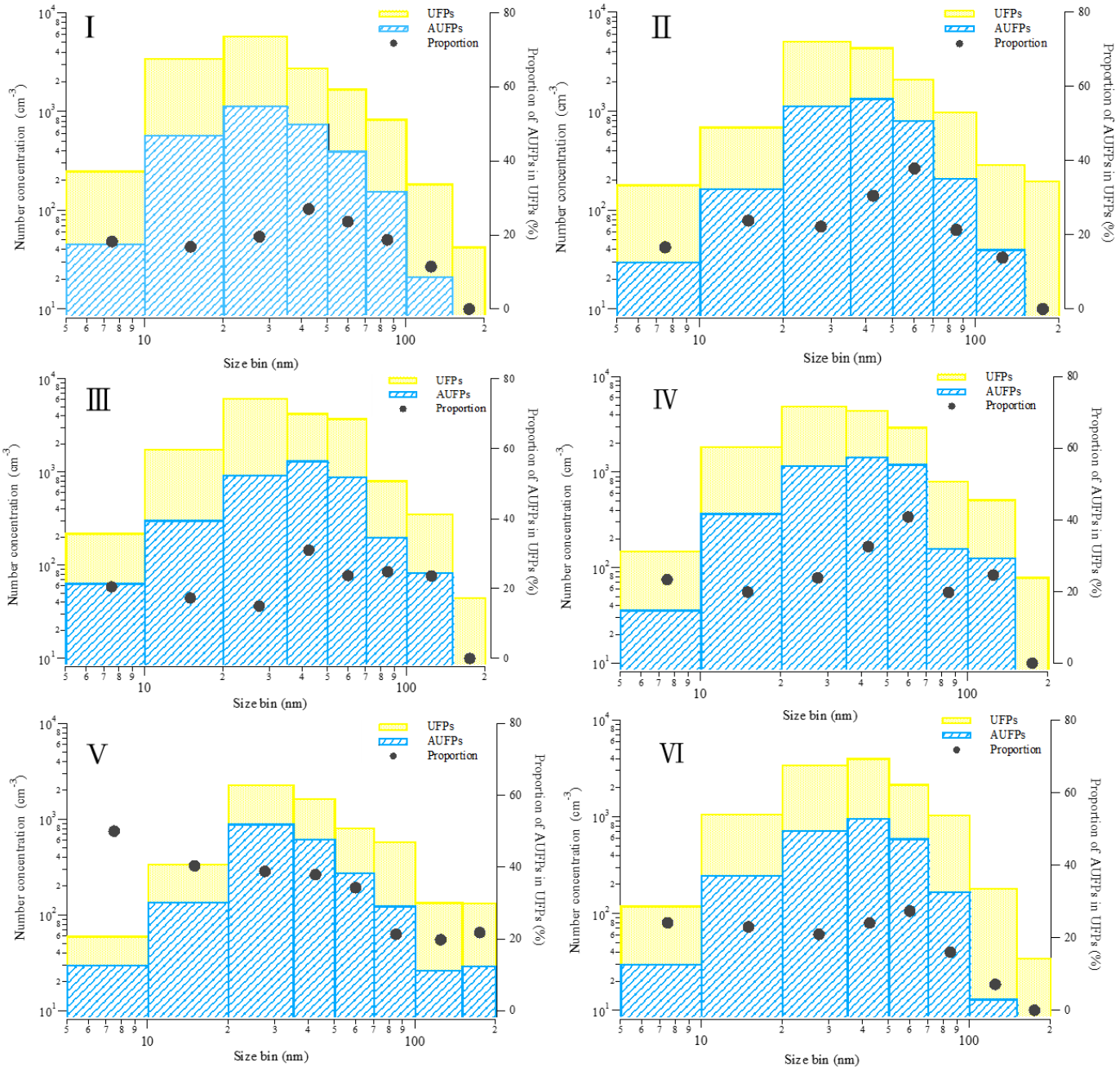

Fig. 4-2 Size distributions of UFPs and AUFPs with the proportions of AUFPs in UFPs in different size bins in different land-use areas and cities.

4.4 Correlation of estimated sulfuric acid vapor with AUFPs

Sulfuric acid vapor has been proved to be related to NPF (Kulmala et al., 2000; Guo et al., 2012; Wang et al., 2014a). Thus, it is expected that some of these newly-formed particles are acidic. Fig. 4-3

illustrates the correlation between proportion of AUFPs in UFPs and sulfuric acid vapor (Q_{sa}) at different concentrations of AUFPs in field measurements. It is noteworthy that the AUFPs data measured in previous studies were used for comparison purpose (Wang et al., 2012 and 2014b). It was found that the proportion of AUFPs in UFPs was positively correlated with the Q_{sa} (R^2 = 0.71), while no obvious relationship was observed between the concentration of AUFPs and the Q_{sa} (R^2 = 0.17), especially in rural areas. In other words, although the levels of Q_{sa} were high in the rural areas, concentrations of AUFPs were even lower than those in urban and roadside areas. It is well known that condensation of compounds with low vapor pressure such as sulfuric acid and nitric acid on preexisting particles and coagulation of these compounds are important mechanisms to form new particles (Schlesinger and Cassee, 2003; Wang et al., 2020a). Both pathways could increase the acidity of particles and lead to the formation of AUFPs if the vapor of those compounds is acidic. Theoretically, a high Q_{sa} level would result in the formation of more AUFPs. However, another factor determining the concentration of AUFPs is also important, namely, the concentration of preexisting particles. If their concentration is higher together with higher Q_{sa} level, more AUFPs will be generated. As such, it is understandable why Q_{sa} does not have positive correlation with the concentration of AUFPs but the proportion of AUFPs in UFPs. In rural areas, although the concentration of Q_{sa} was higher, the concentration of preexisting particles was low, which led to lower AUFPs but higher proportion of AUFPs in UFPs. In comparison, the higher level of preexisting particles in urban and roadside areas was favorable to more AUFPs formation by providing more chances for condensation of sulfuric acid vapor on non-acidic UFPs. However, since the Q_{sa} level in urban/roadside areas was not as high as that in rural area, and the preexisting particles concentration was higher, the proportion of AUFPs in UFPs

would be lower. Moreover, the close relationship of Q_{sa} with AUFPs might indicate the minor contribution of other acids such as nitric or organic acids to the AUFPs. Noteworthily, the AUFPs pollution in urban areas in Hong Kong seemed to be alleviated compared to ten years ago in terms of the AUFPs concentration and the proportion of AUFPs in UFPs. Extremely high AUFPs concentration and proportion of AUFPs in UFPs were found at an urban site in 2010 in Hong Kong (*i.e.*, 9.6×10^3 cm^3 and 45%), significantly higher than those measured at the same urban sites and roadside sites in 2017 and 2019 (all $p < 0.05$). While the meteorological conditions were different in all the measurements, it was still worth mentioning that the significant reduction in SO_2 in China might play an important role in the alleviation of AUFPs pollution. The annual SO_2 concentrations in Hong Kong decreased from 12.0 μg/m^3 in 2010 to 4.0 μg/m^3 in 2019, observed at a roadside monitoring station. In the past, the Hong Kong government implemented several measures to cut the SO_2 emission from vehicles. Although low sulfur fuel oil (LSFO) (Euro IV standard) was set as the minimum requirement for vehicle use in April 2002, the statutory standard has been further tightened to Euro V standard since 2010, which could reduce the SO_2 emissions of existing vehicles by 80% (Hedley et al., 2002; Zhang et al., 2010; https://www.info.gov.hk/gia/general/ 201111/09/P201111090187.htm). Moreover, by the end of 2016, about 50,000 old diesel commercial vehicles (older than Euro IV) were phased out. Low emission zones were set up on busy roads such as Central, Causeway Bay and Mong Kok to only allow buses that met Euro IV emission levels or above to run. The above measures also resulted in lower SO_2/Q_{sa} levels in urban/roadside areas than that in rural area in Hong Kong because LSFO was widely and strictly used in vehicles but not in marine vessels and the standard of LSFO usage in marine vessels (maximum sulfur content: 0.05%) was not as tight as that in vehicles (maximum sulfur content:

0.001%) (https://www.epd.gov.hk/epd/english/environmentinhk/air/air_maincontent.html). Since the rural site was located in a coastal area, it would suffer from more emission of marine vessels and had the higher SO_2/Q_{sa} level. In Shanghai, the SO_2 concentrations sharply decreased from 30 $\mu g/m^3$ to 7 $\mu g/m^3$ during this decade according to the Shanghai environmental bulletin. On one hand, the mandatory usage of LSFO in vehicles was proposed in 2013 and was completely implemented in mainland China at the end of 2017 (http://www.nea.gov.cn/2013-07/09/c_132525509.htm). On the other hand, the SO_2 emissions from industries and power plants were dramatically reduced in these ten years because of the combustion of low sulfur coal (Wang et al., 2018).

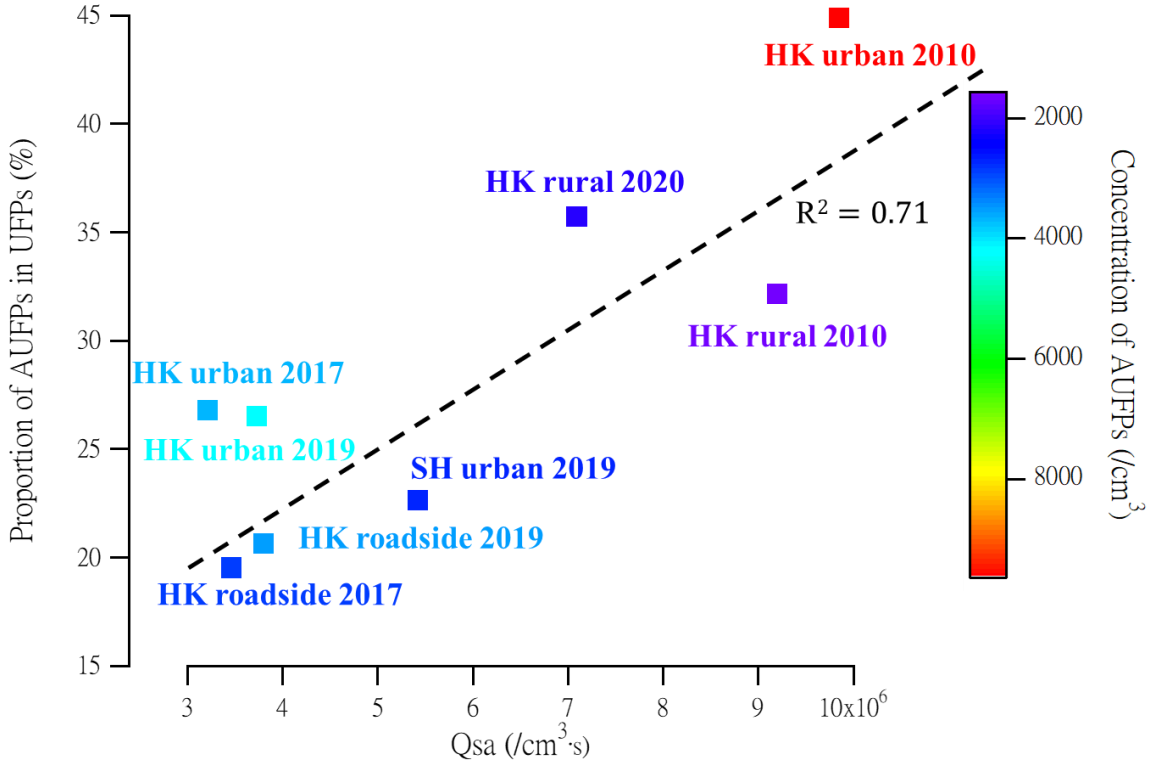

Fig. 4-3 Correlation of sulfuric acid proxy (Q_{sa}) with proportion of AUFPs in UFPs at different concentrations of AUFPs in different field measurements (HK roadside 2017: sampling I, HK urban 2017: sampling II, HK roadside 2019: sampling III, HK urban 2019: sampling IV, HK rural 2020: sampling V, SH urban 2019: sampling VI, HK rural 2010: Wang et al., 2012 and HK urban 2010: Wang et al., 2014b).

4.5 Summary

This is the first study to conduct extensive measurements of UFPs and AUFPs in different land-use areas (*i.e.*, roadside, urban and rural) and cities (*i.e.*, Hong Kong and Shanghai) in China. In total, six field measurements were carried out using the DS+AFM method. The results indicated that the concentration of UFPs was the highest at the roadside site, followed by that at the urban and rural sites. However, an opposite trend was found for the proportion of AUFPs in UFPs. The phenomena suggested the potential transformation of AUFPs from non-acidic UFPs through heterogeneous reaction of acidic vapor with non-acidic UFPs and/or condensation of acidic vapor on the surface of non-acidic UFPs during the transport and aging of air masses and the insignificant emissions of AUFPs from automobile vehicles. In addition, lower concentrations (mean ± SD) of UFPs ((1.21±0.49) $\times 10^4/cm^3$) and AUFPs ((0.27±0.19) $\times 10^4/cm^3$) were found in urban Shanghai than in Hong Kong ((1.48±0.64) and (0.40±0.27) $\times 10^4/cm^3$, respectively) ($p < 0.05$). Regarding size distribution, the sizes of both UFPs and AUFPs were normally distributed at all sampling sites and the GMDs of both UFPs and AUFPs were from 28 nm to 38 nm. Furthermore, the proportion of AUFPs in UFPs peaked in a larger size range (50-75 nm) in urban areas than that in roadside areas (35-50 nm), suggesting the aggregation of AUFPs with non-acidic UFPs during the transport from source areas to receptor areas. In rural area, however, the peak was observed in the smallest size range (*i.e.*, 5-10 nm), indicating the stimulation of NPF with AUFPs as seeds, which were not easily aggregated by other preexisting particles with low concentrations in the relatively clean environment. The GMDs of UFPs and AUFPs in the urban areas between Hong Kong and Shanghai were similar ($p > 0.05$), implying similar

emission sources and/or chemical formation mechanisms of UFPs and AUFPs in these two cities. The Q_{sa} was positively correlated with the proportion of AUFPs in UFPs (R^2=0.71), while no obvious relationship was found between the Q_{sa} and AUFP levels (R^2=0.17). The results suggested significant formation of AUFPs through heterogeneous reaction of sulfuric acid vapor with non-acidic UFPs and/or condensation of sulfuric acid vapor on non-acidic UFPs at high Q_{sa} level, which led to high proportion of AUFPs in UFPs. However, the AUFPs level might not be high even though the Q_{sa} level was high if the concentration of preexisting particles was low. Compared to the AUFPs pollution in urban Hong Kong ten years ago, the pollution was lowered because the concentrations of AUFPs and the proportions of AUFPs in UFPs decreased, possibly due to the successful reduction of SO_2 in China. The reduction in SO_2 in Hong Kong during the last decade was mainly attributed to stricter standards for the use of LSFO and the phase out of old diesel vehicles, while the decrease in SO_2 emissions in Shanghai resulted from the widespread use of LSFO in vehicles nationwide, and the combustion of low sulfur coal in industries and power plants. Although the spatial-temporal variation of AUFPs pollution was explored in this chapter, deficiencies of the DS+AFM method were highlighted and/or emphasized (*i.e.*, usage of AFM) after these field measurements. That is, an immense amount of time was spent on manual scanning of detectors and counting of particle number, which led to the necessity to develop methods for the identification and quantification of AUFPs without using the time-consuming AFM. Therefore, the following two research tasks were conducted.

Chapter 5 Differential removal of nanoparticles on the surface of a thin film substrate

5.1 Introduction

Purposeful identification, selection and collection of particles is essential and common in environmental studies (Cheng, 2018). Analysis of targeted particles can meaningfully minimize the downstream effort on preparation for environmental monitoring and/or analysis, and improve the signal quality. Previous particle identification and selection was mainly accomplished with the aid of microscopic technique. Wang et al. (2012) used atomic force microscope (AFM) to identify and quantify acidic ultrafine particles in the atmosphere by scanning the surface of a detector that collected ambient particles. Kessler et al. (2020) conducted a selective collection of iron-rich dust particles through natural trichodesmium colonies and examined the collected particles using a scanning electron microscope (SEM). Furthermore, through electron microscope and mass spectrometry, nine kinds of particles in East Asia were classified according to their elemental and morphological spectra, including mineral dust, K-rich, sea salt, metal, fly ash, sulfate, nitrate, soot, and organic particles (Li et al., 2016). Although the identification and selection of particles could be achieved by microscopic technique, studies proved that the technique was complex and time-consuming. The properties of each particle were manually identified and/or confirmed based on morphology and spectroscopy. Multiple scans of a sample are required to obtain reliable results, which wastes a lot of resources and leads to high costs. The microscopic technique is also unable to scan the nanoparticles on the entire surface in an acceptable period. In addition, it is impractical to use microscopic technique for analysis if the sample size is huge. Therefore, there is a need to develop a simple method, which can differentially abandon

the non-targeted particles and only detect the targeted particles. Compared to the microscopic technique, the developed method should be highly time-saving and cheap. By differentially removing non-targeted particles on the entire surface, targeted particles can be reserved for further investigation (*e.g.*, numeration and composition analysis). Concentrations of targeted particles can be obtained by considering collection efficiency, number of targeted particles and sample volume, and the impact of targeted particles on human health and the environment can be further evaluated by measuring the chemical components and compositions in the targeted particles with the aid of other instruments (*i.e.*, inductively coupled plasma-mass spectrometry and gas chromatography-mass spectrometry). For example, studies indicated that acidic particles play key roles in new particle formation (NPF) (Fiedler et al., 2005; Kulmala et al., 2006; Yue et al., 2010). Two methods were developed by our group for the measurement of acidic particles in the atmosphere. Nevertheless, the methods are neither convenient nor simple (Wang et al., 2012; Wang et al., 2014b). More importantly, these methods are time-consuming, so intensive detection of acidic particles cannot be achieved. By differentially removing non-acidic particles and purposefully retaining acidic particles to quantify acidic particles in the atmosphere, the key mechanisms of NPF may be explored and explained, and intensive detection of acidic particles can also be achieved. Thus, in aerosol study, the differential removal of non-acidic particles (non-targeted particles) and the intentional retention of acidic particles (targeted particles) on a substrate are both scientifically and practically meaningful.

Removal of nanoparticles from the surface of a substrate is an imperative but challenging issue in micrometer-scale manufacturing and research (Salih et al., 2019; Kohli, 2019). As the particle size decreases, the average adhesion stress, defined as the adhesion force per unit adhesive contact area

between the particle and the substrate, increases according to the fractional power law. The primary force of adhesion of nanoparticles on a dry surface is mainly controlled by the particle-surface interaction and slightly influenced by the particle-particle interaction (Bowling, 1988; Busnaina et al., 2018). Thus, to remove the nanoparticles on the surface, the principle is to overcome the adhesion between the particles and the surface. The adhesion/interaction between particles and the surface is related to several different mechanisms, including van der Waals (VdW) interaction, deformation of particles and substrate, and chemical/hydrogen bonding. Each of these mechanisms is dependent on the interfacial chemical and physical properties of the contact area established between the particles and the surface. Thus, the morphology of the interaction surface plays a controlling role in particle adhesion (Cooper et al., 2000). To change the interaction between the particles and the surface, a thin film coating is commonly adopted to alter the properties of the adhesive surface. A thin film is a layer of material with a thickness ranging from a few nanometers (single layer) to several microns.

Traditional particle removal methods can be divided into two types, *i.e.*, wet-cleaning and dry-cleaning. Liquid ultrasonic cleaning is a common wet-cleaning method (Gale and Busnaina, 1995). This method is thorough because ultrasound can penetrate anywhere the liquid enters. This method can be further categorized into ultrasonic cleaning (less than 100 kHz) and megasonic cleaning (0.8 to 1.2 MHz) (Busnaina et al., 1995). Brems et al. (2013) reviewed the removal techniques of acoustics and pointed out the high effectiveness of the technique in removing nanoparticles. Bakhtari et al. (2006) removed 63 nm polystyrene latex (PSL) particles from bare silicon wafers and wafers with 4 nm Si-cap film by acoustic streaming and the removal efficiency on both surfaces was ~99% in less than 10 min. of processing time. However, damage of surface/materials appeared as the frequency increased,

especially in the range of megasonic (Brems et al., 2013). Furthermore, wet-cleaning may have other disadvantages, such as being re-contaminated by dissolved chemicals, watermarks, etc. (Otani et al., 1995). Dry-cleaning methods are also proposed to remove nanoparticles on the surface. The most common dry-cleaning method is spraying with gas (*i.e.*, air, CO_2 and argon). That is, high-pressure gas passes through the nozzle to generate airflow to sweep particles on the surface (Donovan, 1990; Lee et al., 2009; Kim et al., 2012). Xu et al. (2009) removed 60% - 80% of SiO_2 particles from the surface with a jet spray nozzle, accelerated by N_2 gas flow. In addition to the above traditional methods, several new methods have been proposed to remove particles on the surface, such as gas bullets (Kim et al., 2013), plasma (Park et al., 2012) and electrostatics (Kawamoto and Guo, 2018).

Although the methods were developed to remove nanoparticles on the surface, no approach was reported to differentially remove nanoparticles on the surface based on the property of particles. Previous methods removed all the particles on a surface regardless of particle properties because these methods assumed that removed particles will not react with the surface, which is not always the case. Thus, this study aims to develop a method for differential removal of nanoparticles on the surface. To overcome the defects of microscopic technique, the developed method should be simple and effective. More importantly, the effectiveness of the methods should be able to be controlled. Both wet-cleaning and dry-cleaning methods were attempted. Blowing/air jet method is typically simple and frequently used among all dry-cleaning methods and the effect of this method is related to the pressure of air supply and time interval (Xu et al., 2009). As for the wet-cleaning process, generation of bubbles in the solution is the important mechanism for particle removal on the surface through the cavitation effect. In addition to cavitation, agitation is another but minor physical force to facilitate the particle

removal from the surface in ultrasonic treatment (Hauptmann et al., 2013; Yusof et al., 2016). Nanobubble and ultrasonic are both simple but efficient methods for generating abundant bubbles in the solution. The former one is novel and its effect is controlled by the time of treatment, while the latter one is traditional and the effect is related to the frequency and processing time. Therefore, these three methods were selected and tested. Although all these removal techniques have already existed, previous studies used them to remove all nanoparticles on a surface regardless of their properties. No studies were reported for differential removal of nanoparticles. The novelty of the method introduced in this study is the surface coating that changes the particle-surface interaction and thus non-targeted nanoparticles could be differentially removed while targeted nanoparticles are retained on the surface through this traditional removal technique, which is only a component/tool in the developed method. In this study, acidic particles were regarded as targeted particles that should be collected and reserved on the surface while non-acidic particles were non-targeted particles that would be removed from the surface. The surface was firstly coated with a thin film to alter the particle-surface interaction for potential differential removal of different particles. Atomic Force Microscope (AFM) was used to verify the particle removal efficiency of the developed method based on the differences in particle number before and after the application of the developed method. This is the first attempt to differentially remove unwanted particles and intentionally retain wanted particles on a surface. The method is expected to be targeted, simple, effective, low-cost and timesaving.

5.2 Particle removal efficiency by air-jet method

The AFM images of collected non-acidic and acidic particles on the coated detectors are shown in Fig.

5-1. The acidic particles deposited on the detector coated with a nano-film metal had a clearly distinguishable and unique reaction spot that formed a central elevation with a surrounding yellow halo, visualized through AFM, while no such reaction spot was observed in the image of non-acidic particles (Wang et al., 2012; Wang et al., 2014b; Lu et al., 2020). Noteworthily, there should not be any overlapping particles on the surface. Moreover, due to the difficulty of the standard acidic particle generation (SAPG) system to control the particle size, the sizes of the acidic particles (0.2 – 2 μm) generated were usually larger than those of the non-acidic particles (0.03 - 0.1 μm). In principle, the smaller the particles, the more difficult they are to remove (Bowling, 1988). That is, if the larger acidic particles cannot be removed, the smaller acidic particles will also remain. Therefore, it is not necessary to generate smaller acidic particles (*i.e.*, <0.2 μm). If the non-acidic particles are removed while the acidic particles remain on the surface using a method, it can prove that this method can be used to differentially remove particles.

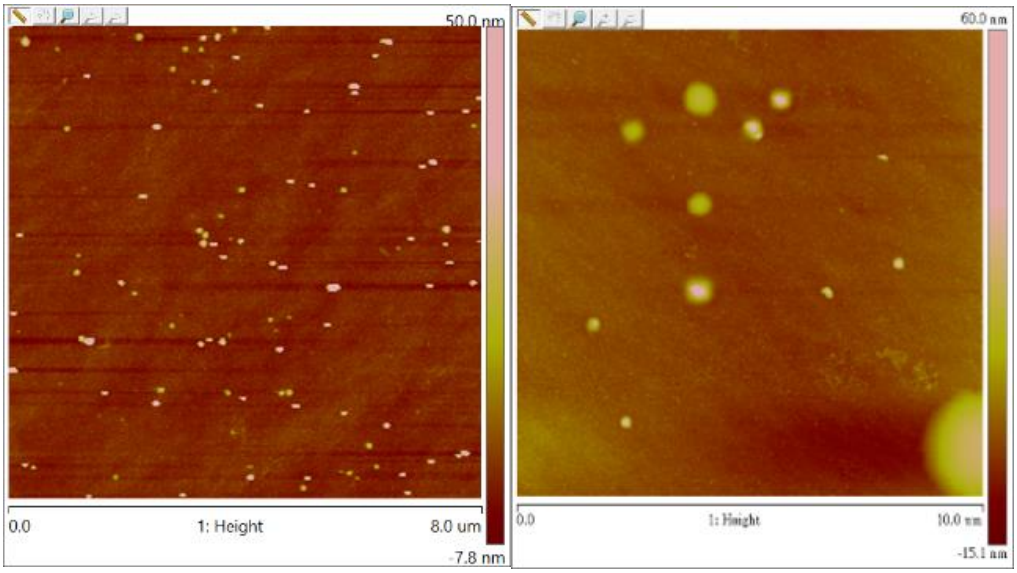

Fig. 5-1 AFM images of the collected standard non-acidic particles (left) and acidic particles (right)

The AFM images of detectors containing acidic and non-acidic particles after air jet treatment are shown in Fig. 5-2. Both acidic particles and non-acidic particles still remained on the surfaces. The

removal efficiency of non-acidic particles was as low as 5.1% ± 3.4%. Moreover, similar number of acidic particles was counted before and after the particle removal treatment. The results indicated that the air jet treatment was ineffective to remove nanoparticles on the surface, regardless of acidic or non-acidic particles. Indeed, the air jet method was commonly effective to remove large particles above 10 μm (Donovan, 1990). For nanoparticles (< 1μm), they were effectively removed from the surface by using some unique gases (*e.g.*, CO_2 or Ar) to generate particle beams (Lee et al., 2009; Kim et al., 2012). However, the process/system is complicated. On one hand, the treated gas (*e.g.*, CO_2 or Ar) needs to be re-cooled to its triple point of about -170℃. On the other hand, the process must be conducted in an ultra-high vacuum environment (*e.g.*, 10 Torr). Thus, the method is too complicated to be widely used.

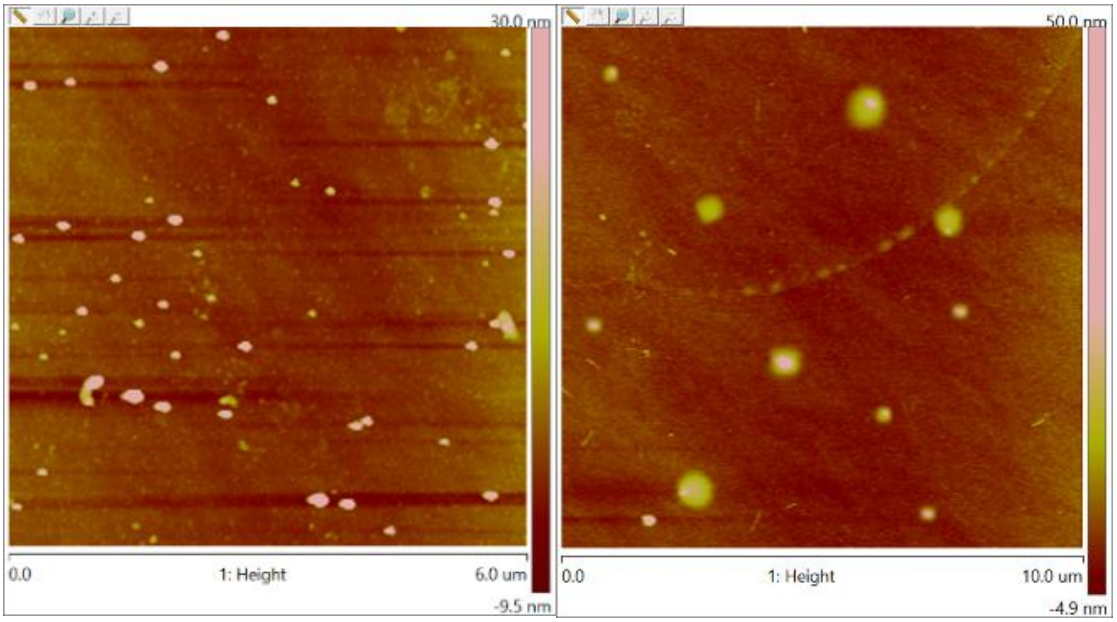

Fig. 5-2 AFM images of non-acidic (left) and acidic particles (right) after air jet treatment

5.3 Particle removal efficiency by nano-bubble method

Fig. 5-3 shows the AFM images of non-acidic and acidic particles after nanobubble treatment for

different times. Similar to the air jet treatment, after 10 nanobubble treatments, acidic particles remained on the surface, and the number of particles was the same as before the treatment (Fig. 5-1 and Fig. 5-3c). In addition, fewer non-acidic particles were observed on the surface, suggesting that the nanobubbles generated by the alcohol-water exchange process had a certain efficiency in removing non-acidic particles from the surface. By increasing the number of nanobubble treatments from 5 to 10, the removal efficiency of non-acidic particles insignificantly increased from 80.8% ± 8.5% to 89.3% ± 4.1% ($p > 0.05$). Nevertheless, this method still could not completely remove non-acidic particles from the surface. The failure of this method might be caused by the incomplete coverage of the nanobubbles on the entire surface, so the cleaning effect is not complete.

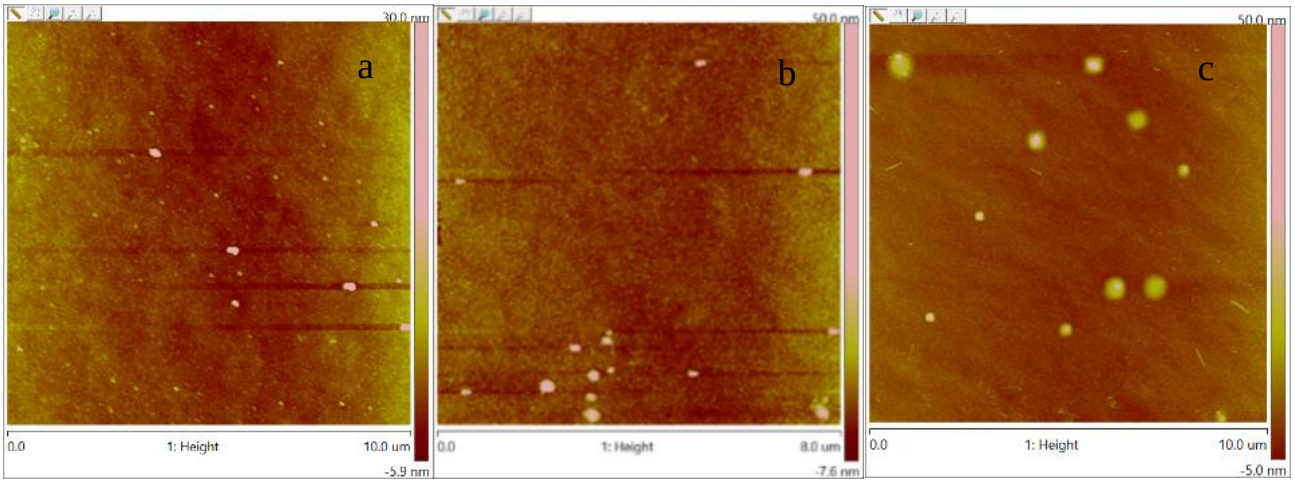

Fig. 5-3 AFM images of non-acidic (a: 5 treatments; b: 10 treatments) and acidic particles (c: 10 treatments) after nanobubble treatment

5.4 Particle removal efficiency by ultrasonic method

5.4.1 Ultrasonic treatment with DI water

Fig. 5-4 presents AFM images of non-acidic and acidic particles after ultrasonic treatment with DI water. On the one hand, both non-acidic and acidic particles were not completely removed from the

surface. On the other hand, after the ultrasonic treatment with DI water, although no visible damage to the surface was noticed, the surfaces seemed to be contaminated because many nano-impurities were observed. The contamination on the surface with acidic particles was much more serious than that with non-acidic particles, which was mainly due to the fact that 1) for the surfaces containing non-acidic particles, the long drying process might cause slight contamination owing to the reception of impurities from the external environment (*e.g.*, ambient air); and 2) for the surfaces with acidic particles, the dissolved acidic particles in DI water could be responsible for the severer contamination because sulfuric acid is soluble in DI water (Margarella et al., 2013). Eventually, the impurities and the dissolved components resulted in the contamination of the surface.

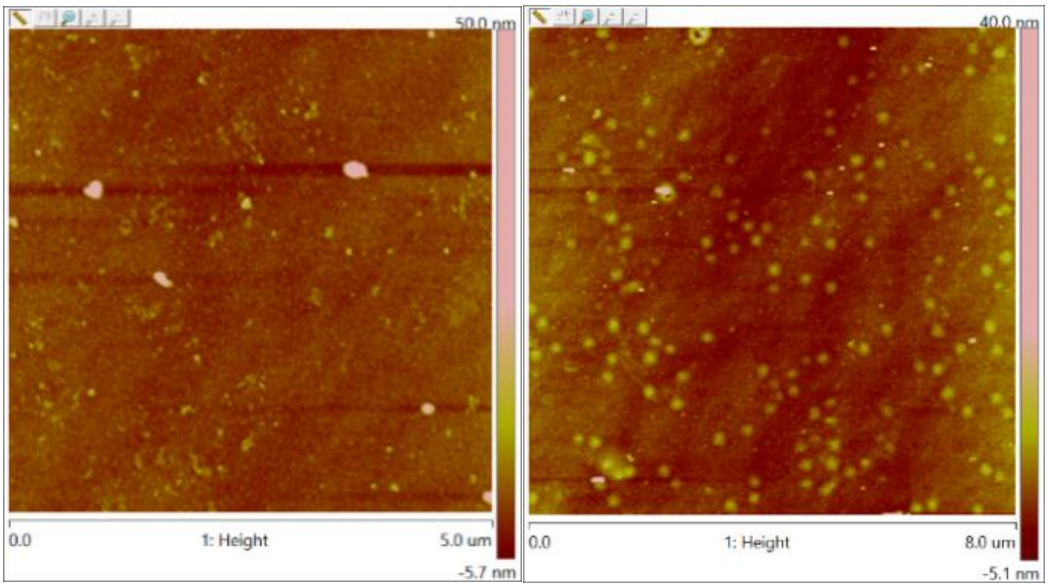

Fig. 5-4 AFM images of non-acidic (left) and acidic particles (right) after ultrasonic treatment with DI water

5.4.2 Ultrasonic treatment with ethanol

Fig. 5-5 shows the AMF images of non-acidic and acidic particles after ultrasonic treatment with ethanol for 30 min. For non-acidic particles, a few particles were still on the surface after the ultrasonic treatment for 10 and 20 min (Fig. 5-6), while the removal efficiency reached 100% after 30 min, *i.e.*,

all the non-acidic particles were removed. As for acidic particles, similar number of acidic particles was counted before and after the treatment, revealing that the ultrasonic treatment with ethanol was unable to remove the acidic particles from the surface of the detectors. Therefore, the ultrasonic treatment with ethanol was likely an effective method for differential removal of particles on the surface. To validate the efficiency of this method, Fig. 5-7 presents the AFM images of a detector surface containing both acidic and non-acidic particles before and after the ultrasonic treatment with ethanol for 30 min. Clearly, all the non-acidic particles were removed through the treatment, while acidic particles were still remained on the surface. It was proved that although the processing time of ultrasonic method (30 min.) was comparable with that of nanobubble method (~30 min.) and less than that of air jet treatment (60 min.), the ultrasonic treatment with ethanol was more effective with a higher removal efficiency (ultrasonic: ~100% vs. nanobubble: ~90% and air jet: ~5%). Noteworthily, the ultrasonic treatment with ethanol did not cause any visible damage and/or contamination to the thin film. Moreover, the intactness of the acidic particles (with a central elevation and a surrounding yellow halo) was maintained during the treatment (Fig. 5-8 and Fig. 5-9). Unlike the nanobubble method that could not provide full coverage of nanobubbles on the surface, the ultrasonic treatment with ethanol constantly generated bubbles where there is liquid by cavitation, leading to complete removal of non-acidic particles from the surface. However, since the interaction force between acidic particles and the surface was stronger, the acidic particles were not removed. In next section, the potential mechanism was further discussed.

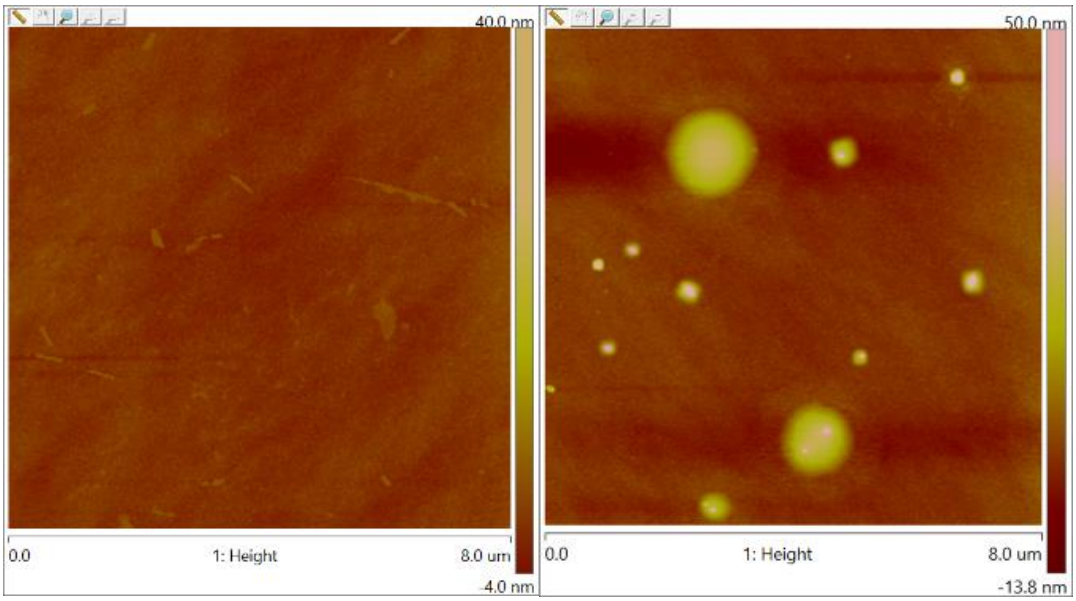

Fig. 5-5 AFM images of non-acidic particles (left) and acidic particles (right) after ultrasonic treatment with ethanol for 30 min.

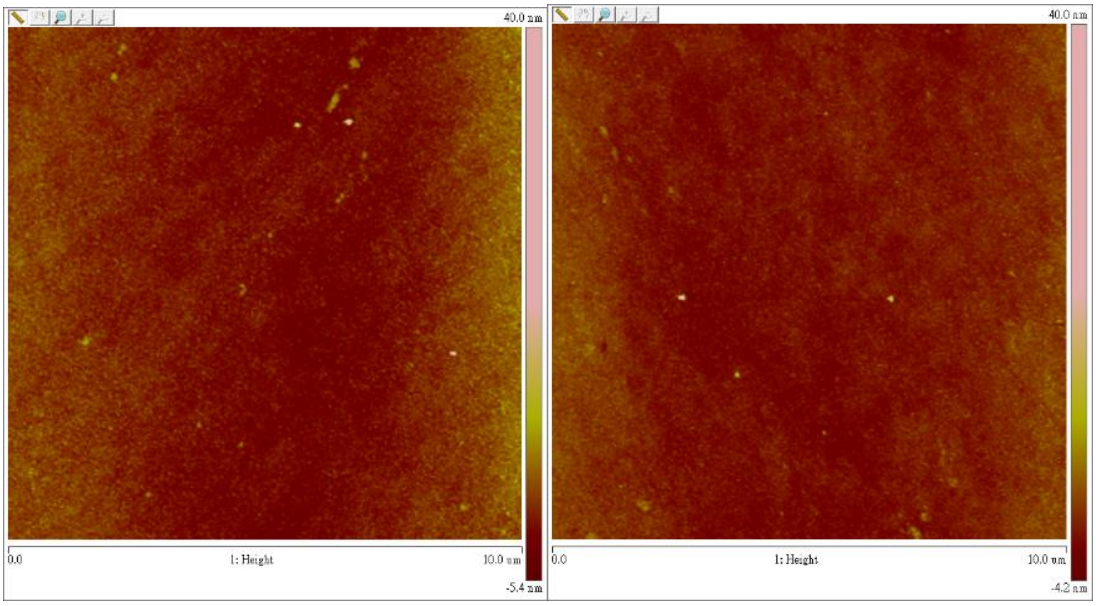

Fig. 5-6 AFM images of non-acidic particles after ultrasonic treatment with ethanol for 10 min. (left) and 20 min. (right)

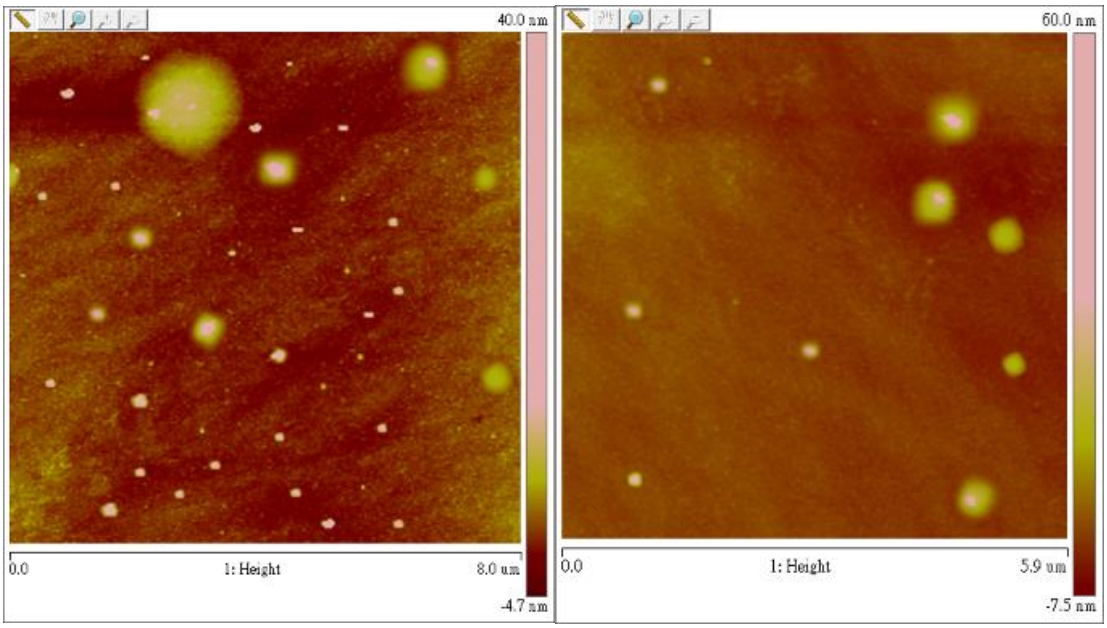

Fig. 5-7 AFM images of a detector surface containing acidic and non-acidic particles before (left) and after (right) ultrasonic treatment with ethanol for 30 min.

Moreover, verification was conducted using the modified QCM+DS system. Both standard acidic and non-acidic particles were generated and collected on the metal-QCM detectors. After a certain reaction time (more than one day), the detectors having non-acidic and acidic particles on the surface were ultrasonically cleaned with ethanol for 30 min., respectively. The frequencies of the metal-QCM detector before and after ultrasonic treatment were obtained. It was found that the frequency of the metal-QCM detector with acidic particles remained almost unchanged after 30 min. of ultrasonic cleaning (*i.e.*, frequency change < 0.1 Hz), revealing that acidic particles were unable to be removed by ultrasonic cleaning. Instead, ultrasonic treatment of the detector with non-acidic particles caused frequency enhancement, opposite to the frequency reduction caused by the mass of deposited particles, suggesting that non-acidic particles were removed during the ultrasonic process. In summary, ultrasonic treatment with ethanol effectively removed non-acidic particles on the surface of the metal-QCM detectors while retaining acidic particles.

5.5 Mechanism and implication

Fig. 5-10 shows the mechanism of differential removal of particles in ultrasonic treatment. The key to ultrasonic cleaning is the bubbles. These bubbles are created by sound waves when they move through water. This is known as cavitation, which is simply the formation of bubbles (cavities) in the solution. Generally, particles collected on the surface of a substrate are either physically adhered particles (*e.g.*, non-acidic particles in this study) or particles that react with the surface (*e.g.*, acidic particles). In the process of differential removal of particles, the physically adhered particles are removed from the surface due to cavitation collapse pressure. The space between physically adhered particles and the surface acts as a crevice, which entraps gas and improves cavitation erosion. The generated bubbles can enter the gaps between the physically adhered particles and the surface. In contrast, for the particles that react with the surface, the space between the particles and the surface is filled and no crevice exists (Fig. 5-8 and Fig. 5-9). Under such circumstance, no cavitation occurs, and bubbles cannot enter the gap to remove the particles.

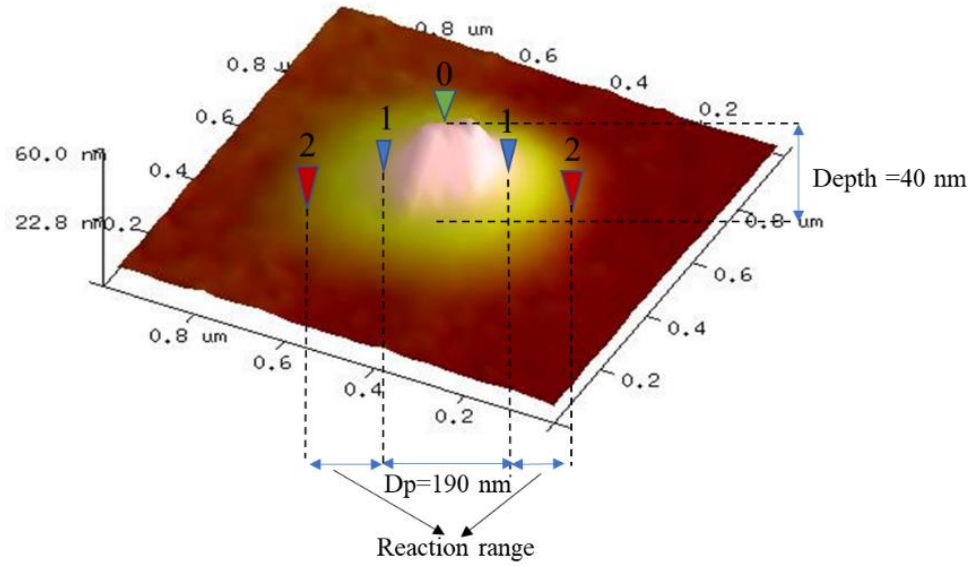

Fig. 5-8 AFM zoomed 3D-image of an acidic particle on the surface coated with a nano-film metal before the ultrasonic treatment

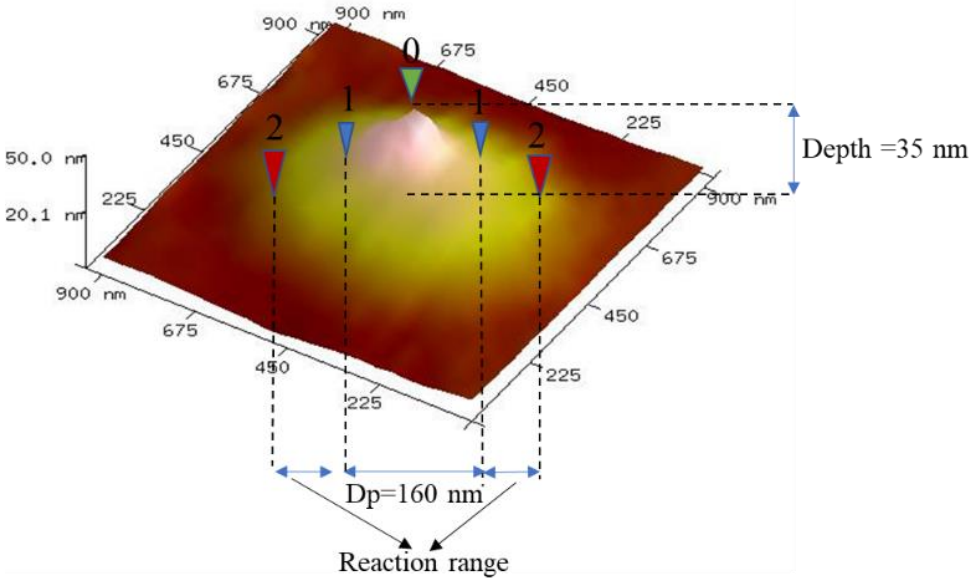

Fig. 5-9 AFM zoomed 3D-image of an acidic particle on the surface coated with a nano-film metal after the ultrasonic treatment

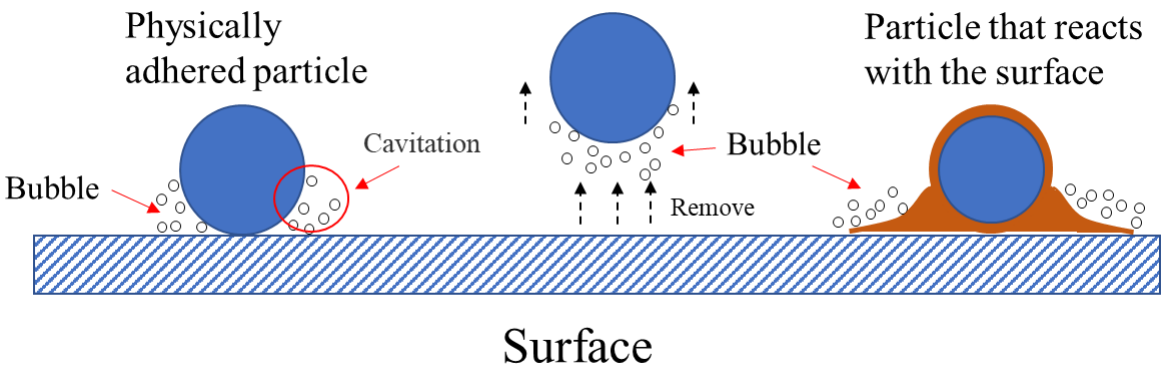

Fig. 5-10 Mechanism of differential removal of particles in ultrasonic treatment

Based on the results obtained from this study, there are several principles that need to be followed to differentiate the removal of nanoparticles on the surface. Firstly, the targeted particles should react with the surface, while the non-targeted particles only adhere to the surface. In order to react, the surface can be coated with a thin film of special material, which can react with the targeted particles. This process ensures the difference in particle-surface interaction between targeted particles and non-targeted particles. Secondly, the components of the targeted particles should not be dissolved in the solution used for sonication. Otherwise, the surface will be contaminated and even the targeted particles will be damaged. Lastly, the solution selected for ultrasonic treatment should be volatile to expedite the drying after treatment, and thus avoid contamination during the drying process.

5.6 Summary

In the study, methods were proposed and trialed for differential removal of nanoparticles on the surface. The aim was to remove non-targeted particles but remain targeted particles on the surface. Acidic particles were treated as the targeted particles. A thin metal film was coated on the surface of a substrate, so that the acidic particles can react with the surface, and subsequently the interaction between the

particles and the surface alters. Three methods were attempted for differential removal of nanoparticles, including air jet, nanobubble and ultrasonic methods. An AFM was used to determine the particle removal efficiency by comparing the difference in particle number before and after the treatment. Due to the strong particle-surface interaction between the acidic particles and the coated surface, the acidic particles adhered to the surface regardless of before or after the treatment. For the non-acidic particles, air jet method and nanobubble method (10 treatments) were not able to completely remove them from the surface with the particle removal efficiency of 5.1% ± 3.4% and 89.3% ± 4.1%, respectively. In contrast, the particle removal efficiency of the non-acidic particles reached 100% in ultrasonic treatment. Noteworthily, ethanol was a better solution than DI water in ultrasonic treatment, which avoided contamination. At last, the mechanism of differential removal of nanoparticles from the surface was discussed. In ultrasonic treatment, the non-acidic particles are removed from the surface by cavitation, which creates bubbles in the gaps between the non-acidic particles and the surface. In contrast, the space between the acidic particles and the surface is filled, so bubbles cannot enter the crevice to remove the particles.

Chapter 6 A novel semi-automatic method for measuring acidic ultrafine particles in the atmosphere

6.1 Introduction

Accumulated evidence strongly suggested that the number of acidic ultrafine particles (AUFPs) is closely correlated with total mortality, morbidity and hospital admissions for respiratory diseases (Thurston et al., 1989, 1992, 1994; Lippmann and Thurston, 1996; Peters et al., 1997; Wichmann et al., 2000; Cohen et al., 2000). In addition to health issues, AUFPs have impacts on climate, visibility and secondary organic aerosol (SOA) production (Kim et al., 1994; Li et al., 2010). Hence, it is critical to be able to distinguish AUFPs from the total number of ultrafine particles (UFPs), and to quantify the number concentrations of AUFPs in the atmosphere. Only with this information can effective control measures be formulated and implemented. However, it was not until 2012 that reliable and methodologically validated measurement techniques appeared to obtain the number concentrations and size distribution of AUFPs (Cohen et al., 2004a and 2004b). Two methods were developed by our group in 2012 and 2014, respectively, to measure the AUFPs in the atmosphere with the nano-film detectors (*i.e.,* electrostatic precipitator (ESP) + atomic force microscope (AFM) and diffusion sampler (DS) + AFM, respectively) (Wang et al., 2012 and 2014b). In the previous methods, nano-film detector was generated by using the magnetron sputtering system to coat a 25 nm metallic film on a silicon wafer. Afterwards, the detectors were deployed in the ESP and/or DS for the collection of UFPs in the atmosphere. Unlike non-acidic UFPs, AUFPs deposited on the detectors caused reaction spots, which were examined by an AFM to distinguish AUFPs from non-acidic UFPs and measure their sizes. Thus, enumeration and size measurement of AUFPs were achieved according to the number and diameter of

particles deposited on the detectors after considering the scanning area, collection efficiency and sampling duration. Both methods proved that nano-metal film detector was a reliable method to differentiate AUFPs from UFPs and to quantify AUFPs.

Although the above methods can be used to quantify the concentration of AUFPs, the fact is that these methods are offline and require enormous resources to support AFM analysis. The AFM is a widely used technique in aerosol studies due to its high imaging resolution (1 nm in lateral and 0.1 nm in vertical) and few limitations (Heath and Scheuring, 2018). The AFM operation does not require special environment (*e.g.*, vacuum and high/low temperature) and sample pre-treatments. However, the AFM instrument is neither inexpensive nor compact, nor easy to operate, which hinders its wide application in field measurements. Moreover, as a manual instrument, AFM analysis is highly time-consuming. Numerous AFM scans are required to reduce the uncertainty caused by incomplete scanning of the entire detector. Thus, it is impractical to obtain vast amounts of AUFPs data using the previous methods. It is necessary to improve/revise the previous methods so that AUFPs can be enumerated and sized online after collection on a nano-film detector without using AFM.

This study developed a novel method for semi-automatic measurement of AUFPs in the atmosphere, named QCM+DS method. Here, the semi-automatic means “partly operated by machinery, not human”. In the study, the QCM+DS system collected AUFPs and non-AUFPs in the atmosphere and measured the masses of deposited particles automatically. Manual work was used to remove the non-AUFPs on the surface of detector so that the QCM system could obtain the mass of AUFPs subsequently. The QCM+DS system was developed by integrating the previous DS with quartz crystal microbalances (QCM). The QCM is an extremely sensitive online mass sensor with a detection capacity in the sub-

nanogram range (Ward and Buttry, 1990; McCallum, 1989, Chen et al., 2016). Noteworthily, the linear relationship of QCM response with mass is only applicable to uniform, rigid and/or thin-film deposition (Buttry, 1991). In the case of depositing soft polymers or biomolecules, the relationship between mass and frequency may be destroyed. Owing to its high sensitivity, fast response and real-time detection capabilities, QCM offers the opportunity to improve the previous DS and nano-film detectors. By functionalizing the surface of the QCM detector with a nano-film of metal, QCM could use its real-time measurement capabilities to monitor the temporal variations of ambient AUFPs. That is, deployment of the coated QCM detectors inside the DS would enable us to conduct long-term online measurements. Prior to sampling, the sensitive response of the QCM system and the collection efficiencies of the QCM+DS system were calibrated using standard acidic and non-acidic particles. Reactions between the AUFPs and nano-film detectors were guaranteed by confirming much lower than one-layer deposition of particles on the detectors. After calibration, the QCM+DS system was deployed in an outdoor measurement together with the previous DS+AFM method and a commercial instrument (*i.e.*, Scanning Mobility Particle Sizer (SMPS)) for method validation.

6.2 Sensitivity factor of QCM

6.2.1 Calibration of sensitivity factor using non-acidic particles

Fig. 6-1 shows the calibrations of sensitivity factor of the QCM system using non-acidic particles with sizes of 32 nm, 53 nm and 102 nm. The mass of deposited particles per unit area of each sample acquired from the CPC was plotted against the frequency changes measured by the QCM system. The slope for each size of particles was the sensitivity factor according to Eq. 3-9. The surface area of the

quartz crystal (A) was equal to 0.4 cm^2. Particles of 102 nm and 53 nm were PSL particles while 32 nm particles were sodium chloride as the particle generator was unable to generate high enough concentrations of 32 nm PSL particles for collection. The densities of PSL and sodium chloride were 1.05 and 2.08 g/cm^3, respectively. Hence, the calibrated K value was 52.23 ± 4.90 $Hz \cdot cm^2/\mu g$ (R^2=0.99) for 102 nm particles, 59.83 ± 6.64 $Hz \cdot cm^2/\mu g$ (R^2=0.99) for 52 nm particles and 52.80 ± 8.49 $Hz \cdot cm^2/\mu g$ (R^2=0.99) for 32 nm particles. It can be seen that the calibrated K values were similar to the initial value of 56.6 $Hz \cdot cm^2/\mu g$ with a deviation of 3.0% set by the manufactory.

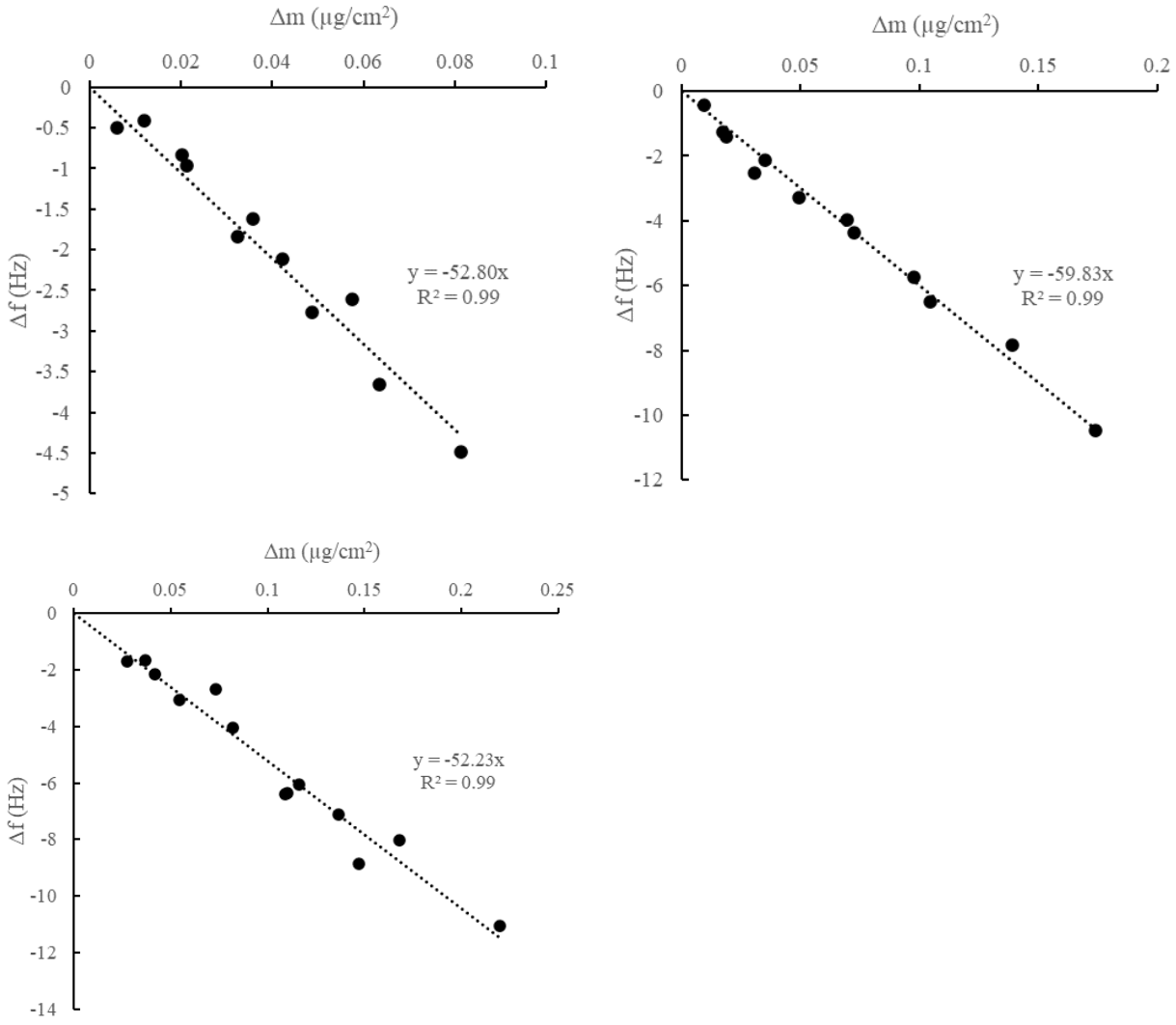

Fig. 6-1 Calibrations of sensitivity factors of the QCM system using different sizes of non-acidic particles (upper left panel: 32 nm; upper right panel: 53 nm; and lower panel: 102 nm)

6.2.2 Calibration of sensitivity factor using acidic particles

The calibration of sensitivity factor using acidic particles was similar to that using non-acidic particles. The same three sizes of acidic particles were generated and measured by both QCM system and CPC with the help of DMA. The density of acidic particles was determined as follows. Because the density of ultrafine carbon black particles was 0.55 g/cm^3 (Gilmour et al., 2004), and sulfuric acid accounted for 44.5%, 27.8% and 14.3% of the mass of 32 nm, 53 nm and 102 nm acidic particles, respectively (Zhang et al., 2008), the density of 102 nm acidic particle was estimated to be 0.73 g/cm^3 (*i.e.* ρ=0.5×(1-14.3%)+1.8×14.3%=0.73 g/cm^3). Likewise, the density of 32 nm and 53 nm acidic particles was 1.11 g/cm^3 and 0.90 g/cm^3, respectively. The calibration results are shown in Fig. 6-2. The calibrated sensitivity factors were 53.97 ± 6.07 Hz·cm^2/μg (R^2=0.96), 57.84 ± 17.98 Hz·cm^2/μg (R^2=0.95) and 59.13 ± 14.17 Hz·cm^2/μg (R^2=0.96) for 32 nm, 53 nm and 102 nm acidic particles, respectively. It can be seen that the results were similar to those of non-acidic particles and the initial value set by the manufactory. The R^2 were not as high (0.95-0.96) as those for non-acidic particles due to the fluctuation of the SAPG system. This uncertainty is unlikely to propagate into the real sampling since the concentration of ambient particles is relatively stable if no emission sources crop up. Overall, the acidic and non-acidic particles produced the same responses on the QCM system, and the initial value of sensitivity factor did not change after modification. Thus, the initial K value set by the manufactory was still adopted (*i.e.*, 56.6 Hz·cm^2/μg) in the QCM+DS system in this study.

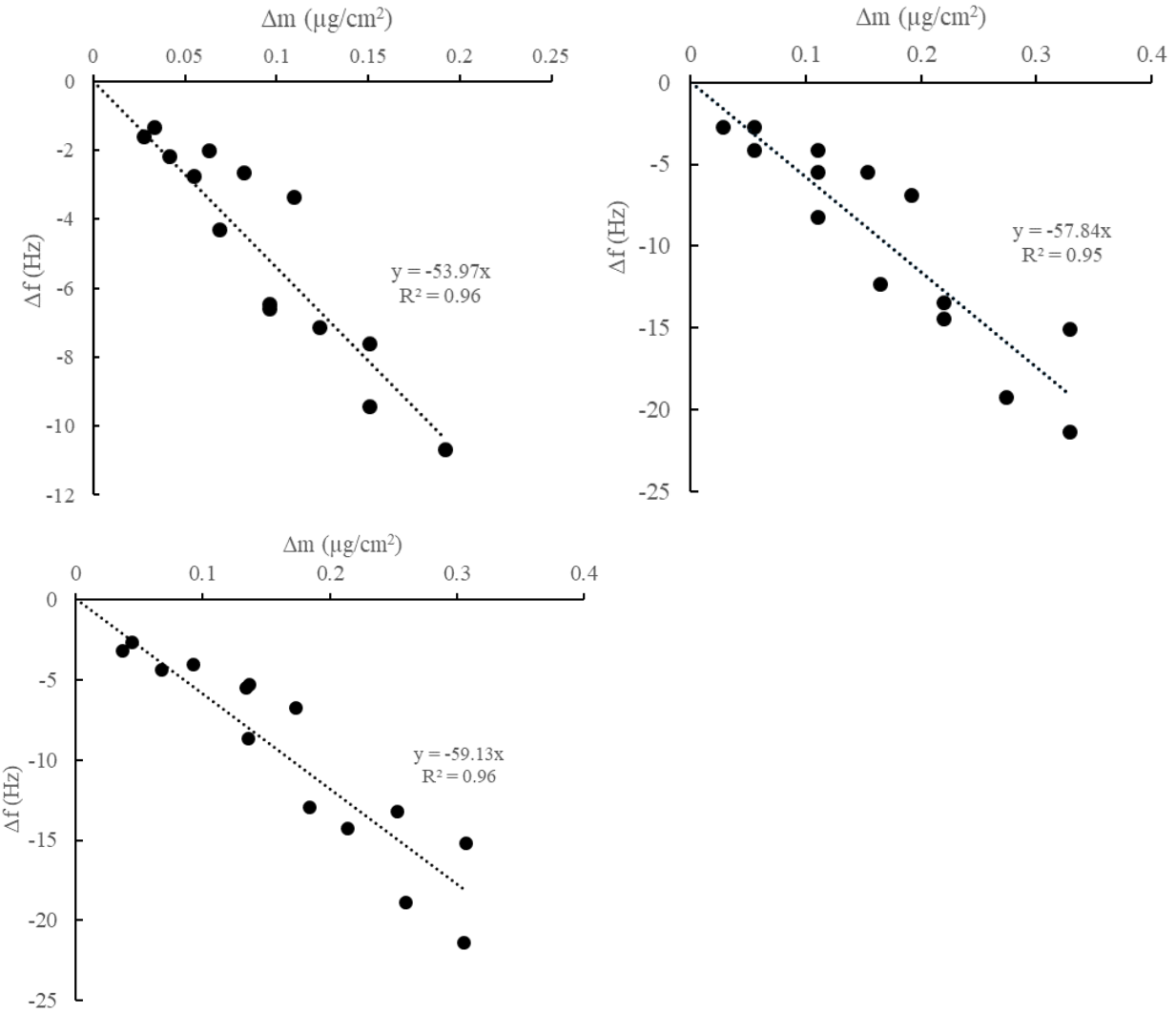

Fig. 6-2 Calibrations of sensitivity factors of the QCM system using different sizes of acidic particles (upper left panel: 32 nm: upper right panel: 53 nm; lower panel: 102 nm)

6.3 Confirmation of less than one-layer deposition

There were two issues about the feasibility of the QCM application into the DS for the measurement of acidic ultrafine particles. One was the recognizability of acidic particles by the QCM system and the other was the mass sensitivity of the QCM system. To distinguish the acidic particles, the deposition of particles was required to strictly fulfil single-layer coverage on the surface of the metal-QCM detectors in order to cause the reaction between a single acidic particle and the coated detector.

The maximum frequency change of the QCM system (*i.e.*, Δf_{max}) during sampling was reached after a single-layer of closely-spaced particles was deposited on the surface. However, in practice, it was impossible to fully obtain/fulfil single-layer coverage of particles on the surface, not to mention the detection of a single-layer deposition. As such, the deposition of particles needed to be far less than single-layer coverage during sampling to avoid particles stacking. Meanwhile, it was essential to ensure that enough frequency change (*i.e.*, Δf_{enough}, > 10 times the detection limit) could be detected in the case of a far less than single-layer deposition based on theoretical calculation (Shrivastava and Gupta, 2011). There were some assumptions in theoretical calculation for Δf_{enough}: i) the coverage rate of particles was twentieth (*i.e.*, 0.05); ii) the particles deposited on the surface had the same diameter; and iii) the average density of particle was $\rho = 2.5$ g/cm^3 (Ferro et al., 2004; Cha and Olofsson, 2018). The surface area of the quartz crystal $A = 0.4$ cm^2. For close-space arrangement of the particles, the surface usage rate $\lambda \approx 0.9$ according to geometry (Binks and Olusanya, 2017). Therefore, the particle number (N) for twentieth coverage rate of single-layer deposition $N = 0.05 \cdot \lambda A/s = 0.05 \cdot \lambda A/\pi r^2$. The s is the cross-sectional area of the particle and r is the geometrical radius of the particle. The mass of a single particle $m = V\rho = 4\pi\rho r^3/3$. Thus, the total mass $M = Nm = 0.05 \cdot 4\rho r\lambda A/3$. As the relationship of frequency change with the mass of particles deposited on the surface followed the Sauerbrey's equation (Eq. 3-7), the theoretical Δf_{enough} for different sizes of particles (*i.e.*, 5-350 nm) were calculated. The frequency changes of 5% coverage for single-layer deposition of particles ranged from 2.1 Hz to 148.6 Hz for 5 nm and 350 nm particles, respectively (Fig. 6-3). In theory, the highest resolution of the QCM system to detect frequency change is able to reach 0.01 Hz, which is significantly lower than the frequency change presented in Fig. 6-3, regardless of particle sizes. In

conclusion, sufficient frequency change could be obtained even in the case of a far less than single-layer deposition of particles.

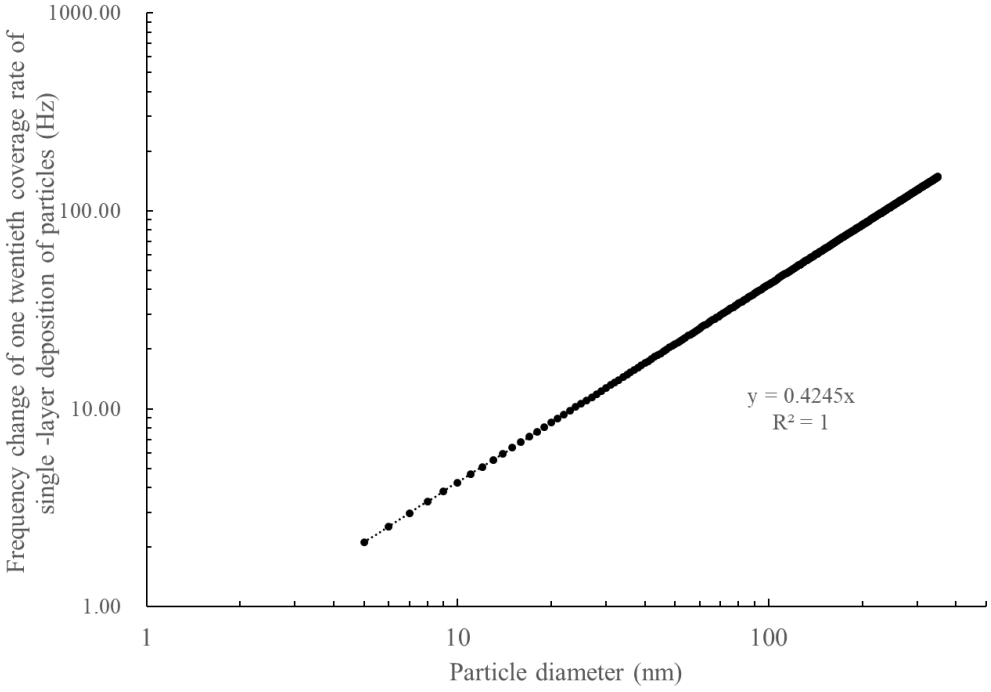

Fig. 6-3 Theoretical frequency change of twentieth coverage rate of single-layer deposition for different sizes of particles

Even so, it was still necessary to confirm that particles stacking would not occur under the circumstance of much lower than 100% coverage for single-layer deposition of particles. Otherwise, some acidic particles might stack upon others and could not react with the coated detector. To confirm the hypothesis, polydisperse sodium chloride particles (~10^6/cm^{-3}) were generated by a particle generator and then collected on the nano-film detectors for a certain time period (*e.g.*, 30 min., 45 min. and 60 min.) using an electrostatic precipitator (ESP) with a flow rate of 0.3 L/min. In theoretical calculation, the coverage percentage was around 5 - 20%. Detectors with different collection times were scanned by an AFM. The specific coverage percentages for each detector were determined through a function in the software of the AFM called bearing analysis. In the analysis, all the bumps

(particles) above the surface of the nano-film were included to determine the coverage percentages. Fig. 6-4 presents deposited ultrafine particles on the metal-QCM detectors under different coverage percentages. All the particles above the surface were marked in blue. From upper left to lower right panels, the coverage percentages were 3%, 5%, 10% and 13%, respectively. It was found that particles were well separated at low coverage percentages (*i.e.*, 3%, 5% and 10%), while particles stacking appeared (inside the circle in green) at high coverage percentage of 13% (Fig. 6-4). Therefore, to definitely avoid particles stacking, the coverage percentage should not be higher than 10% during field measurements. Based on the concentrations of UFPs we measured at the same site in previous study (Wang et al., 2014b) and preliminary calculations, it would need more than 30 days for a 10% coverage percentage of particles on the surface of a detector. Hence, 2-3 days sampling duration for each sample collected by the QCM+DS system in ambient air would be workable. Under such conditions, sufficient frequency change was able to be obtained while particles stacking would not occur.

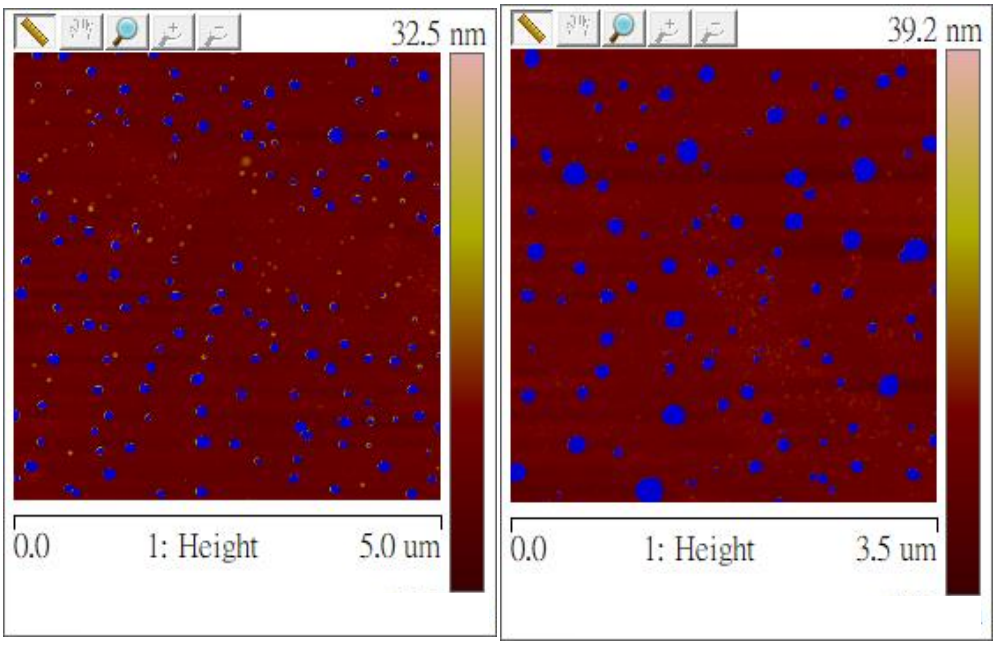

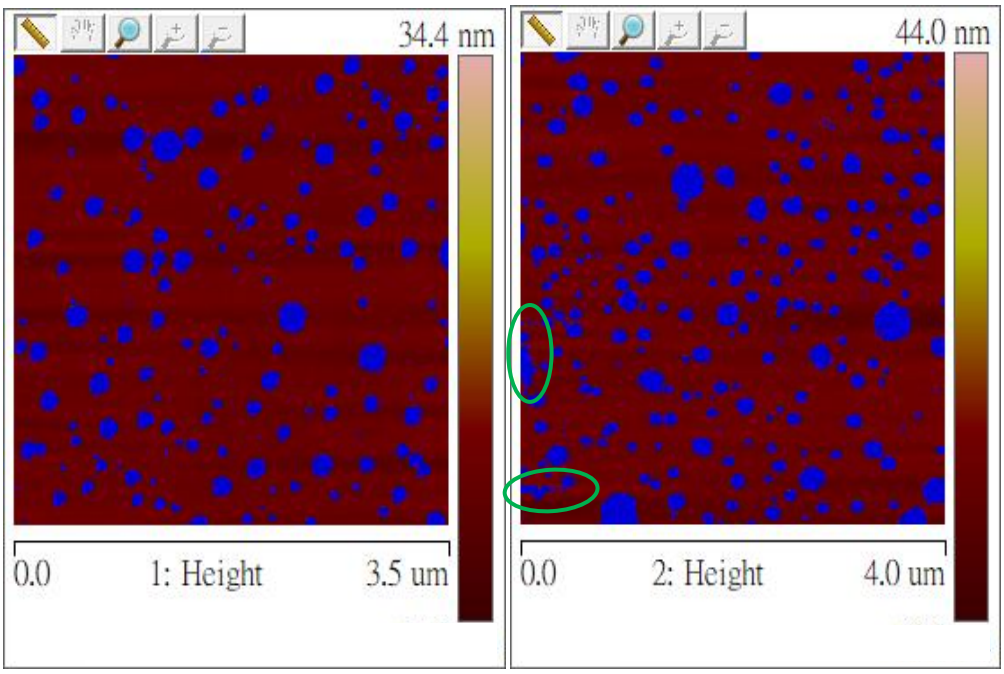

Fig. 6-4 Deposition of ultrafine particles under different coverage percentages. Upper left panel: 3%; upper right panel: 5%; lower left panel: 10%; and lower right panel: 13%

6.4 Collection efficiencies of the QCM+DS system

Fig. 6-5 illustrates the collection efficiencies of the QCM+DS system at different flow rates for different sizes of particles. Obviously, all the stepwise collection efficiencies in the QCM+DS system deceased with the increase of flow rate, regardless of particle size, probably owing to the fact that the deposition positions of the particles were beyond the sampling spots inside the system after the increase of flow rate. It also implied that there was a significant dependence of diffusion deposition on the flow rate. In addition, the collection efficiencies on small particles were higher than those on large particles when the flow rate was the same, consistent with the theory of diffusion deposition, suggesting that the deposition of particles in the QCM+DS system obeyed the principle of diffusion deposition (Hinds, 1999; Wang et al., 2014b). The relationships between the experimentally determined collection efficiencies and deposition parameters were determined by multivariate nonlinear regression analysis

(Origin Pro 2017, USA).

Specifically, at the sampling spot A (Fig. 3-10), the values of deposition parameter (μ) for most experimental scenarios were smaller than 0.003. According to our previous study, the collection efficiency (η_a) had a power–law relationship with μ (Wang et al., 2014b). Thus, the collection efficiency as a function of μ was estimated from the 12 experimental scenarios by a model: $\eta_a = \alpha_1 \times (\mu_2^{\alpha 2} - \mu_1^{\alpha 2})$ using the Quasi-Newton method. The μ_1 and μ_2 are the independent variables. The two parameters α_1 and α_2 are constants. After model simulations, the semi-empirical equation for the diffusive collection efficiency at the sampling spot A was obtained as follows (Eq. 6-4):

$$\eta_a = 20.532 \times (\mu_2^{0.671} - \mu_1^{0.671}) \qquad \text{Eq. 6-4}$$

where μ_1 and μ_2 represent the deposition parameters at the starting and ending points of sampling spot A (*i.e.*, 8.14 cm and 8.86 cm, respectively), and are calculated using Eq. 3-4 and Eq. 3-5; the constant α_1 is a modified factor and α_2 is a power-law exponent obtained from experimental data, which are 20.532 and 0.671 (regression coefficient r = 0.914) in Eq. 6-4, respectively.

However, at the sampling spots B and C, the relationships between collection efficiencies (η_b and η_c) and μ were different. On one hand, most values of μ at the two sampling spots were larger than 0.003, except for large particles (*e.g.* > 200 nm) at high sampling flow rate (*e.g.*, > 0.5 L/min) at sampling spot B, indicating that there was an exponential relationship of μ with η_b and η_c according to the theory of diffusion deposition (Hinds, 1999). On the other hand, the calibrated collection efficiency did not show a power-law function with the sampling flow rate for every size of particles at these two sampling spots in the previous DS (Wang et al., 2014b). Therefore, different exponential models (*i.e.*, $\eta_b = \beta_1 \times [\exp(\beta_2 \times \mu_3) - \exp(\beta_2 \times \mu_4)]$ and $\eta_c = \gamma_1 \times [\exp(\gamma_2 \times \mu_5) - \exp(\gamma_2 \times \mu_6)]$) were adopted to determine the η_b

and η_c as a function of μ by multivariate nonlinear regression method. The constant β_1 and γ_1 were the modified factors for the semi-empirical equations; β_2 and γ_2 were the determined constants for the independent variables at the sampling spots B and C, respectively. By fitting the 12 experimental scenarios at each sampling spot into the two models, the semi-empirical equations for the diffusive collection efficiency at the sampling spots B and C (*i.e.*, η_b and η_c) were obtained (Eq. 6-5 and Eq. 6-6), respectively:

$$\eta_b = 7.435 \times [\exp(-20.132 \times \mu_3) - \exp(-20.132 \times \mu_4)] \quad \text{Eq. 6-5}$$

$$\eta_c = -11.253 \times [\exp(7.520 \times \mu_5) - \exp(7.520 \times \mu_6)] \quad \text{Eq. 6-6}$$

where μ_3, μ_4, μ_5 and μ_6 represent the deposition parameters at the starting and ending points of sampling spots B (19.79 cm and 20.51 cm) and C (46.89 cm and 47.61 cm), respectively; constants β_1 and β_2 are 7.435 and -20.132 ($r = 0.959$) for the collection efficiency of sampling spot B, respectively (Eq. 6-5); and γ_1 and γ_2 are -11.253 and 7.520 ($r = 0.971$) for the collection efficiency of the sampling spot C, respectively (Eq. 6-6).

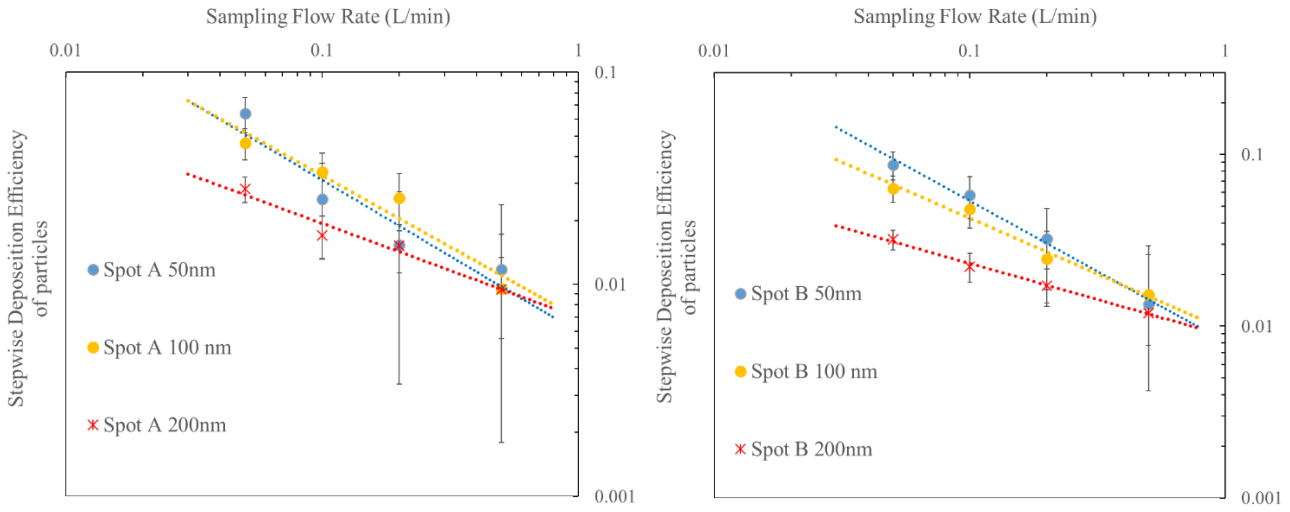

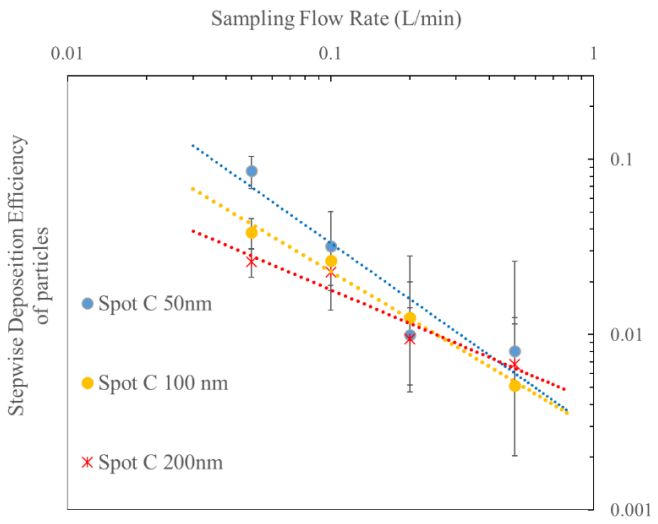

Fig. 6-5 Collection efficiencies of the QCM+DS system at the sampling spot A (upper left), spot B (upper right) and spot C (lower) at four different flow rates for three different sizes of particles

6.5 Validation via a field measurement

Table 6-1 lists the concentrations of AUFPs and total UFPs measured by the QCM+DS system on 11-13 April 2019 as an example. The mass concentrations of UFPs in spots A, B and C were 5.03, 2.85 and 6.49 μg/m^3, respectively. By considering the proportion of AUFPs in UFPs through the removal process of non-AUFPs, the mass concentrations of AUFPs were further determined to be 1.07, 0.74 and 0.97 μg/m^3 at spots A, B and C, respectively. Number concentrations of UFPs and AUFPs were estimated by converting mass concentrations using the assumed density of particles (*i.e.*, 2.5 g/cm^3) (Ferro et al., 2004; Cha and Olofsson, 2018). Noteworthily, although the mass concentrations of UFPs and AUFPs measured at spot B were the lowest among the three sampling spots, the number concentrations were the highest. These were mainly caused by the higher mass concentrations of smaller sizes of particles (*i.e.*, 5.5 - 17 nm) measured at spot B than those at spots A and C, which significantly enhanced the calculated total particle number and thus led to high number concentrations.

Eventually, the values at sampling spots A, B and C were averaged and regarded as the average concentrations of UFPs and AUFPs on these days.

Table 6-1 Concentrations of AUFPs and total UFPs measured by the QCM+DS system on 11-13 April, 2019

Data and Time	*Sampling Spot*	*Particle size bin (nm)*	*Frequency change (Hz)*	*Total mass of particles in the sample air (μg)*	*Estimated total number of particles in the sample air*	*Proportion of AUFPs in UFPs (%)*	*Mass concentration of UFPs ($\mu g/m^3$)*	*Number concentration of UFPs (cm^{-3})*	*Mass concentration of AUFPs ($\mu g/m^3$)*	*Number concentration of AUFPs (cm^{-3})*
11-13 April 2019	Spot A	124~150	1.72	0.79	2.24×10^8	21.2	5.03	1.16×10^4	1.07	2.44×10^3
		75~112	1.09	0.37	4.35×10^8					
		47~69	0.53	0.11	5.04×10^8					
		30~43	0.31	0.03	5.11×10^8					
		19~27	0.22	0.02	8.61×10^8					
		5.5~17	0.12	0.003	5.38×10^8					
	Spot B	124~150	1.10	0.39	1.09×10^8	26.3	2.85	2.10×10^4	0.74	5.47×10^3
		75~112	0.72	0.23	2.76×10^8					
		47~69	0.57	0.08	3.54×10^8					
		30~43	0.22	0.02	2.94×10^8					
		19~27	0.17	0.01	6.65×10^8					
		5.5~17	0.16	0.02	3.86×10^9					
	Spot C	124~150	0.98	1.13	3.20×10^8	15.7	6.49	1.59×10^4	0.97	2.39×10^3
		75~112	0.77	0.41	4.92×10^8					
		47~69	0.42	0.10	4.34×10^8					
		30~43	0.40	0.04	6.69×10^8					
		19~27	0.49	0.02	1.04×10^9					
		5.5~17	0.36	0.01	1.25×10^9					

Table 6-2 Comparisons of concentrations of AUFPs and total UFPs measured by the QCM+DS system, the SMPS and the previous DS+AFM system

Date	***SMPS***		***Previous DS+AFM***				***QCM+DS***			
	Number concentration of UFPs $\times 10^4$ (cm^{-3})	Estimated mass concentration of UFPs ($\mu g/m^3$)	Number concentration of UFPs $\times 10^4$ (cm^{-3})	Estimated mass concentration of UFPs ($\mu g/m^3$)	Number concentration of AUFPs$\times 10^3$ (cm^{-3})	Estimated mass concentration of AUFPs ($\mu g/m^3$)	Mass concentration of UFPs ($\mu g/m^3$)	Estimated number concentration of UFPs $\times 10^4$ (cm^{-3})	Mass concentration of AUFPs ($\mu g/m^3$)	Estimated number concentration of AUFPs $\times 10^3$ (cm^{-3})
11-13 April 2019	0.86±0.39	3.14±1.16	1.69±0.38	2.22±0.50	0.96±0.53	0.13±0.07	4.79±1.68	1.62±0.43	0.93±0.15	3.43±1.62
13-15 April 2019	0.91±0.38	4.84±2.34					4.65±3.00	1.42±0.51	0.84±0.35	2.79±0.71
15-17 April 2019	1.27±0.57	4.28±1.92	1.89±0.78	2.61±0.40	3.61±1.23	0.39±0.16	4.82±3.41	1.32±0.56	0.88±0.54	2.52±0.53
23-25 April 2019	0.67±0.32	2.86±1.27	1.23±0.67	1.91±1.06	4.21±2.45	0.62±0.28	2.88±1.26	0.92±0.11	0.56±0.21	1.94±0.74

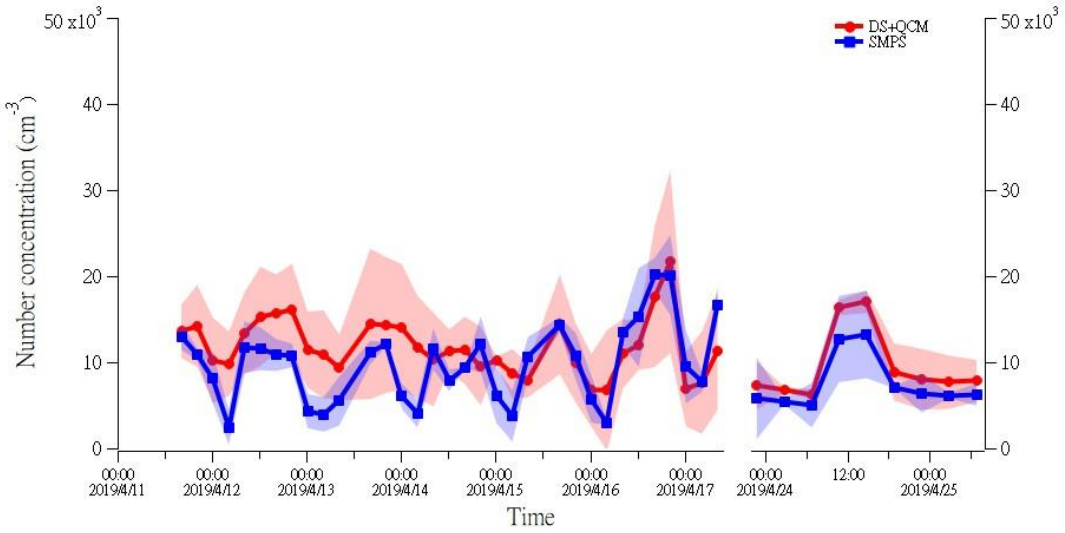

Fig. 6-6 Temporal variations of number concentrations of UFPs measured by QCM+DS system and SMPS on 11-25 April 2019

48.1 8.78 18.3 4.21

Table 6-2 compares the results of SMPS, previous DS+AFM and the QCM+DS system from the field measurement. Note, only one set of detectors was collected on 11-15 April using the previous DS given the levels of particles on these days and the sensitivity of the previous DS detectors. The average UFP number concentrations and mass concentrations measured by the QCM+DS system were in line with those measured by previous DS+AFM method ($p > 0.05$) and SMPS ($p > 0.05$), implying the consistency of the QCM+DS system. To further evaluate the performance of the QCM+DS system, the temporal variations of UFP number concentrations measured by the QCM+DS system and the SMPS on 11-25 April 2019 are shown in Fig. 6-6. Concentrations of UFPs measured by the QCM+DS system and the SMPS were both acquired and compared at a 4-hours interval. Overall, the temporal variation trends of the UFP concentrations measured by both methods were similar with a good index of agreement (IOA = 0.77), which again indicated the consistency of results from both methods. Low levels of UFPs were usually found at night, while high UFP concentrations were observed at daytime hours, in agreement with the pattern of human activities. The discrepancy of results was mainly attributed to two factors. On one hand, the QCM+DS system estimated the UFP number concentrations based on the density of UFPs reported in previous study, which might cause uncertainties. On the other hand, the QCM+DS system was not as sensitive as the SMPS, not only in time-resolution but also in size-resolution, which likewise led to a certain degree of uncertainty in determining UFP concentrations. Specifically, SMPS measured the particle concentration every 10s for a

specific size, while the QCM+DS system acquired the particle concentration in a size bin every 15 min. To achieve a higher time-resolution and/or size-resolution, improvements could be made by replacing the 5 MHz QCM detector in the study to a more sensitive QCM detector (*e.g.*, 10 MHz, 20 MHz and 50 MHz QCM detectors) (Pohanka, 2017).

As for the concentrations of AUFPs, only the data obtained from the previous DS+AFM method and the QCM+DS system were compared since the SMPS was unable to measure the AUFP concentrations (Table 6-2). Generally, the AUFP concentrations measured by the QCM+DS system were higher than those measured by the previous DS+AFM method. Difference was significant in mass concentration ($p < 0.05$) but not obvious in number concentration ($p > 0.05$). In addition to the impact of assumed particle density, the difference may be caused by the random selection of the AFM scanning areas in the DS+AFM method and the measurement deviation of the QCM system. The proportions of AUFPs in UFPs measured in the study (DS+AFM: 17.5% ± 5.8% and QCM + DS: 20.3% ± 7.0%) were significantly decreased compared to those measured in 2010 (DS+AFM: 44.9% ± 8.6%) at the same site regardless of methods ($p < 0.05$), while the number concentrations of UFPs were comparable to those observed in 2010 ($p > 0.05$) (Wang et al., 2014b). The decreased proportions of AUFPs in this study against those in 2010 implied effective control of SO_2 which is the precursor of acidic particles (*i.e.*, sulfuric and hydrogen sulfate). Indeed, SO_2 levels in Hong Kong and adjacent inland Pearl River Delta region from 2010 to 2019 have been significantly reduced by 55.4% and 63.0%, respectively, reported

by the Hong Kong Environmental Protection Department (https://www.epd.gov.hk/epd/tc_chi/resources_pub/publications/m_report.html). Compared with the proportion measured by the QCM+DS, the lower proportion of AUFPs in UFPs obtained by the DS+AFM method might be underestimated due to the uncertainties in the selection of the AFM scanning areas, especially when the concentrations of AUFPs in the atmosphere were low.

Overall, based on comparison with the results of SMPS and previous DS + AFM methods, the QCM+DS system was satisfactory for the measurements of UFPs and AUFPs. Compared to the previous method (DS+AFM), the QCM+DS system abandoned a time-consuming and complicated instrument (*i.e.*, AFM) and developed from an offline method to a semi-online method. The DS + AFM method required about one day to scan one set of samples (Wang et al., 2014b). Moreover, the large size (60cm×60cm×80cm) and heavy weight (~ 100 kg) made the AFM difficult to be widely used in the field measurements. Overall, the QCM+DS method was portable, compact and user-friendly. Nevertheless, time-resolution and/or size-resolution of the QCM+DS system could be further improved. At this stage, the QCM + DS system cannot be used to obtain the size distribution of AUFPs, which is a challenge for the development of methods to determine the size distribution of AUFPs in future study.

6.6 Summary

In this study, a QCM+DS method was developed to semi-automatically determine the

concentrations of ambient AUFPs and UFPs, based on the diffusion deposition of ultrafine particles in a diffusion sampler and the online detection of the mass of UFPs using a metal-QCM detector. The QCM+DS method was accomplished by combining the previous DS and three QCM systems. Modifications were made to the inlet of the sampler and the sampling spots inside the sampler to collect size-resolved particles and place detectors inside the sampler, respectively. Furthermore, the QCM detector was altered by coating a nano-metal film on its surface using a magnetron sputtering system to generate a metal-QCM detector for collecting and identifying AUFPs. According to the different attraction of AUFPs and non-acidic UFPs to metal film, ultrasonic treatment by ethanol removed the non-acidic particles on the surface of the detector, while retaining the acidic particles. AUFPs were identified and quantified based on the frequency change of the metal-QCM detectors during ultrasonic processing and sampling. Prior to field measurements for method validation, calibration experiments were conducted to determine the sensitivity factor of the modified QCM detector and the relationship of collection efficiency with particle size and sampling flow rate in the QCM+DS system.

In the field sampling campaigns, the total UFPs number and mass concentrations measured by the QCM+DS system showed fairly good agreements with the results of the other two methods (*i.e.*, SMPS and DS+AFM). In addition, the concentrations of AUFPs measured by the DS+AFM system were lower than those obtained by the QCM+DS method, which might be caused by underestimation of the DS+AFM method due to the uncertainties in the selection of the AFM

scanning areas. The difference between these two methods was significant in mass concentration but insignificant in number concentration. In short, the QCM+DS system is satisfactory and reliable for the measurements of ambient UFPs and AUFPs. Improvements can be further made by increasing the time-resolution and/or size-resolution of the method and obtaining the size distribution of AUFPs.

Chapter 7 Conclusions and suggestion for future study

7.1 Conclusions

The focus of this research is the method development of acidic ultrafine particles (AUFPs) measurement technology and the application of novel methods for the measurement of AUFPs in the atmosphere. Specifically, this study measured ultrafine particles (UFPs) and AUFPs in different land-use areas in Hong Kong and in urban area of Shanghai using the previous diffusion sampler (DS) + atomic force microscope (AFM) method; invented a new method for differential removal of non-acidic particles on the surface of nano-film metal detector; and developed and validated a novel method for semi-automatically measuring AUFPs in the atmosphere in Hong Kong, namely quartz crystal microbalance (QCM) + DS system. The main findings are drawn as follows.

(i) Six field measurements of UFPs and AUFPs were conducted in Hong Kong (two at urban sites, two at a roadside site and one at a rural site) and Shanghai (one at an urban site) using the DS+AFM method. The concentration of UFPs was the highest at the roadside site, followed by that at the urban site and at the rural site. However, the proportion of AUFPs in UFPs showed a reverse trend to that of UFPs. The trend of proportion of AUFPs in UFPs implied the potential transformation of AUFPs from non-acidic UFPs by condensation of acidic vapor on the surface of preexisting non-acidic particles and/or heterogeneous reaction of acidic vapor with non-acidic particles during the transport and aging of air masses. It also suggested the insignificant role of

anthropogenic sources in AUFPs emission. In addition, the urban area in Hong Kong suffered from heavier pollution of UFPs and AUFPs than that in Shanghai. However, the DS+AFM method was found to be high-cost and time-consuming through the field measurements.

(ii) The sizes distributions of UFPs and AUFPs measured in the six field measurements were all normal. The peak of proportion of AUFPs in UFPs was found in the size range of 35-50 nm in the roadside areas, while the peak in urban areas was observed in 50-70 nm. The lag of peak in urban areas was mainly due to the aggregation of AUFPs with non-acidic UFPs during the transport from source areas to receptor areas. In contrast, in rural area, the highest proportion of AUFPs in UFPs was in the smallest size range of 5-10 nm. The peak in nucleation-mode indicated the stimulation of NPF event with AUFPs as seeds and the minor aggregation of AUFPs with preexisting particles in a relatively clean environment. Moreover, similar geometric mean diameters (GMDs) of UFPs and AUFPs were found in the urban areas between Hong Kong and Shanghai ($p > 0.05$), perhaps suggesting the similar emission sources and/or chemical formation mechanisms of UFPs and AUFPs in these two cities.

(iii) Positive correlation of the estimated sulfuric acid vapor (Q_{sa}) with the proportion of AUFPs in UFPs was found (R^2=0.71), while the correlation between AUFP level and Q_{sa} was not obvious (R^2=0.17). The results suggested the important roles of both Q_{sa} and the concentration of preexisting particles in determining the concentration of AUFPs and the proportion of AUFPs in UFPs. That is, the AUFPs level is not necessarily high if sulfuric acid vapor is sufficient (high

Q_{sa}) but the level of preexisting particles is low. Besides, the pollution of AUFPs was reduced in the past ten years with the evidence of lower AUFPs concentrations and proportions of AUFPs in UFPs. The successful reduction in SO_2 emissions in China was probably the main cause. Significant reductions in SO_2 levels were observed in both Hong Kong and Shanghai. In addition to the use of LSFO in vehicles, the elimination of old diesel vehicles and the combustion of low sulfur coal in industries and power plants were the other main factor responsible for the reduction in SO_2 levels in Hong Kong and Shanghai, respectively.

(iv) To realize the identification of AUFPs without using AFM and quantification of AUFPs using the QCM system, three methods were tested for differential removal of nanoparticles on the surface of nano-film metal detector, including air jet, nanobubble and ultrasonic methods. Due to the strong particle-surface interaction between acidic particles and nanofilm metal detector, the acidic particles were retained on the surface regardless of methods. For non-acidic particles, only the ultrasonic method with ethanol was able to completely remove them from the surface. In ultrasonic treatment, the non-acidic particles are effectively removed from the surface due to the cavitation collapse pressure, which creates bubbles in the spaces between the non-acidic particles and the surface. In contrast, the gaps between the acidic particles and the surface are filled, so the acidic particles cannot be removed by bubbles.

(v) Because of the drawbacks of the previous DS+AFM methods (*i.e.*, offline, time-consuming, complicated and expensive), a QCM+DS method was developed to semi-automatically

determine the concentrations of ambient AUFPs and UFPs. The QCM+DS device was accomplished by combining the previous DS and three QCM systems, but the inlet of the DS and the sampling spots inside the DS were modified. A metal-QCM detector was generated and inserted into the QCM+DS device to collect and identify AUFPs. After sampling, the non-acidic particles on the surface of the detector were removed using ultrasonic method, while the acidic particles were retained. AUFPs were identified and quantified based on the frequency change of the metal-QCM detectors after the ultrasonic treatment and in the sampling. Namely, the frequency change after ultrasonic treatment referred to the mass of deposited non-acidic particles while the frequency change in the sampling was related to the mass of total UFPs (*i.e.*, both AUFPs and non-acidic particles). Calibration experiments indicated that after modification of the QCM detector, the sensitivity factor remained the same value as that set by the manufactory (*i.e.*, 56.6 $Hz \cdot cm^2/\mu g$), and three equations were obtained to calculate the collection efficiency of particles in different sizes under different flow rates in the three sampling spots of the QCM+DS device.

(vi) The QCM+DS system was validated in a field measurement. The results of the UFPs measured by the QCM+DS system showed good agreements with the results of the other two methods (*i.e.*, SMPS and DS+AFM), while the concentrations of AUFPs measured by the previous DS+AFM system were lower than those obtained using the newly-developed QCM+DS method, which might be caused by underestimation of the DS+AFM method due to

the uncertainties in the selection of the AFM scanning areas and the impact of assumed particle density. Nevertheless, the difference was insignificant in number concentration. In short, the QCM+DS system is satisfactory and reliable for the measurements of ambient UFPs and AUFPs.

7.2 Suggestion for future study

Although this study has improved the understanding of AUFPs pollution and enhanced the AUFPs measurement technology, limitations still exist and more research is necessary in the future. Suggestions are proposed as follows.

(i) Spatial and temporal variations of AUFPs pollution are worth further investigating. Though this study measured AUFPs in different land-use areas and cities in China, the database is far from enough in terms of sample sites and time periods. More and prolonged field measurements are required to obtain comprehensive and sufficient data of AUFPs. In particular, to better understand the AUFPs pollution, data of other air pollutants especially its potential precursors and meteorological parameters should also be continuously monitored. As such, relationships of AUFPs with their precursors, other pollutants, and meteorological parameters, as well as the formation mechanisms of AUFPs could be more in-depth explored.

(ii) The major sources of AUFPs and the formation mechanisms of AUFPs in the atmosphere are still unknown, which deserve further research. Sulfuric acid is known to form AUFPs. However, there are some other chemicals are acidic, such as ammonium bisulfate and

organic acids. To understand the major sources of these possible precursors/components of AUFPs, multi-approaches such as field measurements, chamber experiments and model simulations are required.

(iii) The chemical composition of AUFPs in the atmosphere can be further explored. Previous studies and this study mainly focused on the identification of AUFPs through morphological characteristics of UFPs and subsequent measurements of concentrations and size distributions of AUFPs in the atmosphere. The chemical properties of AUFPs have not comprehensively studied. In addition, although toxicological studies have clearly demonstrated the adverse health impact of AUFPs and suggested that acidity is the possible reason, it is difficult to ascertain which chemicals are actually responsible. Using the differential particle removal method introduced in Chapter 5, AUFPs collected from the atmosphere can be selectively retained on the surface and then the chemical composition of the retained AUFPs can be further analyzed with the aid of other instruments such as Nano-Fourier Transform Infrared Spectroscopy, X-ray Photoelectron Spectroscopy, Inductively Coupled Plasma-Mass Spectrometry and Gas Chromatography-Mass Spectrometry.

(iv) Although the developed QCM+DS device is time-saving, portable, compact and user-friendly, the time-resolution and size-resolution are still not perfect. Improvements can be made by replacing the 5 MHz QCM detector in the study to a more sensitive QCM

detector (*e.g.*, 10 MHz, 20 MHz and 50 MHz QCM detectors) to increase the resolution. Moreover, the current QCM+DS device is unable to obtain the size distribution of AUFPs, which is a challenge for future study to develop a method for online acquisition of size distributions of AUFPs.

(v) The developed QCM+DS system is not fully automatic. The measurement using the QCM+DS method involves several manual jobs, such as keeping sampled metal-QCM detectors in inert atmosphere to extend reactions of acidic particles with nanofilm of metal, and immersing the exposed detectors in ethanol for ultrasonic treatment to remove non-acidic particles. To reduce cost and save manpower, a fully online measurement technique of AUFPs is expected to be developed in future study, which can automatically monitor the concentration and size distribution of AUFPs in a long-term measurement.

References

Adams, K., Greenbaum, D. S., Shaikh, R., van Erp, A. M., and Russell, A. G. 2015. Particulate matter components, sources, and health: Systematic approaches to testing effects. *Journal of the Air and Waste Management Association*, *65*(5), 544-558.

Amdur, M. O., and Chen, L. C. 1989. Furnace-generated acid aerosols: speciation and pulmonary effects. *Environmental Health Perspectives*, 79, 147-150.

Arouca, F. O., Feitosa, N. R., and Coury, J. R. 2010. Effect of sampling in the evaluation of particle size d athanasios istribution in nanoaerosols. *Powder Technology*, *200*(1-2), 52-59.

Bakhtari, K., Guldiken, R. O., Makaram, P., Busnaina, A. A., and Park, J. G. 2006. Experimental and numerical investigation of nanoparticle removal using acoustic streaming and the effect of time. *Journal of the Electrochemical Society*, *153*(9), G846.

Baldauf, R. W., Devlin, R. B., Gehr, P., Giannelli, R., Hassett-Sipple, B., Jung, H., Martini, G., McDonald, J., Sacks, J. D., and Walker, K. 2016. Ultrafine particle metrics and research considerations: review of the 2015 UFP workshop. *International Journal of Environmental Research and Public Health*, *13*(11), 1054.

Bigg, E. K., Ono, A., and Williams, A. J. 1974. Chemical tests for individual submicron aerosol particles. *Atmospheric Environment,* 8, 1-13.

Binks, B. P., and Olusanya, S. O. 2017. Pickering emulsions stabilized by coloured organic pigment particles. *Chemical Science*, *8*(1), 708-723.

Bowling, R. A. 1988. A theoretical review of particle adhesion. In *Particles on Surfaces 1*, 129-142. Springer, Boston, MA.

Boy, M., Kulmala, M., Ruuskanen,T. M., Pihlatie, M., Reissell, A., Aalto, P.P., Keronen, P., Dal Maso, M., Hellen, H., Hakola, H., Janson, R., Hanke, M., and Arnold, F. 2005. Sulphuric acid closure and contribution to nucleation mode particle growth. *Atmospheric Chemistry and Physics,* 5, 863- 878.

Bräuner, E. V., Forchhammer, L., Møller, P., Simonsen, J., Glasius, M., Wåhlin, P., Raaschou-Nielsen, O., and Loft, S. 2007. Exposure to ultrafine particles from ambient air and oxidative stress- induced DNA damage. *Environmental Health Perspectives,* 115, 1177- 1182.

Brems, S., Hauptmann, M., Camerotto, E., Pacco, A., Kim, T. G., Xu, X., Wostyn, K., Mertens, P., and De Gendt, S. 2013. Nanoparticle removal with megasonics: a review. *ECS Journal of Solid State Science and Technology, 3(1)*, N3010.

Buonanno, G., Ficco, G., and Stabile, L. 2009. Size distribution and number concentration of particles at the stack of a municipal waste incinerator. *Waste Management,* 29,749-755.

Busnaina, A. A., and Gale, G. W. 1995. Ultrasonic and megasonic particle removal. *Proceeding. Precise. Cleaning,* 15, 347-359.

Busnaina, A., Bakhtari, K., and Park, J. G. 2018. Particle deposition and adhesion. In *Handbook of Silicon Wafer Cleaning Technology*, 153-184. William Andrew Publishing.

Buttry, D. A. 1991. Applications of the quartz crystal microbalance to electrochemistry. *Electroanalytical Chemistry: A Series of Advances*, In: Bard, A. J. (Ed.), Vol 17, Marcel Dekker, New York, 1-85.

Campagnolo, D., Cattaneo, A., Corbella, L., Borghi, F., Del Buono, L., Rovelli, S., Spinazzé, A., and Cavallo, D. M. 2019. In-vehicle airborne fine and ultra-fine particulate matter exposure: The impact of leading vehicle emissions. *Environment International*, 123, 407-416.

Casati, R., Scheer, V., Vogt, R., and Benter, T. 2007. Measurement of nucleation and soot mode particle emission from a diesel passenger car in real world and laboratory in situ dilution. *Atmospheric Environment*, *41*(10), 2125-2135.

Cha, Y., and Olofsson, U. 2018. Effective density of airborne particles in a railway tunnel from field measurements of mobility and aerodynamic size distributions. *Aerosol Science and Technology*, *52*(8), 886-899.

Charasseangpaisarn, T., and Wiwatwarrapan, C. 2015. The effect of various frequencies of ultrasonic cleaner in reducing residual monomer in acrylic resin. *Ultrasonics*, 63, 163-167.

Chen, L. C., Wu, C. Y., Qu, Q. S., and Schlesinger, R. B. 1995. Number concentration and mass concentration as determinants of biological response to inhaled irritant particles. *Inhalation Toxicology,* 7:577-588.

Chen, M., Romay, F. J., Li, L., Naqwi, A., and Marple, V. A. 2016. A novel quartz crystal cascade impactor for real-time aerosol mass distribution measurement. *Aerosol Science and Technology*, *50*(9), 971-983.

Cheng, M. D. 2018. Selective collection of airborne particulate matter. *Aerosol and Air Quality Research*, *18*(6), 1361-1365.

Cheng, Y., Yu, C. W. F., Huang, Y., Zhang, Y. W., Gao, Y., Yau, P. S., Chan, C. S., and Lee, S. C. 2012. Particle counts and size distributions in the roadside environment. *Indoor and Built Environment*, *21:* 633–641.

Clifford, S., Mazaheri, M., Salimi, F., Ezz, W. N., Yeganeh, B., Low-Choy, S., Walker, K.,

Mengersen, K., Marks, G. B., and Morawska, L. 2018. Effects of exposure to ambient ultrafine particles on respiratory health and systemic inflammation in children. *Environment International*, 114, 167-180.

Cohen, B. S., Li, W., Xiong, J. Q., Lippmann, M. 2000. Detecting H+ in ultrafine ambient aerosol using iron nano-film detectors and scanning probe microscopy. *Applied Occupational and Environmental Hygiene,* 15, 80-89

Cohen, B. S., Heikkinen, M. S., and Hazi, Y. 2004a. Airborne fine and ultrafine particles near the world trade center disaster site. *Aerosol Science and Technology*, *38*(4), 338-348.

Cohen, B. S., Heikkinen, M. S., Hazi, Y., Guo, H., Peters, P., and Lippmann, M. 2004b. Field evaluation of nanofilm detectors for measuring acidic particles in indoor and outdoor air. *Research report (Health Effects Institute)*, (121), 1-35.

Cooper, K., Gupta, A., and Beaudoin, S. 2000. Substrate morphology and particle adhesion in reacting systems. *Journal of Colloid and Interface Science*, *228*(2), 213-219.

Dassen, W., Brunekreef, B., Hoek, G., Hofschreuder, P., Staatsen, B., Groot, H. D., Schouten, E., and Biersteker, K. 1986. Decline in children's pulmonary function during an air pollution episode. *Journal of the Air Pollution Control Association*, *36*(11), 1223-1227.

Dockery, D. W., Pope III, C. A., Xu, X., Spengler, J. D., Ware, J. H., Fay, M. E., Ferris, B. G., and Speizer, F. E. 1993. An association between air pollution and mortality in six U.S. Cities. *New England Journal of Medicine,* 329, 1753-1759.

Donovan, R. P. 1990. Particle control for semiconductor manufacturing. New York: Dekker.

Edney, E. O., Kleindienst, T. E., Jaoui, M., Lewandowski, M., Offenberg, J. H., Wang, W., and Claeys, M., 2005. Formation of 2-methyltetrols and 2-methylglyceric acid in secondary organic aerosol from laboratory irradiated isoprene/NO_x/SO_2/air mixtures and their detection in ambient PM2.5 samples collected in the eastern United States. *Atmospheric Environment,* 39, 5281-5289.

Fernández-Camacho, R., Rodríguez, S., Rosa, J. L., Sánchez De La Campa, A. M., Viana, M., Alastuey, A., and Querol, X. 2010. Ultrafine particle formation in the inland sea breeze airflow in Southwest Europe. *Atmospheric Chemistry and Physics*, *10*(19), 9615-9630.

Ferro, A. R., Kopperud, R. J., and Hildemann, L. M. 2004. Elevated personal exposure to particulate matter from human activities in a residence. *Journal of Exposure Science and Environmental Epidemiology*, *14*(1), S34-S40.

Fiedler, V., Maso, M. D., Boy, M., Aufmhoff, H., Hoffmann, J., Schuck, T., Birmili, W., Hanke, W., Uecker, J., Arnold, F., and Kulmala, M. 2005. The contribution of sulphuric acid to

atmospheric particle formation and growth: a comparison between boundary layers in Northern and Central Europe. *Atmospheric Chemistry and Physics*, *5*(7): 1773-1785.

Franken, R., Maggos, T., Stamatelopoulou, A., Loh, M., Kuijpers, E., Bartzis, J., et al. 2019. Comparison of methods for converting dylos particle number concentrations to $PM_{2.5}$ mass concentrations. *Indoor Air*, *29*(3), 450-459.

Gale, G., and Busnaina, A. 1995. Removal of particulate contaminants using ultrasonics and megasonics: a review. *Particulate science and Technology,* 13**,** 197-211.

Gerhard, E. R., and Johnsone, H. F. 1955. Micro-determination of sulfuric acid aerosol. *Analytical Chemistry*, 27, 732.

Gilmour, P. S., Ziesenis, A., Morrison, E. R., Vickers, M. A., Drost, E. M., Ford, I., et al. 2004. Pulmonary and systemic effects of short-term inhalation exposure to ultrafine carbon black particles. *Toxicology and Applied Pharmacology*, *195*(1), 35-44.

González, Y., Rodríguez, S., Guerra García, J.C., Trujillo, J.L., and García, R. 2011. Ultrafine particles pollution in urban coastal air due to ship emissions. *Atmospheric Environment,* 45, 4907-4914.

Guo, H., Ding, A. J., Morawska, L., He, C., Ayoko, G., Li, Y. S. and Hung, W. T. 2008. Size distribution and new particle formation in subtropical eastern Australia. *Environmental Chemistry,* 56, 382-390.

Guo, H., Morawska, L., He, C., Zhang, Y. L., Ayoko, G., and Cao, M. 2010. Characterization of particle number concentrations and $PM_{2.5}$ in a school:influence of outdoor air pollution on indoor air. *Environmental Science and Pollution Research,* 176, 1268-1278.

Guo, H., Wang, D. W., Cheung, K., Ling, Z. H., Chan, C. K., and Yao, X. H. 2012. Observation of aerosol size distribution and new particle formation at a mountain site in subtropical Hong Kong. *Atmospheric Chemistry and Physics*, *12*(20), 9923-9939.

Hauptmann, M., Frederickx, F., Struyf, H., Mertens, P., Heyns, M., De Gendt, S., Glorieux, C., and Brems, S. 2013. Enhancement of cavitation activity and particle removal with pulsed high frequency ultrasound and supersaturation. *Ultrasonics sonochemistry*, *20*(1), 69-76.

Hagler, G. S. W., Baldauf, R. W., Thoma, E. D., Long, T. R., Snow, R. F., Kinsey, J. S., Oudejans, L., and Gullett, B. K. 2009. Ultrafine particles near a major roadway in Raleigh, North Carolina: Downwind attenuation and correlation with traffic-related pollutants. *Atmospheric Environment,* 43, 229-1234.

Han, Y., Stroud, C. A., Liggio, J., and Li, S. M. 2016. The effect of particle acidity on secondary organic aerosol formation from α-pinene photooxidation under atmospherically relevant

conditions. *Atmospheric Chemistry and Physics*, *16*(21), 13929-13944.

Hattis, D., Wasson, J. M., Page, G. S., Stern, B., and Franklin, C. A. 1987. Acid particles and the tracheobronchial region of the respiratory system: an "irritation-signaling" model for possible health effects. *Journal of the Air Pollution Control Association,* 37, 1060-1066.

Hayashi, H., Koshi, S., and Sakabe, H. 1961. Determination of mist size by metal coated glass slide. *Bullet of National Institute of Industrial Health,* 6, 35.

Hazi, Y., Heikkinen, M. S. A., and Cohen, B. S. 2003. Size distribution of acidic sulfate ions in fine ambient particulate matter and assessment of source region effect. *Atmospheric Environment*, *37*(38): 5403-5413.

Heath, G. R., and Scheuring, S. 2018. High-speed AFM height spectroscopy reveals μs-dynamics of unlabeled biomolecules. *Nature Communications*, *9*(1), 1-11.

Hedley, A. J., Wong, C. M., Thach, T. Q., Ma, S., Lam, T. H., and Anderson, H. R. 2002. Cardiorespiratory and all-cause mortality after restrictions on sulphur content of fuel in Hong Kong: an intervention study. *The Lancet*, *360*(9346), 1646-1652.

Heinzerling, A., Hsu, J., and Yip, F. 2016. Respiratory health effects of ultrafine particles in children: A literature review. *Water, Air, and Soil Pollution*, *227*(1), 32.

Hinds, W. C. 1999. Properties, behavior, and measurement of airborne particles. Aerosol Technology, 2nd ed, John Wiley and Sons Press, New York, 182-204.

Hoek, G., Boogaard, H., Knol, A., de Hartog, J., Slottje, P., and Ayres, J. G. 2010. Concentration response functions for ultrafine particles and all-cause mortality and hospital admissions: results of a European expert panel elicitation. *Environment Science and Technology*, 44, 476-48

Holmes, N. S. 2007. A review of particle formation events and growth in the atmosphere in the various environments and discussion of mechanistic implications. *Atmospheric Environment*, *41*(10), 2183-2201.

Horstman, Jr., Sanford, W., and Wagman, J. 1967. Size analysis of acid aerosols by a metal film technique. *American Industrial Hygiene Association Journal, 28*(6), 523-530.

Hu, D., Qiao, L., Chen, J., Ye, X., Yang, X., Cheng, T., and Fang, W. 2010. Hygroscopicity of inorganic aerosols: size and relative humidity effects on the growth factor. *Aerosol and Air Quality Research*, *10*(3), 255-264.

Huang, P. F., and Turpin, B. 1996. Reduction of sampling and analytical errors for electron microscopic analysis of atmospheric aerosols. *Atmospheric Environment*, *30*(24), 4137-4148.

Jang, M. S., Czoschke, N. M., Lee, S., and Kamens, R. M. 2002. Heterogeneous atmospheric aerosol production by acid-catalyzed particle-phase reactions. *Science*, 298:814-817.

Jang, I. R., Park, J., and joon Kim, H. 2019. High precision mass sensing of in-liquid particles using CNT coated quartz crystal microbalance. In *2019 IEEE SENSORS*. IEEE, 1-4.

Karottki, D. G., Spilak, M., Frederiksen, M., Jovanovic Andersen, Z., Madsen, A. M., Ketzel, M., and Loft, S. et al., 2015. Indoor and outdoor exposure to ultrafine, fine and microbiologically derived particulate matter related to cardiovascular and respiratory effects in a panel of elderly urban citizens. *International Journal of Environmental Research and Public Health*, *12*(2), 1667-1686.

Kawamoto, H., and Guo, B. 2018. Improvement of an electrostatic cleaning system for removal of dust from solar panels. *Journal of Electrostatics,* 91, 28-33.

Kessler, N., Armoza-Zvuloni, R., Wang, S., Basu, S., Weber, P. K., Stuart, R. K., and Shaked, Y. 2020. Selective collection of iron-rich dust particles by natural Trichodesmium colonies. *The ISME journal*, *14*(1), 91-103.

Kim, I., and Lee, J. 2013. The removal of 10-nm contaminant particles from micron-scale trenches using CO_2 nano bullets. *Journal of Nanoparticle Research, 15(4)*, 1-13.

Kim, I., Hwang, K., and Lee, J. 2012. Removal of 10-nm contaminant particles from Si wafers using CO_2 bullet particles. *Nanoscale Research Letters*, *7*(1), 211.

Kim, Y. P., Pun, B., Chan, C. K., Flagan, R. C., and Seinfeld, J. H. 1994. Determination of water activity in ammonium sulfate and sulfuric acid mixtures using levitated single particles. *Environmental Science and Technology*, 20, 275-284.

King, W. H. 1964. Piezoelectric sorption detector. *Analytical Chemistry*, *36*(9), 1735-1739.

Knutson, E. O. 1999. History of diffusion batteries in aerosol measurements. *Aerosol Science and Technology*, *31*(2-3), 83-128.

Kohli, R. 2019. Electrostatic removal and manipulation of small particles and surface cleaning applications. In *Developments in Surface Contamination and Cleaning: Applications of Cleaning Techniques*, Elsevier, 391-421.

Kumari, S. V., and Vaidyan, V. K. 1988. Surface morphological investigation of iron films during oxidation. *Bulletin of Materials Science*, *10*(3), 223-231.

Kumar, P., Morawska, L., Birmili, W., Paasonen, P., Hu, M., Kulmala, M., and Britter, R. et al., 2014. Ultrafine particles in cities. *Environment International*, 66, 1-10.

Kumar, P., Robins,A., Vardoulakis, S., and Britter, R. 2010. A review of the characteristics of

nanoparticles in the urban atmosphere and the prospects for developing regulatory controls. *Atmospheric Environment,* 44, 5035-5052.

Kulmala, M., Vehkamaki, H., Petaja, T., Dal Maso, M., Lauri, A., Kerminen, V.-M., Birmili, W., and McMurry, P. H. 2004a. Formation and growth rates of ultrafine particles: a review of observations. *Journal of Aerosol Science,* 35, 143-176.

Kulmala, M., Laakso, L., Lehtinen, K. E. J., Riipinen, I., Dal Maso, M., Anttila, T., Kerminen, V.-M., Hõrrak, U., Vana, M., and Tammet, H. 2004b. Initial steps of aerosol growth. *Atmospheric Chemistry and Physics,* 4, 2553-2560

Kulmala, M., Lehtinen, K. E. J., and Laaksonen, A. 2006. Cluster activation theory as an explanation of the linear dependence between formation rate of 3nm particles and sulphuric acid concentration. *Atmospheric Chemistry and Physics*, *6*(3): 787-793.

Kulmala, M., Pirjola, U., and Makela, J. M. 2000. Stable sulphate clusters as a source of new atmospheric particles. *Nature, 404*(6773), 66- 69.

Lee, J. W., Hwang, K. S., Lee, K. H., Yi, M. Y., and Lee, M. J. 2009. Removing 20 nm particles using a supersonic argon particle beam generated with a contoured Laval nozzle. *Journal of Adhesion Science and Technology*, *23*(5), 769-777.

Li, W., Shao, L., Zhang, D., Ro, C. U., Hu, M., Bi, X., Geng, H., Matsuki, A., Niu H., and Chen, J. 2016. A review of single aerosol particle studies in the atmosphere of East Asia: morphology, mixing state, source, and heterogeneous reactions. *Journal of Cleaner Production*, 112, 1330-1349.

Li, X., Wang, J., Tu, X. D., Liu, W., and Huang, Z. 2007. Vertical variations of particle number concentration and size distribution in a street canyon in Shanghai, China. *Science of the Total Environment*, *378*(3), 306-316.

Li, Y. J., Cheong, G., Lau, A. P. S., and Chan, C. K. 2010. Acid-catalyzed particle-phase reactions of limonene and terpineol and their impacts on gas-to-particle partitioning in the formation of organic aerosols. *Environmental Science and Technology*, 44, 5483-5489.

Liang, D., Shih, W. P., Chen, C. S., and Dai, C. A. 2010. A miniature system for separating aerosol particles and measuring mass concentrations. *Sensors*, *10*(4), 3641-3654.

Lingard, J. J. N., Agus, E. L., Young, D. T., Andrews, G. E., and Tomlin, A. S. 2006. Observations of urban airborne particle number concentrations during rush-hour conditions: analysis of the number based size distributions and modal parameters. *Journal of Environmental Monitoring,* 8, 1203-1218.

Lioy, P. J, and Waldman, J. M. 1989. Acidic sulfate aerosols: characterization and exposure.

Environment Health Perspectives, 79, 15-34.

Lippmann, M. 1989. Progress, prospects, and research needs on the health effects of acid aerosols. *Environmental Health Perspectives*, 79, 203-205.

Lippmann, M. 2000. Environmental toxicants: human exposures and their health effects--Sulfur oxides: acidic aerosols and SO_2. New York, John Wiley and Sons: 771-809.

Lippmann, M., and Thurston, G. D. 1996. Sulfate concentrations as an indicator of ambient particulate matter air pollution for health risk evaluations. *Journal of Exposure Analysis and Environmental Epidemiology*, *6*(2), 123-146.

Lodge, J. P., and Havlik, B. R. 1960. Evaporated metal films as indicators of atmospheric pollution. *International Journal of Air and Water Pollution,* 3, 249.

Lu, H., Lyu, X., and Guo, H. 2020. A novel semi-automatic method for measuring acidic ultrafine particles in the atmosphere. *Atmospheric Environment*, 245, 118044.

Lung, C. C., Jonathan, M. F., Qu, Q. S., Amdur, M. O., and Gordon, T. 1992. Effects of fine and ultrafine sulfuric acid aerosols in guinea pigs:Alterations in alveolar macrophage function and intracellular pH. *Toxicology and Applied Pharmacology,* 1131, 109-117.

Lv, R., Peng, J., Chen, S., Hu, Y., Wang, M., Lin, J., Zhou, X., and Zheng, X. 2017. A highly linear humidity sensor based on quartz crystal microbalance coated with urea formaldehyde resin/nano silica composite films. *Sensors and Actuators B: Chemical*, 250, 721-725.

Mamane, Y., and De Pena, R. G. 1978. A quantitative method for the detection of individual submicrometer size sulfate particles. In *Sulfur in the Atmosphere*, Pergamon, 69-82.

Malm, W. C., and Day, D. E. 2001. Estimates of aerosol species scattering characteristics as a function of relative humidity. *Atmospheric Environment,* 35, 2845-2860.

Margarella, A. M., Perrine, K. A., Lewis, T., Faubel, M., Winter, B. and Hemminger, J. C. 2013. Dissociation of sulfuric acid in aqueous solution: determination of the photoelectron spectral fingerprints of H_2SO_4, HSO_4^-, and SO_4^{2-} in water. *The Journal of Physical Chemistry C,* 117**,** 8131-8137.

Marple, V. A., Rubow, K. L., and Olson, B. A. (3^{rd} Eds). 2001. Inertial, gravitational, centrifugal, and thermal collection techniques. *Aerosol Measurement: Principles, Techniques, and Applications*, 2:229–260.

Martin, M., Mader, W., and Fromm, E. 1994. Oxidation of iron, aluminium and titanium films in the temperature range 50-200° C. *Thin Solid Films*, *250*(1-2), 61-66.

Marczyńska, A., Skoryna, J., Lewandowski, M., and Smardz, L. 2015. Oxidation Kinetics of Thin

and Ultrathin Fe Films. *Acta Physica Polonica, A.*, *127*(2).

Mathis, U., Ristimäki, J., Mohr, M., Keskinen, J., Ntziachristos, L., Samaras, Z., and Mikkanen, P. 2004. Sampling conditions for the measurement of nucleation mode particles in the exhaust of a diesel vehicle. *Aerosol Science and Technology*, *38*(12), 1149-1160.

McCallum, J. J. 1989. Piezoelectric devices for mass and chemical measurements: an update. *Analyst*, 114, 1173.

McGranahan, G., and Murray, F. (Eds.). 2012. *Air pollution and health in rapidly developing countries*. Earthscan.

Mikkonen, S., Korhonen, H., Romakkaniemi, S., Smith, J. N., Joutsensaari, J., Lehtinen, K. E. J., Hamed, A., Breider, T. J., Birmili, W., Spindler, G., Plass-Duelmer, C., Facchini, M. C., and Laaksonen, A. 2011. Meteorological and trace gas factors affecting the number concentration of atmospheric Aitken (D_p=50nm) particles in the continental boundary layer: parameterization using a multivariate mixed effects model. *Geoscientific Model Development*, *4*(1), 1-13.

Morawska, L., He, C., Johnson, G., Guo, H., Uhde, E., and Ayoko, G. 2009. Ultrafine particles in indoor air of a school: possible role of secondary organic aerosols. *Environmental Science and Technology*, *43*(24), 9103-9109.

Morawska, L., Moore, M. R., and Ristovski, Z. D. 2004. Health impacts of ultrafine particles. Canberra (Australia): Australian Department of the Environment and Heritage.

Morawska, L., Ristovski, Z., Jayaratne, E. R., Keogh, D. U., and Ling, X. 2008. Ambient nano and ultrafine particles from motor vehicle emissions: Characteristics, ambient processing and implications on human exposure. *Atmospheric Environment*, *42*(35), 8113-8138.

Morawska, L., Wierzbicka, A., Buonanno, G., Cyrys, J., Schnellekreis, J., Kowalski, M., Querol, X. et al., 2020. Ambient ultrafine particles: evidence for policy makers. *A Report Prepared by the 'Thinking Outside The Box' Team*.

Narsto, 2003. Particulate matter science for policy makers: a NARSTO assessment. In: McMurry, P., Shepher, M., Vicker, J. (Eds.), EPRI, Palo Alto, CA, USA.

Ngo, N. D., Lee, J., Kim, M. W., and Jang, J. 2019. Measurement of $PM_{2.5}$ mass concentration using an electrostatic particle concentrator-based quartz crystal microbalance. *IEEE Access*, *7*, 170640-170647.

Oh, N., and Park, J. H. 2014. Endocytosis and exocytosis of nanoparticles in mammalian cells. *International Journal of Nanomedicine*, *9*(Suppl 1), 51.

Oberdörster, G., Finkelstein, J. N., Johnson, C., Gelein, R., Cox, C., Baggs, R., and Elder, A. C. P. 2000. Acute pulmonary effects of ultrafine particles in rats and mice. *Research Report 96*. Health Effects Institute, Cambridge MA.

Oberdörster, G., Oberdörster, E., and Oberdörster, J. 2005. Nanotoxicology: an emerging discipline evolving from studies of ultrafine particles. *Environmental Health Perspectives,* 113, 823- 839.

Oberdörster, G., Sharp, Z., Atudorei, V., Elder, A., Gelein, R., Kreyling, W., and Cox, C. 2004. Translocation of inhaled ultrafine particles to the brain. *Inhalation Toxicology*, *16*(6-7), 437-445.

Otani, Y., Namiki, N., and Emi, H. 1995. Removal of fine particles from smooth flat surfaces by consecutive pulse air jets. *Aerosol Science and Technology*, *23*(4), 665-673.

Paniwnyk, L., Alarcon-Rojo, A., Rodriguez-Figueroa, J. C., and Toma, M. 2017. The use of ultrasound as an enhancement aid to food extraction. In *Ingredients Extraction by Physicochemical Methods in Food*, 399-440. Academic Press.

Park, J. K., Yoon, J. W., Whang, K. H., and Cho, S. H. 2012. Removal of nanoparticles on silicon wafer using a self-channeled plasma filament. *Applied Physics A, 108*(2), 269-274.

Peters, A., Dockery, D. W., Heinrich, J., and Wichmann, H. E. 1997. Short-term effects of particulate air pollution on respiratory morbidity in asthmatic children. *European Respiratory Journal*, 10, 872-879.

Pohanka, M. 2017. The piezoelectric biosensors: principles and applications. *International Journal of Electrochemical Science*, 12, 496-506.

Reipa, V., Purdum, G., and Choi, J. 2010. Measurement of nanoparticle concentration using quartz crystal microgravimetry. *The Journal of Physical Chemistry B*, *114*(49), 16112-16117.

Riipinen, I., Sihto, S. L., Kulmala, M., Arnold, F., Dal Maso, M., Birmili, W., Saarnio, K., Teinila, K., Kerminen, V. M., Laaksonen, A., and Lehtinen, K. E. J. 2007. Connections between atmospheric sulphuric acid and new particle formation during QUEST IIIIV campaigns in Heidelberg and Hyytiälä. *Atmospheric Chemistry and Physics,* 7, 1899-1914.

Rim, D., Choi, J. I., and Wallace, L. A. 2016. Size-resolved source emission rates of indoor ultrafine particles considering coagulation. *Environmental Science and Technology*, *50*(18), 10031-10038.

Salih, H. H., El Badawy, A. M., Tolaymat, T. M., and Patterson, C. L. 2019. Removal of stabilized silver nanoparticles from surface water by conventional treatment processes. *Advances in Nanoparticles*, *8*(2), 21.

Sarangi, B., Aggarwal, S. G., Sinha, D., and Gupta, P. K. 2016. Aerosol effective density measurement using scanning mobility particle sizer and quartz crystal microbalance with the estimation of involved uncertainty. *Atmospheric Measurement Techniques*, *9*(3), 859-875.

Sauerbrey, G. 1959. Verwendung von Schwingquarzen zur Wägung dünner Schichten und zur Mikrowägung. *Z. Phys*, *155*(2):206–222.

Savolainen, K., and Pietroiusti, A. 2017. Exposure Assessment. In *Adverse Effects of Engineered Nanomaterials*. Academic Press, 103-123.

Schlesinger, R. B., and Cassee, F. 2003. Atmospheric secondary inorganic particulate matter: the toxicological perspective as a basis for health effects risk assessment. *Inhalation Toxicology*, *15*(3), 197-235

Shrivastava, A., and Gupta, V. B. 2011. Methods for the determination of limit of detection and limit of quantitation of the analytical methods. *Chronicles of Young Scientists*, *2*(1), 21.

Sipilä, M., Berndt, T., Petäjä, T., Brus, D., Vanhanen, J., Stratmann, F., Patokoski, J., Roy L. Mauldin III, R., Hyvärinen A.,, Lihavainen, H., and Kulmala, M. 2010. The role of sulfuric acid in atmospheric nucleation. *Science*, *327*(5970), 1243-1246.

Šmejkalová, A. H., Zíková, N., Ždímal, V., Plachá, H., and Bitter, M. 2020. Atmospheric aerosol growth rates at different background station types. *Environmental Science and Pollution Research*, 1-13.

Solomon, P. A., Hopke, P. K., Froines, J., and Scheffe, R. 2008. Key scientific findings and policy and health-relevant insights from the U.S. Environmental protection agency's particulate matter supersites program and related studies: an integration and synthesis of results. *Journal of the Air and Waste Management Association, 58*(12), S3.

Stolzenburg, M. R., and McMurry, P. H. 1991. An ultrafine aerosol condensation nucleus counter. *Aerosol Science and Technology*, *14*(1), 48-65.

Sturm, R. 2016. Local lung deposition of ultrafine particles in healthy adults: experimental results and theoretical predictions. *Annals of Translational Medicine*, *4*(21).

Subramanian, S., Simon, S., Gao, B., and Sjöblom, J. 2016. Asphaltene fractionation based on adsorption onto calcium carbonate: Part 1. Characterization of sub-fractions and QCM-D measurements. *Colloids and Surfaces A: Physicochemical and Engineering Aspects*, 495, 136-148.

Thurston, G. D., Ito, K., Hayes, C. G., Bates, D. V., and Lippmann, M. 1994. Respiratory hospital admissions and summertime haze air pollution in toronto, ontario: consideration of the role of acid aerosols. *Environmental Research*, 65, 271-290.

Thurston, G. D., Ito, K., Kinney, P. L., and Lippmann, M. 1992. A multi-year study of air pollution and respiratory hospital admissions in three new york state metropolitan areas: results for 1988 and 1989 summers. *Journal of Exposure Analysis and Environmental Epidemiology*, 2, 429-450.

Thurston, G. D., Ito, K., Lippmann, M., and Hayes, C. G. 1989. Re-examination of London mortality in relation to exposure to acidic aerosols during 1962-1973 winters. *Environmental Health Perspectives*, 79, 73-82.

Thurston, G.D. 2000. Particulate matter and sulfate: evaluation of current California air quality standards with respect to protection of children. *Prepared for California Air Resources Board (CARB) and California Office of Environmental Health Hazard Assessment (OEHHA)*, 29-36.

Tsai, Y. I. 2005. Atmospheric visibility trends in an urban area in Taiwan 1961-2003. *Atmospheric Environment,* 39, 5555-5567.

Tzou, T. Z. 1999. Aerodynamic particle size of metered-dose inhalers determined by the quartz crystal microbalance and the Andersen cascade impactor. *International Journal of Pharmaceutics*, *186*(1), 71-79.

Utell, M. J., Morrow, P. E., and Hyde, R. W. 1982. Comparison of normal and asthmatic subjects'responses to sulphate pollutant aerosols. In *Inhaled Particles V*, Pergamon, 691-697.

Ushakov, S., Valland, H., Nielsen, J. B., and Hennie, E. 2013. Effects of high sulphur content in marine fuels on particulate matter emission characteristics. *Journal of Marine Engineering & Technology*, *12*(3), 30-39.

Venkatasubramanian, A., Navaei, M., Bagnall, K. R., McCarley, K. C., Nair, S., and Hesketh, P. J. 2012. Gas Adsorption characteristics of metal–organic frameworks via quartz crystal microbalance techniques. *The Journal of Physical Chemistry C*, *116*(29), 15313-15321.

Ward, M. D., and Buttry, D.A. 1990. In situ interfacial mass detection with piezoelectric transducer. *Science*, 249, 1000-1007.

Wang, M., Kong, W., Marten, R., He, X. C., Chen, D., Pfeifer, J., and Donahue, N. M. et al., 2020a. Rapid growth of new atmospheric particles by nitric acid and ammonia condensation. *Nature*, *581*(7807), 184-189.

Wang, F., Yu, H., Wang, Z., Liang, W., Shi, G., Gao, J., Li, M., and Feng, Y. 2020b. Review of online source apportionment research based on observation for ambient particulate matter. *Science of the Total Environment*, 144095.

Wang, D. W., Guo, H., and Chan, C. K. 2012. Measuring ambient acidic ultrafine particles using iron nanofilm detectors: method development. *Aerosol Science and Technology,* 46, 521–532.

Wang, D., Guo, H., Cheung, K., and Gan, F. 2014a. Observation of nucleation mode particle burst and new particle formation events at an urban site in Hong Kong. *Atmospheric Environment*, 99, 196-205.

Wang, D. W., Guo, H., and Chan, C. K. 2014b. Diffusion sampler for measurement of acidic ultrafine particles in the atmosphere. *Aerosol Science and Technology*, *48*(12), 1236-1246.

Wang, J., Zhu, J., and Liew, P. J. 2019. Material removal in ultrasonic abrasive polishing of additive manufactured components. *Applied Sciences*, *9*(24), 5359.

Wang, S. C., and Flagan, R. C. 1990. Scanning electrical mobility spectrometer. *Aerosol Science and Technology*, *13*(2), 230-240.

Wang, T., Wang, P., Theys, N., Tong, D., Hendrick, F., Zhang, Q., and Roozendael, M. V. 2018. Spatial and temporal changes in SO_2 regimes over China in the recent decade and the driving mechanism. *Atmospheric Chemistry and Physics*, *18*(24), 18063-18078.

Wehner, B., Uhrner, U., von Löwis, S., Zallinger, M., and Wiedensohler, A. 2009. Aerosol number size distributions within the exhaust plume of a diesel and a gasoline passenger car under on-road conditions and determination of emission factors. *Atmospheric Environment,* 43, 1235-1245.

Weichenthal, S., Bai, L., Hatzopoulou, M., Ryswyk, K., Kwong, J. C., Jerrett, M., Donkelaar, A., Martin, R. V., Burnett, R. T., Lu, H., and Chen, H. 2017. Long-term exposure to ambient ultrafine particles and respiratory disease incidence in in Toronto, Canada: a cohort study. *Environmental Health*, *16*(1), 64.

Wichmann, H. E., Mueller, W., Allhoff, P., Beckmann, M., Bocter, N., Csicsaky, M. J., Schoeneberg, G. et al., 1989. Health effects during a smog episode in West Germany in 1985. *Environmental Health Perspectives*, *79*, 89-99.

Wichmann, H. E., Spix, C., Tuch, T., Wolke, G., Peters, A., Heinrich, J., Kreyling, W. G., and Heyder, J. 2000. Daily mortality and fine and ultrafine particles in Erfurt, Germany Part I: role of particle number and particle mass. *Research Report (Health Effects Institute)*, (98), 5-86.

Wiedensohler, A. E. M. C., Lütkemeier, E., Feldpausch, M., and Helsper, C. 1986. Investigation of the bipolar charge distribution at various gas conditions. *Journal of Aerosol Science*, *17*(3), 413-416.

Wyzga, R. E., and Folinsbee, L. J. 1995. Health effects of acid aerosols. *Water, Air, and Soil Pollution,* 85, 177-188.

Xu, K.; Pichler, S., Wostyn, K., Cado, G., Springer, C., Gale, G. W., Dalmer, M., Mertens, P. W., Bearda, T., Gaulhofer, E., and Podlesnik, D. 2009. Removal of nano-particles by aerosol spray:

effect of droplet size and velocity on cleaning performance. *Solid State Phenomena,* 145, 31-34.

Xue, J., Lau, A. K., and Yu, J. Z. 2011. A study of acidity on $PM_{2.5}$ in Hong Kong using online ionic chemical composition measurements. *Atmospheric Environment*, *45*(39), 7081-7088.

Yang, J. Y., Kim, J. Y., Jang, J. Y., Lee, G. W., Kim, S. H., Shin, D. C., and Lim, Y. W. 2013. Exposure and toxicity assessment of ultrafine particles from nearby traffic in urban air in Seoul, Korea. *Environmental Health and Toxicology*, 28.

Yang, S. and Duisterwinkel, A. 2011. Removal of nanoparticles from plain and patterned surfaces using nanobubbles. *Langmuir,* 27**,** 11430-11435.

Yao, X., Choi, M. Y., Lau, N. T., Lau, A. P., Chan, C. K., and Fang, M. 2010. Growth and shrinkage of new particles in the atmosphere in Hong Kong. *Aerosol Science and Technology*, *44*(8), 639-650.

Yusof, N. S. M., Babgi, B., Alghamdi, Y., Aksu, M., Madhavan, J., and Ashokkumar, M. 2016. Physical and chemical effects of acoustic cavitation in selected ultrasonic cleaning applications. *Ultrasonics sonochemistry*, *29*, 568-576.

Yue, D. L., Hu, M., Zhang, R. Y., Wang, Z. B., Zheng, J., Wu, Z. J., Wiedensohler, A., He, L. Y., Huang, X. F., and Zhu, T. 2010. The roles of sulfuric acid in new particle formation and growth in the mega-city of Beijing. *Atmospheric Chemistry and Physics,* 10, 4953-4960.

Zampetti, E., Macagnano, A., Papa, P., Bearzotti, A., Petracchini, F., Paciucci, L., and Pirrone, N. 2017. Exploitation of an integrated microheater on QCM sensor in particulate matter measurements. *Sensors and Actuators A: Physical*, 264, 205-211.

Zhai, W., Wen, D., Xiang, S., Hu, Z., and Noll, K. E. 2016. Ultrafine-particle emission factors as a function of vehicle mode of operation for LDVs based on near-roadway monitoring. *Environmental Science and Technology*, *50*(2), 782-789.

Zhao, J., Liu, M., Liang, L., Wang, W., and Xie, J. 2016. Airborne particulate matter classification and concentration detection based on 3D printed virtual impactor and quartz crystal microbalance sensor. *Sensors and Actuators A: Physical*, 238, 379-388.

Zhang, Q. F., and Zhu, Y. F. 2010. Measurements of ultrafine particles and other vehicular pollutants inside school buses in South Texas. *Atmospheric Environment,* 44:253-261.

Zhang, K., Hu, J., Gao, S., Liu, Y., Huang, X., and Bao, X. 2010. Sulfur content of gasoline and diesel fuels in northern China. *Energy Policy*, *38*(6), 2934-2940.

Zhang, Q., Jimenez, J. L., Worsnop, D. R., and Canagaratna, M. 2007. A case study of urban

particle acidity and its influence on secondary organic aerosol. *Environmental Science and Technology*, *41*(9), 3213-3219.

Zhang, R.Y., Alexei, F. K., Joakim, P., Zhang, D., Xue, H. X., and McMurry, P. H. 2008. Variability in morphology, hygroscopicity, and optical properties of soot aerosols during atmospheric processing. *Proceedings of the National Academy of Sciences of the United States of America*, 30, 10291-10296.

Zhang, Y. N., Zhang, Z. S., Chan, C. Y., Engling, G., Sang, X. F., Shi, S., and Wang, X. M. 2012. Levoglucosan and carbonaceous species in the background aerosol of coastal southeast China: case study on transport of biomass burning smoke from the Philippines. *Environmental Science and Pollution Research*, *19*(1), 244-255.

Zhang, K., Hu, R., Fan, G., and Li, G. 2017. Graphene oxide/chitosan nanocomposite coated quartz crystal microbalance sensor for detection of amine vapors. *Sensors and Actuators B: Chemical*, 243, 721-730.